5-1-2019

DEVELOPMENT AND VALIDATION OF NEW MODELS AND METRICS FOR THE ASSESSMENTS OF NOISE-INDUCED HEARING LOSS

Wisam Subhi Talib Al-Dayyeni
Southern Illinois University Carbondale, wisam.subhi@gmail.com

DEVELOPMENT AND VALIDATION OF NEW MODELS AND METRICS FOR THE ASSESSMENTS OF NOISE-INDUCED HEARING LOSS

by

Wisam Subhi Talib Al-Dayyeni

B.Sc., Al-Nahrain University at Baghdad, Iraq, 2005
M.Sc., Al-Nahrain University at Baghdad, Iraq, 2009

A Dissertation
Submitted in Partial Fulfillment of the Requirements for the
Doctor of Philosophy Degree

Department of Electrical and Computer Engineering
in the Graduate School
Southern Illinois University Carbondale
May 2019

DISSERTATION APPROVAL

DEVELOPMENT AND VALIDATION OF NEW MODELS AND METRICS FOR THE ASSESSMENTS OF NOISE-INDUCED HEARING LOSS

by

Wisam Subhi Talib Al-Dayyeni

A Dissertation Submitted in Partial

Fulfillment of the Requirements

for the Degree of

Doctor of Philosophy

in the field of Electrical and Computer Engineering

Approved by:

Dr. Jun Qin, Chair

Dr. Lalit Gupta

Dr. Chao Lu

Dr. Mohammad Sayeh

Dr. Henry Hexmoor

Graduate School
Southern Illinois University Carbondale
March 21, 2019

AN ABSTRACT OF THE DISSERTATION OF

WISAM SUBHI TALIB AL-DAYYENI, for the Doctor of Philosophy degree in Electrical and Computer Engineering, presented on March 21, 2019, at Southern Illinois University Carbondale.

TITLE: DEVELOPMENT AND VALIDATION OF NEW MODELS AND METRICS FOR THE ASSESSMENTS OF NOISE-INDUCED HEARING LOSS

MAJOR PROFESSOR: Dr. Jun Qin

Noise-induced hearing loss (NIHL) is one of the most common illnesses that is frequently reported in the occupational and military sectors. Hearing loss due to high noise exposure is a major health problem with economic consequences. Industrial and military noise exposures often contain high-level impulsive noise components. The presence of these impulsive noise components complicates the assessment of noise levels for hearing conservation purposes. The current noise guidelines use equal energy hypothesis (EEH) based metrics to evaluate the risk of hearing loss. A number of studies show that the current noise metrics often underestimates the risk of hearing loss in high-level complex noise environments. The overarching goal of this dissertation is to develop advance signal processing based methods for more accurate assessments of the risk of NIHL. For these assessments, various auditory filters that take into account the physiological characteristics of the ear are used. These filters will help to understand the complexity of the ear's response to high-level complex noises.

In this study, the F-weighting and the fatigue model are evaluated using animal noise exposure data. The results show that both the F-weighting and the fatigue model demonstrate better correlations with the hearing loss indicators compared with conventional noise metrics. Also, the dual resonance nonlinear filter and the rounded-exponential filter are applied to

develop the velocity excitation pattern and the loudness excitation pattern. The results show that both excitation patterns can potentially be used as noise hazardous level indexes for the assessment of NIHL. Moreover, six noise metrics derived from six different auditory models are developed based on excitation patterns to assess NIHL. The designed noise metrics are evaluated by their correlations with chinchilla noise exposure data. The results show that the developed metrics have better correlation with hearing loss assessment compared to conventional metrics.

ACKNOWLEDGMENTS

Praise be to God for everything. I would like to express my deepest appreciation to my advisor Dr. Jun Qin for his assistance and guidance throughout my doctoral degree program. He constantly conveyed a spirit of adventure in regards to research. His guidance to me was vital to finishing this dissertation.

I would like to thank the members of my dissertation committee: Dr. Mohammad Sayeh, Dr. Lalit Gupta, Dr. Chao Lu, and Dr. Henry Hexmoor. Furthermore, I would like to express my gratitude to all the faculty and the staff of the Electrical and Computer Engineering Department for their support.

I'm deeply indebted to the Higher Committee for Education Development (HCED) in Iraq for granting me the opportunity to pursue my doctoral degree in the United States of America. Also, I am extremely grateful to all the members of my family for their extensive support and encouragement throughout my study.

Finally, I would like to thank my lab mates Ali Mahdi, Ibrahim Shebani, and Pengfei Sun for the time we spent together.

TABLE OF CONTENTS

LIST OF TABLES

LIST OF FIGURES

CHAPTER 1

INTRODUCTION

1.1 Background

Noise-induced hearing loss (NIHL) is one of the most common health related problems in the world. In 2018, the World Health Organization (WHO) estimated that around 466 million people worldwide suffer from hearing loss [1]. By 2050, WHO expects that over 900 million individuals will have disabling hearing loss [1]. WHO estimates that 1.1 billion people (aged between 12–35 years) are at risk for hearing loss because they are exposed to hazardous loud noise [1]. In the United States, hearing loss as a prevalent chronic disability is estimated to affect 29 million Americans of working age (equating 16.1% of American population) [2, 3]. Approximately, one-third of these impairments among the Americans can be attributed to noise exposure [4]. Exposure to loud noise over the time can cause a serious damage to the hair cells inside the cochlea. The exposure to the hazardous noise could result in a permanent shift in the hearing threshold, known as NIHL.

NIHL is a disease of the modern world because it is associated with the growing use of industrial tools in different forms [5]. People are exposed to harmful noise levels on a daily basis without knowing the consequences of the long-term exposure. Long-term exposure to noise, either high level continuous Gaussian noise or impulsive noise, can lead to hearing loss. Such types of noise can cause serious damage to the auditory system. Occupational groups at particular risk of hearing loss are [3]:

1. Military groups exposed to gunfire, explosions, and aircraft engines.
2. Transportation workers like flight crew, ambulance drivers, and motorcycle riders.

3. Industrial groups including manufacturing, mining, construction, farming, carpentry, musicians, etc.

Approximately 22 million workers in the United States are exposed to hazardous levels of occupational noise in the workplaces [6, 7]. The United States military spent over $1.2 billion of entitlement for compensation and hearing loss care for over 1.8 million Veterans in 2012 [8]. Hearing loss has a strong negative impact on the quality of life. Hearing loss can cause depression, impairs social interactions, and increases the risk of accidents [9-11].

1.2 Types of hearing loss

Hearing loss can be categorized into *conductive hearing loss*, *cochlear hearing loss*, and *retrocochlear hearing loss* [12].

1.2.1 Conductive hearing loss

Conductive hearing loss occurs when sound transmission efficiency of the outer and/or middle ear is reduced. This may be caused by cerumen (earwax) or a foreign body in the ear canal, irritation or infection of the outer ear, damage to the eardrum produced by trauma, an ear canal tumor, damage to the ossicles in the middle ear, middle ear tumor, or fluid in the middle ear caused by infection [13, 14]. Conductive hearing loss results in an attenuated sound reaching the cochlea in the inner ear. As a result, the sound will be heard lower than normal. The amount of loss may differ with the frequency, so that the sound may appear to have a different tonal quality from normal [12].

1.2.2 Cochlear hearing loss

Cochlear hearing loss includes damage to the structures inside the cochlea. It occurs in many ways, for example by exposure to intense noise or sound, metabolic disturbances, infection, autoimmune disorders, and genetic factors. Moreover, the damage may extend beyond

the cochlea and neural structures, such as an auditory nerve and higher centers in the auditory pathway. The term sensorineural hearing loss is used when both the cochlear and the neural structures are involved [12].

1.2.3 Retrocochlear hearing loss

Retrocochlear hearing loss occurs if the neural system is damaged at a level beyond the cochlea. For example, in the auditory nerve or the auditory cortex. Some causes of the retrocochlear hearing loss include vascular disorders, ototoxic medications, and tumors of the auditory nerve or the auditory cortex [15].

NIHL studied in this dissertation is focused on the hearing loss that arises from damages to the cochlea caused by different types of noise.

1.3 Sound

Sound can be defined as a physical phenomenon or a psychological phenomenon. In physics, sound is generated by a vibrating object and is propagated through a transmission medium or substance such as a gas, liquid or solid [16]. In psychology, sound refers to a perceptual sense of hearing these vibrations [17]. Sound can be seen as a wave motion in an elastic medium such as air [18]. The sound signal can be described by three main characteristics: intensity, frequency, and duration.

The intensity is defined as the power transmitted per second per unit area. The frequency can be defined as the number of cycles of vibration occur in one second. It is measured in Hertz (Hz). A healthy human ear can detect the sounds ranged approximately from 20 Hz to 20,000 Hz (20 kHz). The period is defined as the time required for one cycle of vibration [16].

1.4 Noise

The word “noise” is originally derived from the Latin word “nausea” which means sea sickness. Humans perceive different sounds and various noises in daily live. Many people consider noise as an intense sound. Noise also can be defined as a non-harmonic and a non-periodical complex sound with usually unwanted or unpleasant sense. The noise can be multi-frequency, intermittent, and impulsive in nature. From the psychological perspective, noise is just any sound undesired by the recipient and may affect the health of individuals [19]. Noise can be harmful when it is loud, even for a short time period like the noise of firearms or firecrackers. The loud noise can cause a damage to the sensitive structure in the inner ear and cause NIHL.

Noise generally can be classified into different types: (a) Continuous Gaussian noise, also called steady-state noise, this type of noise remains constant with negligible fluctuation over the time. (b) Impact noise which has a low background with intermittent noise levels that increase and decrease rapidly. (c) Impulse noise which has a short burst with sharp rise in the level and rapid decay. (d) Complex noise which has a combination of two or more of the previous types of noises [20-23]. Figure 1.1 illustrates different types of noise using simulated waveforms.

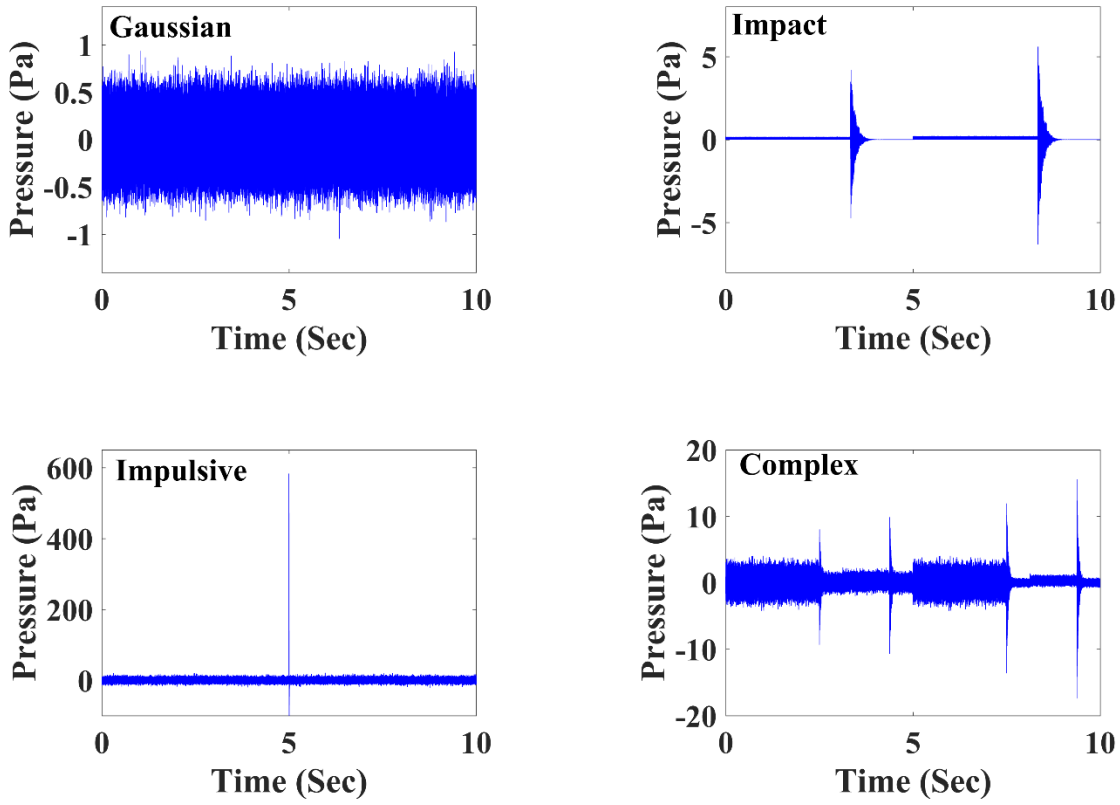

Figure 1.1. Types of noise with their simulated waveforms.

1.5 Measurement of sound

Sound pressures and intensities are normally described using logarithmic scales known as *sound levels*. The common logarithmic scale used for describing the sound levels is *decibel* (dB). The decibel is a relative unit and based on the ratio of two similar power quantities like sound power or intensity. In acoustics, the mathematical definition of the *Sound Pressure Level* (SPL) is described as below [24]

$$SPL = 10\log_{10}\left(\frac{\bar{p}^2}{p_0^2}\right) \tag{1.1}$$

where $\bar{p}$ is the time mean sound pressure in Pa and p_0 is the reference sound pressure. The reference pressure is equal to 20 µPa, which was adopted to be closer to 0 dB for a healthy normal-hearing person in the frequency range of best hearing [25]. This reference pressure was utilized in the first sound level meter standard Z24.3-1963 [25, 26].

1.6 Dissertation objectives

This dissertation focuses on the following objectives:

- Comparing and evaluating the existing noise metrics using animal noise exposure data.
- Designing of new noise metrics based on auditory models for better assessment of hearing loss.
- Evaluating and comparing the performance of the proposed noise metrics using animal noise exposure data.

1.7 Dissertation outline

The content of this dissertation is organized as follows:

- Chapter Two explores literature reviews of the studies related to the assessment of the NIHL.
- Chapter Three presents a basic overview of the physiology of the mammalian auditory system. Also, it summarizes the theoretical background of seven auditory filters.
- Chapter Four compares the two newly developed noise metrics with the three conventional noise metrics using animal experimental data.
- Chapter Five investigates the use of the excitation patterns of two auditory filters to evaluate the hazardous levels caused by different types of noises.

- Chapter Six develops and compares new noise metrics for NIHL assessment using various the auditory filters.
- Chapter Seven summarizes the main conclusions and future research directions.

CHAPTER 2

LITERATURE REVIEW

Most standards or policies use A-weighted sound pressure level as the main metric for evaluating the risk of a sound to produce hearing loss from long-term exposures [25]. The use of A-weighting reflects the fact that humans hear best in the mid-frequency region of audibility, with poor thresholds in the lower and the higher frequency regions of audibility [27]. However, numerous studies have shown that the A-weighting might underestimate the risk of NIHL [28-30]. For example, Cohen *et al.* [31] found that the A-weighted SPL underestimated the observed temporary threshold shift in human hearing for some noises, especially those with high low-frequency noise. Cohen *et al.* pointed out that the sharp roll-off at the low frequencies of the A-weighting curve minimizes their effect on the overall reading. Over the last decades, multiple researchers have sought to find a better metric for the NIHL evaluation. A chronological review is provided in this chapter for the studies that looked for more accurate way to improve the assessment of NIHL.

In 1994, Lei *et al.* [32] used the kurtosis statistic measured in the time domain and the frequency domain to predict the relative magnitude and the frequency distribution of the acoustic trauma. Lei *et al.* applied five different temporal structure noises but with the same average spectrum and the same unweighted SPL of 100dB to produce hearing loss in five groups of chinchillas. Animals were exposed to a given noise for five consecutive days. Each noise exposure produced a different magnitude and frequency distribution of the hearing loss. Lei *et al.* found that the time domain kurtosis is a suitable metric for ordering the severity of the trauma from a series of exposures whose total energy and spectra are the same. Moreover, Lei *et al.* pointed out that the temporal-spectral variables of the noise signal are important determinants of

the hearing loss. The results indicated that there is a consistent relation between the time domain kurtosis and the total loss of the outer hair cell. Also, there is a systematic relationship between the frequency domain kurtosis and the frequency specific profile of outer hair cell loss across the basilar membrane. This study showed that the equal energy hypothesis (EEH) is not an adequate predictor of NIHL. The results indicated that in addition to an EEH based metric, the kurtosis statistic of an exposure needs to be considered in the prediction of the hazards of an exposure.

In 2001, Hamernik *et al.* [33] extended the results of Lei *et al.* [32] by considering more generalized non-Gaussian noise signals. Five noises (four non-Gaussian noise and one Gaussian noise) each having an A-weighted SPL of 100 dB were exposed to five groups of chinchillas. The animals were exposed to a given noise for five consecutive days. The five noise signals differed only in their temporal structure. The results showed that the four non-Gaussian noises produced considerably greater hearing and sensory cell loss than did the Gaussian noise. The results also suggested that energy-based metrics are not sufficient for the prediction NIHL.

In 2003, Hamernik *et al.* [20] furthered the results of Lei *et al.* [32] and his previous experiment [33] by (1) extending the range of the kurtosis for each of the two series of noise exposures whose transients have different spectra, and (2) the kurtosis was varied by changing the peak histograms and the interval of the noise signals. This will result in changing the probability of the occurrence of a transient. Hamernik *et al.* exposed seventeen groups of chinchillas to seventeen different noises (one Gaussian condition and sixteen non-Gaussian conditions) at 100 dB SPL for five consecutive days. The results showed that the non-Gaussian noise exposures produce more hearing loss than the Gaussian noise. Also, the kurtosis in conjunction with an energy metric can differentiate exposure conditions not identified by conventional EEH based metrics alone.

In 2006, Qiu *et al.* [34] investigated the impact of complex noises that were generated using broadband noise bursts and band limited impacts within a continuous Gaussian background noise at 90, 100 and 110 dB SPL. Nine experimental groups of chinchillas were exposed to nine different noises (two Gaussian noises and seven non-Gaussian noises) for five consecutive days. The results showed that at SPL of 90 dB, there were no differences in the trauma produced by the Gaussian and non-Gaussian noise exposures. At SPL greater than 90 dB, the non-Gaussian noise exposures produced increased trauma comparative to the equivalent Gaussian noise exposures. In this study, Qiu *et al.* also showed that the kurtosis metric combined with the equivalent energy metric can improve the assessment of the complex noise that can cause more hearing damage.

In 2013, Qiu *et al.* [35] implemented more animal experiments to investigate the extent to which the kurtosis could be utilized to grade the hazard of a noise trauma produced by the exposures. Twenty-nine groups of chinchilla were exposed to Gaussian and non-Gaussian noise exposures at 97 dB SPL. Two groups of animals were exposed to either five days continuous Gaussian noise or to a nineteen days interrupted Gaussian noise. Three groups of animals were exposed for five days to one of the three continuous non-Gaussian noises. Twenty four groups were exposed to an interrupted non- Gaussian noise for nineteen days. All of the non-Gaussian noises were different in the level of the kurtosis or in the temporal characteristics of the noise. The non-Gaussian noise was defined by different intervals, peak SPLs, and duration histograms of the impact noise transients embedded in the noise signals. The results showed that the NIHL depends on the total acoustic energy of exposure to the noise, is not valid for high kurtosis exposures. In addition, the noise exposures which have the same spectral energy hearing trauma

also increases with the higher kurtosis. Moreover, the detailed temporal characteristics of an exposure does not have a strong effect on the trauma for the same level of kurtosis.

In 2009, Zhu *et al.* [36] used the analytic wavelet transform (AWT) to develop new noise metrics for a more accurate assessment of the hazard of the complex noise. The AWT is a hybrid combination of the windowed Fourier transform and the wavelet transform [37]. This blend will use the advantages of the wavelet transform while retaining usual definitions such as amplitude and frequency [37, 38]. The AWT is ideal to characterize time and frequency components in highly transient noises like an impulsive or complex noise [36]. This transform was utilized to obtain time-frequency (T-F) characteristics of the noise signal. Zhu *et al.* derived fourteen noise metrics from six basic forms to identify the most promising metric that can be used for better assessment of the risks of complex noises. The derived metrics were evaluated using existing animal data that were obtained by exposing twenty-three groups of chinchillas to different types of noise [20, 34, 39]. Zhu *et al.* used the permanent threshold shift measured in the chinchillas to assess the correlation with the noise metrics.

In 2011, Goley *et al.* [40] designed new noise metrics by combing the equivalent SPL and a temporal correction term defined as a function of kurtosis of the noise. The kurtosis serves as a good differentiator of the risk of the complex noises which have the same energy but different temporal characteristics [20, 33]. The form of the proposed noise metrics was designed to be no corrections with Gaussian noises, but higher corrections with the complex noises. Goley *et al.* added the correction term to three noise metrics: the equivalent SPL (L_{eq}), A-weighted SPL (L_{Aeq}), and the mean of the equivalent SPL defined at 0.5, 1, 2, and 4 kHz full-octave components ($L_{eq,5124}$). Multiple predictor regression models were constructed for each of the three metrics as well. The developed noise metrics were evaluated using chinchilla noise

exposure data to assess their correlations with NIHL [20, 34, 39]. The results showed that the kurtosis correction term improves the correlation of the noise metric with hearing losses measured in chinchillas. The $L'_{eq,5124}$ metric (which is kurtosis corrected $L_{eq,5124}$) showed the highest correlation with hearing loss compared with the other tested metrics.

In 2016, Sun *et al.* [41] proposed an adaptive weighting metric (F-weighting) which is based on the idea of blending the two traditional metrics (*i.e.,* A-weighting and C-weighting). The kurtosis and the oscillation coefficient were used in the implementation of the F-weighting metric. The performance of the F-weighting was evaluated using the chinchilla noise exposure data to assess its correlation with the hearing loss [20, 34, 39]. The results showed that the F-weighting metric has better performance than the traditional metrics (*i.e.,* A-weighting and C-weighting) on the assessment of hearing loss.

Moreover, controversy has arisen over the need for an advance method for better assessment of NIHL. Recently, several auditory filter based models have been developed for better assessment of NIHL [42-44]. Such auditory filter based models can reflect the fundamental physical properties of the ear [45]. This may lead to a better understanding of the NIHL based on the characteristics of the conductive path of the ear [43, 46].

In 1991, the US Army Research Laboratory (ARL) [42, 47, 48] developed the Auditory Hazard Assessment Algorithm for the Human Ear (AHAAH) to predict hazard of impulse noise in military fields. The AHAAH model is a theoretically based electro-acoustic analog of the ear that is conformal with the structure of the auditory system. The model reproduces the measured transfer functions from the free field to the stapes in the middle ear and translates stapes motion into basilar membrane displacements [49]. The AHAAH model takes into account the middle ear muscle effects, the displacement limiting by the middle ear, the spectral tuning, the change of

loss mechanism with level, and the operation in the time domain [42, 45, 47, 48, 50]. The model keeps track of the basilar membrane displacements at twenty-three locations. The final output of AHAAH model is an auditory risk unit which is calculated by squaring the peak amplitude of each upward displacement of the basilar membrane and summing them. The AHAAH model designed to predict the mechanical damage in the ear caused by a high level impulse noise. The results showed that the AHAAH model is a good predictor for the auditory hazard from intense acoustic impulses, such as firearms or airbags [49].

In 2015, Sun *et al.* [51] developed two auditory fatigue models to predict gradually developing hearing loss. Each one of these models contain two parts: the auditory system and the fatigue theory. The auditory system of each model consists of: the outer ear transfer function, the middle ear transfer function, and the triple-path nonlinear (TRNL) filter. The fatigue theory for the first model is based on the stress-cycles (S-N) curve and for the second model is based on the Miner's rule in the high-cycle fatigue theory. The auditory part is applied to obtain the basilar membrane velocities at each partition in the cochlea. The fatigue theory is applied to calculate the noise induced cumulative hazard represented by the number of fatigue cycles. High cycle fatigue theory was utilized in both models because the gradually developing hearing loss caused by the industrial noise is considered a long-term process of physical stretching compression of the Corti organ [43, 51, 52]. Sun *et al.* used chinchilla noise exposure data to validate the effectiveness of the fatigue models [20, 34, 39]. The results showed that the models can accurately predict hearing loss in the chinchilla.

In 2016, Sun *et al.* [44] developed two Excitation Patterns (EPs) based models (loudness EP and velocity EP) to evaluate NIHL. The loudness EP model contains: the outer ear transfer function, the middle ear transfer function, and the rounded-exponential (ROEX) filter. The

velocity EP model contains: the outer ear transfer function, the middle ear transfer function, and the dual resonance nonlinear (DRNL) filter. The ROEX auditory filter is derived from psychophysical data, and it has been used to represent the magnitude response of the auditory filter [53, 54]. The DRNL filter is a computational model used to obtain the velocity of the basilar membrane [55]. Two noise metric based EPs were developed to evaluate the hazard caused by the Gaussian noise and the impact noise. The results show that the velocity EP and the loudness EP are comparable in the case of the Gaussian noise. For the case of the impact noise, the velocity EP can more accurately estimate the hazard of noise exposure than the loudness EP [44].

CHAPTER 3

AUDITORY SYSTEM AND AUDITORY MODELS OVERVIEW

3.1 The auditory system

This section will present a basic overview of the physiology of the mammalian auditory system. The auditory system is usually divided into three regions: the outer ear, the middle ear, and the inner ear, as shown in Figure 3.1.

3.1.1 The outer ear

The outer (or external) ear consists of the pinna (outer part of the auditory system) and the ear canal (meatus). The pinna gathers sound from the environment in the form of acoustic energy and funnels it down the auditory canal. The shape of the outer ear, by its reverse horn structure, passively amplifies the sound [56]. The outer ear ends at the tympanic membrane (eardrum). When the tympanic membrane oscillates, it will cause the middle ear ossicles to displace.

3.1.2 The middle ear

The middle ear covers the region from the rear side of the eardrum to the oval window. Functionally, the middle ear acts as an impedance transformer buffering the impedance mismatch between the medium of lower impedance (*i.e.,* air in the auditory canal) and the medium of higher impedance (*i.e.,* water-like liquid called perilymph in the inner ear) [57]. The middle ear consists of three tiny bones: malleus (hammer), incus (anvil), and stapes (stirrup). These three tiny bones are called ossicles. The motion of the stapes generates hydrodynamic movement in the cochlea.

3.1.3 The inner ear

The inner ear is the sensory organ of the auditory system, which comprises the cochlea (a snail-like auditory organ). The cochlea is a fluid-filled structure completely covered in hard bone except for the oval window and the round window, which are enclosed by pliable membranes rather than bone. The cochlea is considered to be a time-frequency analyzer located in the temporal bones [57]. The cochlea has three chambers: scala vestibuli, scala tympani, and the scala media. The scala vestibuli and the scala tympani are located within the bone labyrinth and are filled with a fluid called perilymph. The scala media, or the cochlea duct, is filled with endolymph. Helicotrema is the part where the scala tympani and the scala vestibuli meet at the apex of the cochlea. The organ of Corti is located in the cochlea duct and rests on the basilar membrane. The basilar membrane has a higher stiffness and a lower mass at the base of the cochlea, and it vibrates maximally in response to high-frequency signals. In contrast, the basilar membrane has a lower stiffness and a higher mass at the apex of the cochlea, and it vibrates maximally in response to low-frequency signals [58]. Because of this structure of the basilar membrane, it will result in different resonance frequencies depending on the location of the basilar membrane. The resonant frequency of each location on the basilar membrane is based on the average stiffness, mass, and damping of the basilar membrane at that location. Moreover, the organ of Corti has a single row of inner hair cells and three rows of outer hair cells. Each hair cell has tiny sensory hair bundles called stereocilia, whose bending movement opens or closes mechanically-gated ion channels. The inner hair cells are the sensory receptors that convert sound vibrations in the fluids of the cochlea into neural spikes, which are transferred along the auditory nerve to higher centers of the auditory pathways. The main function of the outer hair

cells is to mechanically amplify the sound-induced vibrations and to sharpen the frequency observed in the cochlea [59].

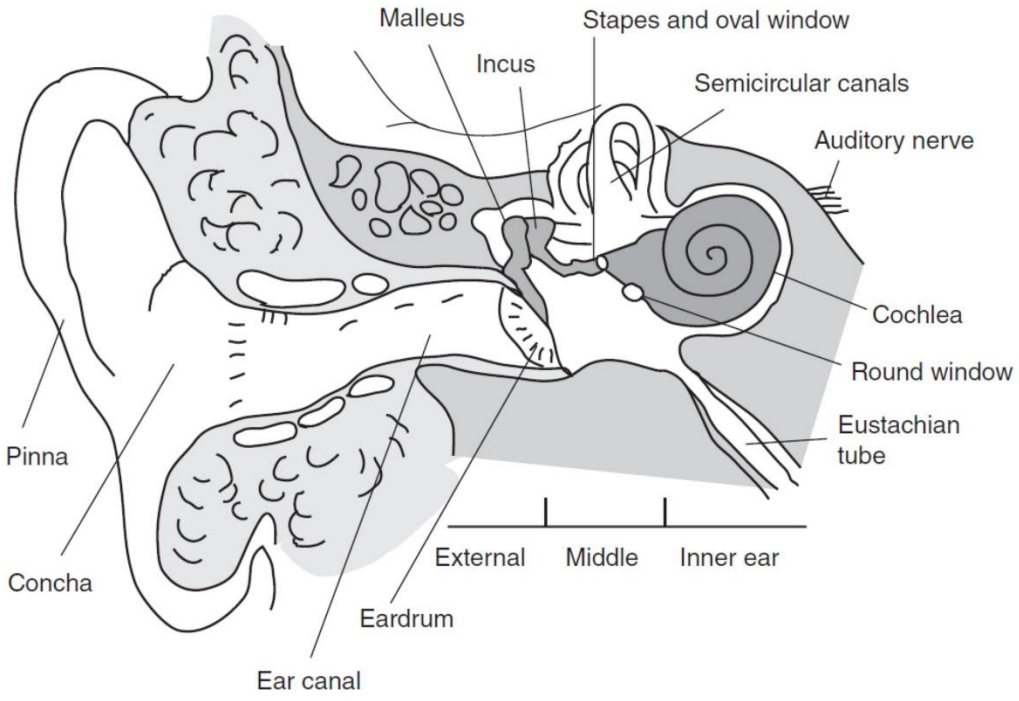

Figure 3.1. Cross-sectional diagram for the human ear, showing the external, middle, and inner ear [60].

3.2 Equal-loudness contours

In 1993, Fletcher and Munson [61] conducted a series of experiments on how the human's ear hears different frequencies at different sound levels. They measured perceived loudness as a function of tonal intensity and frequency. In these experiments, the observers of the loudness determined the level of a tone of a specific frequency that they judged equal in

perceived loudness to a 1000 Hz pure tone presented at a specific level and expressed in dB SPL. The loudness curves of Fletcher-Munson experiments show the ear's average sensitivity to various frequencies at different sound levels. The Fletcher-Munson loudness curves are known as the Equal-Loudness Contours.

In 1937, Churcher and King [62] performed a second determination on the equal-loudness contours under free-field conditions. However, the two previous determinations showed considerable discrepancies over parts of the auditory diagram [63]. There were discussions at the Committee on Noise Measurement of the British Standards Institution about the need for a standard set of contours. Therefore, it was decided that a new investigation on equal-loudness relations should be carried out at the National Physical Laboratory [63].

In 1956, Robinson and Dadson [63] produced a new set of equal-loudness curves for listeners in an anechoic room with a frontal sound source. The Robinson-Dadson curves became a standard of International Organization for Standardization (ISO 226) in 1986. When ISO revised the standard again, based on equal-loudness contours collected from 12 international research groups worldwide in 2003, it developed a new standard known as (ISO 226:2003) [64].

Figure 3.2 illustrates the simulated equal-loudness contours curves based on ISO 226:2003 [64]. Each point on any certain equal-loudness contour represents the level (on the Y-axis) and the frequency (on the X-axis) which was judged by the observers of the loudness to be similarly as loud as the 1000 Hz standard tone at the specified SPL. The "*phon*" is defined as a measure of loudness level based on the equal-loudness contours [61]. The equal-loudness contour curves show that the ear is less sensitive to low frequencies at low intensities. Also, the curves show that the ear is most sensitive to the mid-range frequencies, and slightly less sensitive to higher-range frequencies, compared to mid-range frequencies at the same intensity.

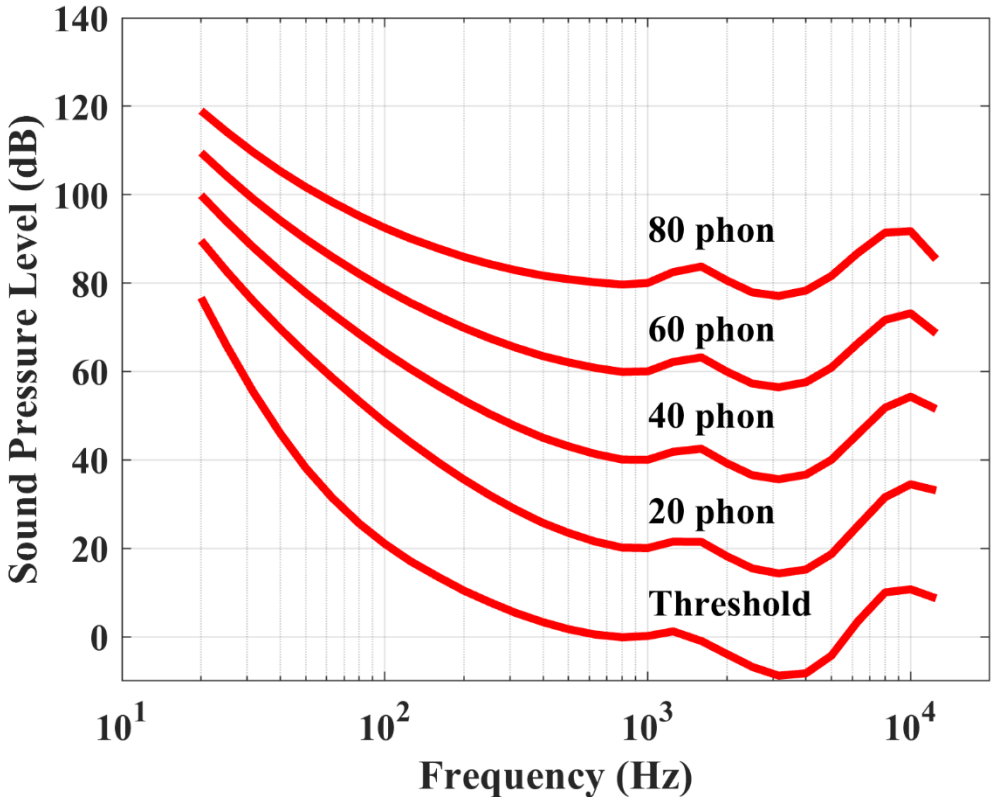

Figure 3.2. Simulated equal-loudness contours curves from ISO 226:2003 [64].

3.3 Auditory weighting functions

Auditory weighting functions for humans are based on the equal-loudness contours curves. Approximately, three years after the publication by Fletcher and Munson on equal-loudness contours curves, a sound level meter standard (Z24.3-1936) was developed by the sponsorship of the American Standards Association [which is now known as the American National Standards Institute (ANSI)] [26]. After a few decades, both international and national standards added several weighting filters for sound level meters. These weighting filters are: A-, B-, C-, D-, and Z-weighting which are largely based on equal-loudness contours. Today, the frequency-weighting B and D have been abandoned and they are no longer included in the standards because of the broad use of A-weighting. The ZERO frequency-weighting or the Z-

weighting has a flat frequency response (within ±1.5 dB) from 10 Hz to 20 kHz. The Z-weighting was introduced in the International Standard IEC 61672 in 2003 to replace the “Flat” or “Linear” filters [25]. A-weighting and C-weighting are used for noise measurements nowadays. Figure 3.3 shows the simulated A-weighting and C-weighing curves.

A-weighting is the most used auditory weighting function for noise and other acoustic measurements. The A-weighting curve is based on the 40-phon equal-loudness contour of Fletcher and Munson. 40 phon is a sort of a level that is likely to exist in a quiet acoustic environment. Therefore, A-weighting was originally intended for measurements at low sound levels. However, A-weighting is now commonly used for the measurement of noise. The use of A-weighting as a sound measurement was started in late 1960’s when regulatory organizations began imposing limits on the noise exposure after the detection of hearing loss caused by long term exposure to noise. A number of studies showed that humans were more sensitive to the hearing loss in the 1 kHz to 4 kHz range [27, 29]. Because the A-weighting curve intensifies this frequency range (*i.e.*, 1 kHz to 4 kHz), it was utilized as the standard for measuring the noise in the workplace.

Moreover, the C-weighting curve is based on the 100-phon equal-loudness contour. The ear’s response for higher sound level does not change with the frequency as much as it does for low sound level. That’s why the C-weighting curve is flatter than the A-weighting curve, because it was designed based on the100-phon while the A-weighing curve is based on the 40-phon. Also, this will result in the C-weighting curve to have a shallower low-frequency roll off than the A-weighting curve. C-weighting is usually used for peak measurements because it gives a better estimate of the auditory systems response to high sound levels than the A-weighting. The sound levels measured with the A-weighting and C-weighting have units of "dBA" and "dBC,"

respectively. In this dissertation, A-weighting and C-weighting will be used as the conventional metrics for the comparison purposes because they are specified in the health legislation [65].

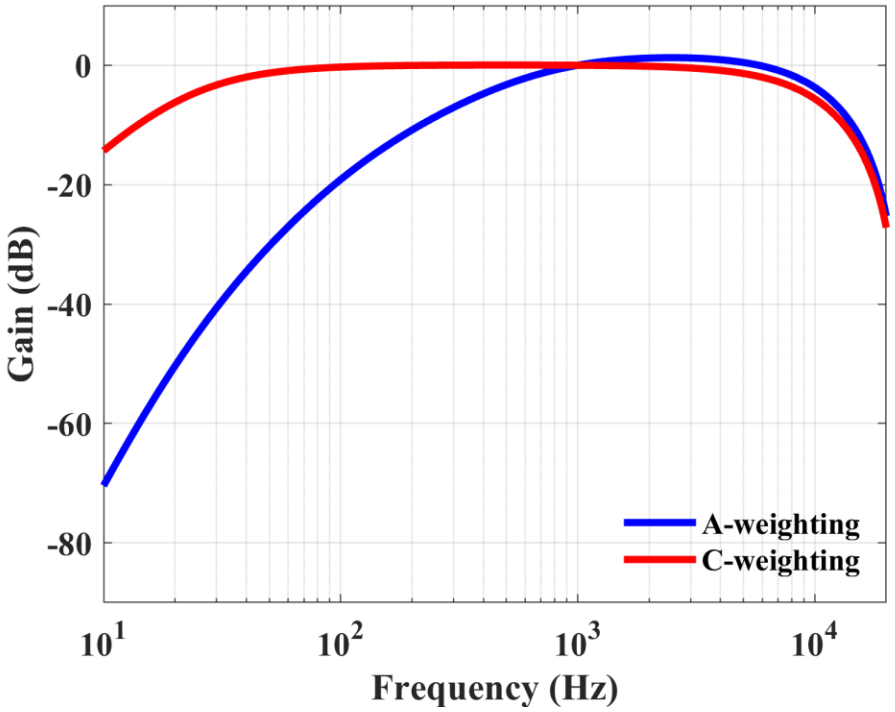

Figure 3.3. A-weighting and C-weighing curves based on IEC 61672-1 and ANSI S1.42 standards [66, 67].

3.4 Auditory models

The auditory models play a major role as powerful analytical tools to understand the auditory processing. Auditory models have been utilized as realistic sound processors for many hearing applications. This section presents theoretical and mathematical background for auditory filters. Table 3.1 summarizes the selected auditory models for this dissertation and the modeling approaches they belong to.

These auditory models can be divided into two categories: (i) mechanical models which include: DRNL, CARFAC, and Verhulst (ii) perceptual models which include: Gammatone, Loudness, ROEX, and Zilany. The mechanical models are able to simulate the mechanical

vibration of the basilar membrane in the cochlea. The perceptual models are designed to reproduce the perceptual data without making explicit predictions of the cochlea mechanics.

Moreover, the auditory models can be classified according to their design nature into three categories: (i) parallel filterbank models which include: Gammatone, Loudness, ROEX, DRNL, and Zilany (ii) cascaded model which includes, CARFAC, and (iii) transmission-line model which includes, Verhulst. The parallel filterbank models consist of a number of discrete filters that are independently activated by the common input. The cascade model and the transmission-line model are based on the Wentzel-Kramers-Brillouin (WKB) approximation for simulating the wave propagation in a one-dimensional non-uniform media [68, 69].

Table 3.1. The auditory models selected in this dissertation. The models are named according to the specific technical name or according to the first author's name if there is no assigned technical name.

Auditory Model	(Author's Name, year)	Design strategy	Design nature
Gammatone	(Hohmann, 2002)	Parallel filterbank	Perceptual data
Loudness	(Moore *et al.,* 1997)	Parallel filterbank	Perceptual data
Rounded-exponential filter (ROEX)	(Patterson *et al.,* 1982)	Parallel filterbank	Perceptual data
Dual Resonance Nonlinear filter (DRNL)	(Meddis *et al.*, 2001)	Parallel filterbank	Mechanical vibrations
Cascade of Asymmetric Resonators with Fast-Acting Compression model (CARFAC)	(Lyon, 2011)	Cascaded filterbank	Mechanical vibrations
Nonlinear time-domain cochlear model	(Verhulst *et al.,* 2012)	Transmission line	Mechanical vibrations
Computational auditory-nerve fiber responses model	(Zilany *et al.*, 2006)	Parallel filterbank	Auditory-nerve fiber response

3.4.1 Gammatone model

Gammatone filters are used in computational auditory models to simulate the peripheral filtering in the cochlea [70-72]. The Gammatone filterbank follows a linear relationship, so that it cannot simulate the nonlinear features of the cochlear biophysics. The Gammatone filters provide a linear and symmetric approximation of the shape and the bandwidth of the peripheral filtering [73]. Moreover, the center frequencies of the Gammatone filterbank are linearly spaced

on the Equivalent Rectangular Bandwidth (ERB) frequency scale [72]. In this chapter, a fourth-order linear Gammatone implementation based on an impulse-invariant, all-pole designed by Hohmann [72] will be used; which is available online at AMtoolbox [74].

For the Gammatone filter design, the complex analog Gammatone impulse response can be given by the below equation [72]

$$G_\gamma(n) = n^{\gamma-1} \,.\, \tilde{a}^n \tag{3.1}$$

where γ represents the filter order and n represents the sample index. $\tilde{a}$ is given by the below equation [72]

$$\tilde{a} = \lambda \,.\, \exp(i\mu) \tag{3.2}$$

where λ represents the bandwidth or the damping parameter and μ represents the oscillation frequency. In the Gammatone implementation, the concept of the ERB of the auditory filters is used for the derivation of the bandwidth as a function of its center frequency. The analytic expression for the ERB as a function of frequency in Hz is given by [72, 75]

$$ERB_{aud}(f) = l + f/q \tag{3.3}$$

where l equal to 24.7 and q equal to 9.265. The relation between the ERB and the damping parameter of a Gammatone filter is approximated by Patterson *et al.* [70] as shown below [70, 72]

$$\lambda = \exp(-2\pi b/f_s) \tag{3.4}$$

where $b = ERB/a_\gamma$ and $a_\gamma = 2(2\gamma - 2)!\, 2^{-(2\gamma-2)}/(\gamma - 1)!^2$

The center frequencies of the auditory filterbank are linearly spaced on the ERB frequency scale. As the auditory filters have constant ratio of bandwidth and center frequency

according to equation (3.3), the ERB scale is logarithmic. the value on the ERB scale as a function of frequency can be given by the following [72]

$$ERB_{Scale}(f) = q.\log(1 + \frac{f}{l.q}) \quad (3.5)$$

where l equal to 24.7 and q equal to 9.265.

3.4.2 Loudness model

Loudness can be considered as one of the most essential parameters of psychoacoustics. Moore *et al.* [76] implemented a model of loudness perception which is mainly intended to predict the loudness of the sounds. The model of loudness perception by Moore was developed originally from a model proposed by Zwicker [77-79]. Moore's model takes into account the specification of the conditions of presentation of the sounds. The options under these conditions are free field, diffused field, or headphone and binaural or monaural.

Moreover, the loudness model considers the transfer functions of the outer ear and the middle ear. The cochlea is modeled as a bank of bandpass auditory filters with overlapping passbands. The shapes and the bandwidths of the filters depend on both center frequency and the level. The output can be specified either in terms of excitation level or as linear power [80]. Moore's model has been used as the standardization method for the calculation of loudness in the American National Standards Institute (ANSI) and in the international standardization (ISO) [80, 81]. However, this model is based on the average results of a large number of listeners with normal hearing which can be considered as a limitation for this model [76]. In this dissertation, the loudness model for time-varying sounds by Glasberg *et al.* [82] will be used.

For the loudness model calculations, Moore *et al.* [76] model the auditory filters by the ERB bands. The ERB of the auditory filter is described by [76]

$$ERB = 24.7(4.37\ f_c + 1) \tag{3.6}$$

where f_c is the center frequency in kHz.

Moore's method for the calculation of the excitation diagram for time-varying sounds is based on a multi-resolution spectral analysis by Fourier Transform [82]. Six Fast Fourier Transforms (FFTs) are calculated in parallel, with temporal windows durations of 2, 4, 8, 16, 32, and 64 ms. The FFT calculations are used to measure the level in bands 4050-15000, 2540-4050, 1250-2540, 500-1250, 80-500, and 20-80 Hz, respectively.

3.4.3 Rounded-exponential filter (ROEX model)

The ROEX filter was originally derived from psychophysical data [83]. It is a descriptive model, which describes the shape of the transfer function of an auditory filter [83]. The ROEX filter formula can be defined as [44, 84]

$$W(g) = (1 + pg)\exp(-pg) \tag{3.7}$$

where g is the normalized deviation from the center frequency of the filter divided by the center frequency, and p is a parameter controlling the slope and the bandwidth of the filter.

The EP for the ROEX filter is calculated according to the standard procedure described in ANSI 3.4-2005 [85]. To calculate the input level at each Equivalent Rectangular Bandwidth, p in Equation (3.7) is set to be $4f/ERB$. The ERB is a psychoacoustic measurement of the width of the auditory filter in each location along the cochlea. The ROEX model ERB bands calculation are based on Glasberg *et al.* [75] as shown in equation (3.6). The ERB obtained according to the input level used to determine the ROEX filter shape. The energy in each ERB can be obtained by [44]

$$E_i = \frac{\sum W(g_{i,j}) P_j^2}{{P_0}^2} E_0 \tag{3.8}$$

where W represents local ROEX filter in the *i*th ERB. P_j^2 refers to the power in the *j*th frequency band. E_0 is the reference energy at 1 kHz center frequency and 0 dB SPL, and P_0 is the reference pressure referring to 2×10^{-5} Pa. For the selected frequencies, E_i will be transformed to loudness levels according to the values of the excitation threshold [86]

$$N = C\left[\left(GE + 2E_{THRQ}\right)^{\alpha} - \left(2E_{THRQ}\right)^{\alpha}\right] \tag{3.9}$$

where E is the energy, and G is the low level gain. C and α are two constants, where C =0.046871, and α is related to the G value. E_{THRQ} refers to lower threshold of human perception.

Figure 3.4 shows the shape of the ROEX filter at 0.5, 1, 2, 4, and 8 kHz center frequencies when the levels change from 10 to 100 dB in 10-dB steps. The ROEX filter is a dynamic filter, which has different frequency gains when the sound pressure level changes. As the SPL level increases, the curve of the ROEX filter becomes more flat. In general, when the SPL increases, there will be more energy passing through the ROEX filter. From this perspective, the ROEX filter is consistent with the loudness contours [84, 86].

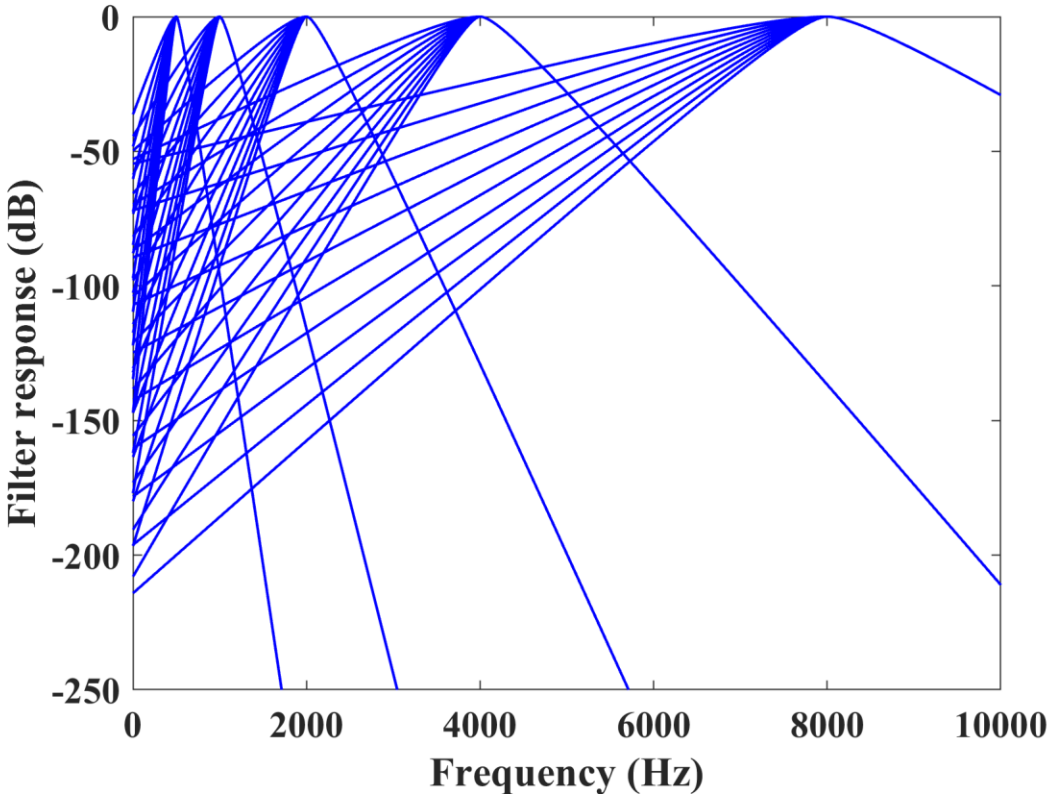

Figure 3.4. The shape of the ROEX filter centered at 0.5, 1, 2, 4, and 8 kHz for levels from 10 dB to 100 dB with 10-dB step.

3.4.4 Dual resonance nonlinear model

Meddis *et al.* [55] implemented a computational algorithm to mimic the response of the basilar membrane. The input to the system is stapes velocity (m/s), and its output characterizes the vibration velocity of the basilar membrane. The model uses two processing paths operating in parallel: linear and compressively nonlinear [55]. The linear path characterizes the vibration of the passive cochlea structures while the compressively nonlinear path represents the active contribution of the outer hair cells to the system. The output result from the algorithm is the sum of the outputs of the linear path and nonlinear path. This output characterizes the basilar membrane motion.

Furthermore, Lopez-Poveda and Meddis [87] developed a human nonlinear filterbank which is based on the DRNL filter. The model includes two stages: (1) an outer/middle-ear transfer function, which converts a headphone-delivered sound pressure waveform into a stapes motion waveform, and (2) a DRNL filter which simulates the basilar membrane motion in response to stapes velocity [87]. The aim of the model is to reproduce the nonlinear mechanical responses of the basilar membrane. Moreover, Lopez-Najera *et al.* [88] introduced the improved DRNL filter by adding a third parallel path acting as a *linear, zero-phase, all-pass* filter to the original DRNL filter. The output from the improved DRNL filter is the sum of the outputs from the main DRNL filter and the third path. This third path allows modeling of the phase plateaus and the high-frequency amplitude observed in basilar membrane tonal responses [88, 89]. The DRNL filter and the improved DRNL filter has been used before in NIHL field to evaluate the hearing loss [43, 44, 90, 91]. In this dissertation, the MATLAB implementation of the code for the DRNL model was used from the AMtoolbox [74].

3.4.4.1 DRNL model

The DRNL filter is utilized to obtain the basilar membrane movements in the human cochlea [55]. The DRNL filter simulates the velocity of basilar membrane as a response to the stapes velocity in the middle ear. As shown in Figure 3.5, the input of the DRNL filter is the linear stapes velocity. Each individual site is represented as a tuned system with two parallel independent paths. The right path is the linear one and the left path is the nonlinear one in the figure. The linear path consists of a gain/attenuation factor, a bandpass function, and a low pass function in a cascade. The nonlinear path is a cascade combination of the 1^{st} bandpass function, a compression function, the 2^{nd} bandpass function, and a low pass function. The output of the DRNL filter is the sum of the linear and nonlinear paths. The result is the basilar membrane

velocity at a particular location along the cochlear partition. In both paths, each of the three bandpass functions consists of a cascade of two or three 1st order Gammatone filters [92] with a unit gain at the center frequency. Two low-pass functions are the same and also have a cascade of four 2nd order Butterworth low pass filters. Moreover, the compressive function shape in the nonlinear path is derived from the animal data, and it is defined as [55]

$$y[t] = \text{sign}\,(x[t]) \times MIN\,(a|x[t]|, b|x[t]|^c) \tag{3.10}$$

where $x[t]$ is the output from the first filter in the nonlinear path. a, b, and c are models parameters.

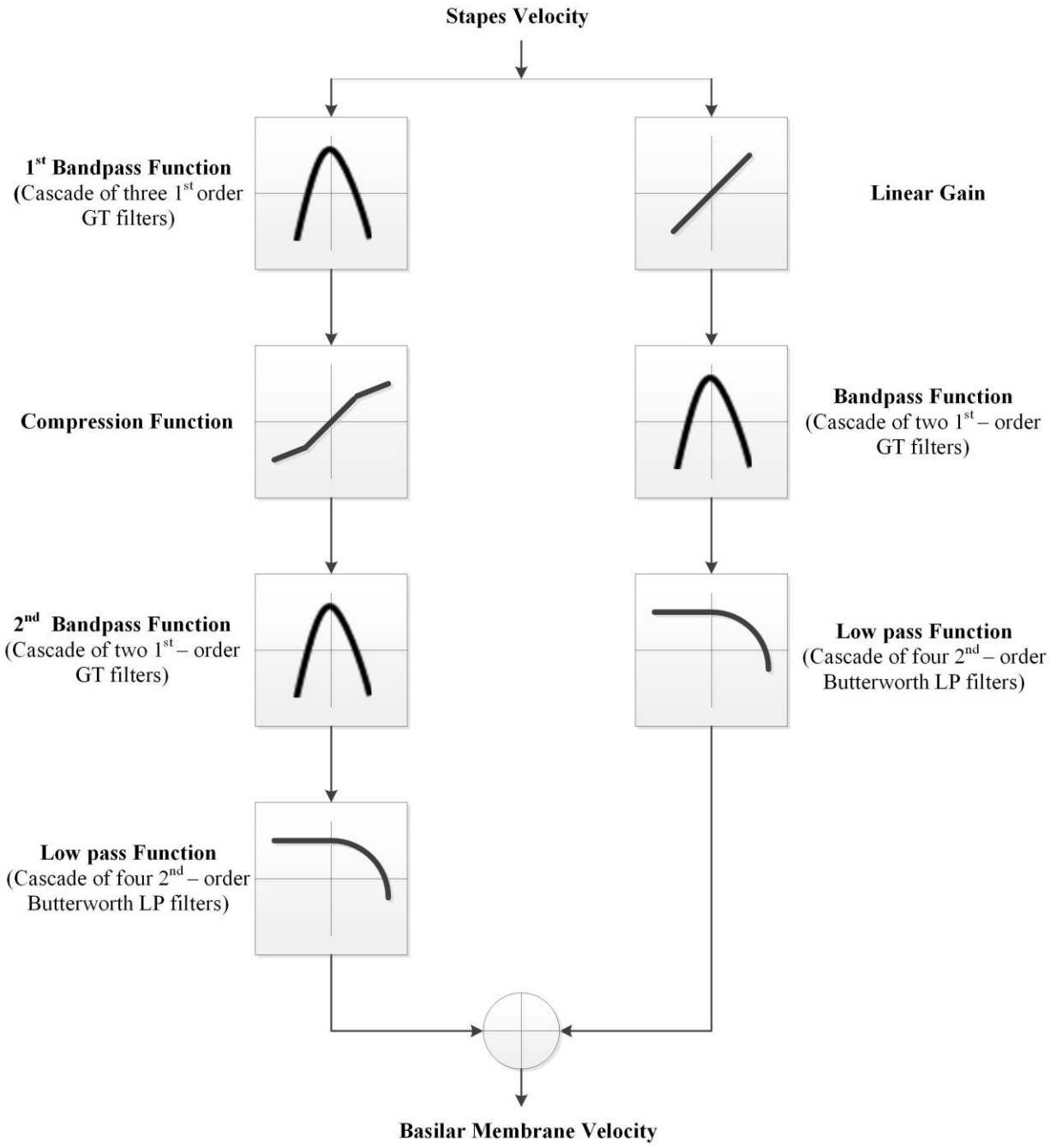

Figure 3.5. Schematic diagram of the DRNL filter, in which the velocities of stapes in middle ear are passed through two parallel branches to obtain the velocities of the basilar membrane [55].

3.4.4.2 TRNL model

The triple-path nonlinear (TRNL) filter [88] was applied to obtain the basilar membrane responses along the cochlea partitions. Figure 3.6 shows the structure of the TRNL filter, in which the input is the middle ear stapes velocity and the output represents the velocity of the basilar membrane of a particular location at the cochlea partitions.

The TRNL filter consists of three parallel independent paths: Linear path (right), nonlinear path (middle), and low-gain linear path (left). The linear path contains a gain /attenuation factor, a bandpass function, and a low pass function in a cascade. The nonlinear path is a cascade combination of the 1^{st} bandpass function, a compression function, the 2^{nd} bandpass function, and a low pass function [55]. Each individual bandpass function contains a cascade of two or more gammatone filters [92] with unit gain at the center frequency. The third path is used to allow modeling of the amplitude and the phase plateaus at high frequency observed in the basilar membrane responses [88, 89]. The third path contains a linear low-gain, and all-pass filter. Moreover, the compression function in the nonlinear path was based on the animal data that is defined in equation (3.10).

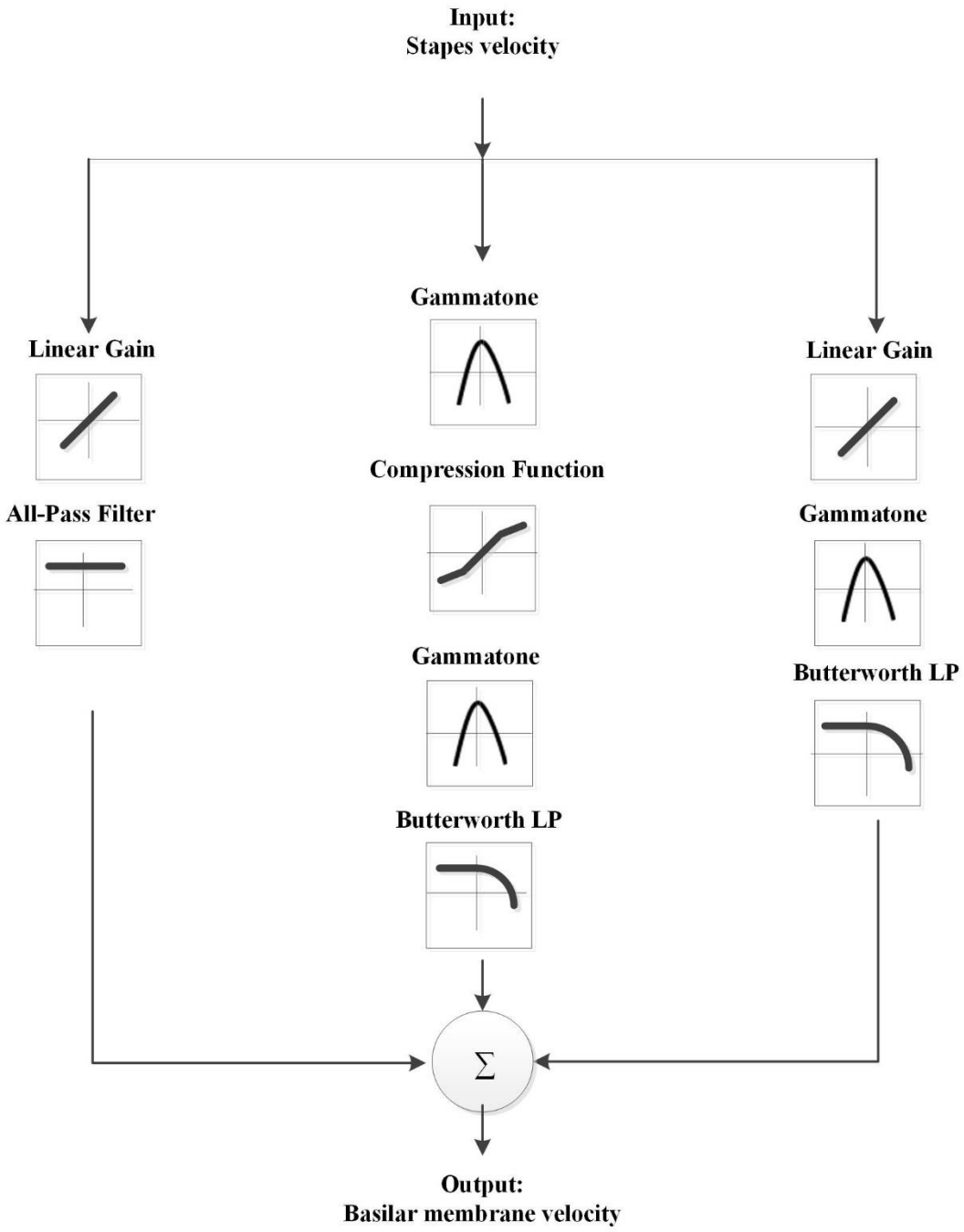

Figure 3.6. Schematic diagram of the TRNL filter, in which the input is the middle ear stapes velocities and the output is the velocity of the basilar membrane [51, 55, 88].

3.4.5 Cascade of asymmetric resonators with fast-acting compression model (CARFAC model)

The structure of the filter cascades is based on the Wentzel-Kramers-Brillouin (WKB) method for simulating the wave propagation in non-uniform media such as the cochlea [68, 93]. This method says that if a wave is propagating along one dimension from the input, then the response from the input to any location can be found by composing the relative responses from each location to the next along that dimension using specific local parameters as if the medium were uniform [94].

Lyon *et al.* [69, 93] introduced the CARFAC model which is based on the previous work of pole-zero filter cascade models. This model consists of second order filters in which each filter is described by a complex-conjugate pair of zeros and a complex-conjugate pair of poles. The zeros are located slightly above the poles in frequency which will lead to peak in gain near the pole frequency, followed by a gain drop at higher frequencies. The level dependence of the model is achieved by moving the pole damping in each stage in response to the output levels of the filterbank. This modification of pole damping corresponds to moving the pole along a circular trajectory in the *s* plane. Thus, the peak frequency of the resonance moves a little as the bandwidth and the gain of the resonance changes. In this dissertation, the software implementation of the CARFAC model is used from the publicly available online open-source website [95].

For the implementation of the CARFAC model, the structure of the filter cascades originates from a simple observation of how filter cascades can make models of wave propagation in non-uniform systems like the cochlea. The outer ear and the middle ear are not

included in this model. In this dissertation, the transfer function of the outer ear and the middle ear is will be added to the CARFAC model to build a complete auditory system.

The complex transfer function of the linearized pole–zero filter cascade for one stage is a rational function of a second order Laplace transform variable (*s*) in both numerator and denominator. This will be corresponding to a pair of zeros (roots of the numerator) and a pair of poles (roots of the denominator) as shown below [93]

$$H(S) = \frac{s^2/\omega_z^2 + 2\zeta_z s/\omega_z + 1}{s^2/\omega_p^2 + 2\zeta_p s/\omega_p + 1} \tag{3.11}$$

where ω_p and ω_z are the frequencies of the poles and zeros, respectively. ζ_p and ζ_z are the damping ratios of the poles and zeros.

Moreover, the CARFAC model ERB bands calculation are based on Glasberg *et al.* [75] as shown in equation (3.6).

3.4.6 Nonlinear time-domain cochlear model (Verhulst model)

Verhulst *et al.* [96] introduced a nonlinear transmission-line model of the cochlea for human otoacoustic emission generation and transient stimulation. The cochlea is modeled as an uncoiled fluid-filled tube containing a series of 1000 oscillators that are coupled through the incompressible basilar membrane fluid. In this model, the pressure was assumed to be uniformly distributed in perpendicular directions to the basilar membrane. Each stage of the model consists of a shunt admittance and an impedance. The shunt admittance characterizes the basilar membrane transverse impedance and the structures that load it. Moreover, the impedance represents the impedance of the fluid which moves longitudinally. The active forces and the nonlinearity of the cochlea are simulated by varying the poles of shunt admittance [73, 96, 97]. The main benefit of the transmission-line model is the possibility to simulate the forward and the

reverse traveling waves which gives rise to otoacoustic emissions. In this dissertation, the computer implementation of this model is used from the AMtoolbox [74].

For the implementation of the Verhulst model, the outer ear is not included in original design of this model because it is used to investigate the otoacoustic emission (OAE) generation that was delivered directly to the tympanic membrane in the middle ear via earbars. Outer ear transfer function will be considered for this model to build a complete auditory system to evaluate the input acoustic signal from the free-field.

For the middle ear and the inner ear implementation of this model, the Helicotrema boundary at the apex was modeled as a short circuit. The middle ear boundary was modeled as an impedance matching network [96]. The resistance at the middle ear boundary can be expressed as follow [96]

$$R_{ME} = \left(\omega_{c0}^2 M_{p0} M_{s0}\right)^{\frac{1}{2}} \tag{3.12}$$

where ω_{c0} is the characteristic angular frequency at base. M_{p0} and M_{s0} are the acoustical mass at base expressed as below [96]

$$M_{s0} = 2\rho/bh \tag{3.13}$$

$$M_{p0} = M_{s0} l^2/(4N_w)^2 \tag{3.14}$$

where ρ is the cochlear fluid density. b is the basilar membrane width. h is the scala height. l and N_w are constants.

Moreover, for the inner ear, Figure 3.7 shows the schematic diagram of the nonlinear transmission-line model of the cochlea. The model consists of the series admittance (Y_{sn}) and the parallel admittance (Y_{pn}). The input pressure is the sound pressure on the stapes. The series

admittance (*i.e.*, Y_{sn}) and the parallel admittance (*i.e.*, Y_{pn}) can be defined as a function of the complex Laplace transform variable, *s*, as shown below [97]

$$Y_{sn}(s) = (\omega_0 M_{s0} S)^{-1} \tag{3.15}$$

$$Y_{pn}(s) = s\left[\omega_0 M_{p0}\left(s^2 + \delta_n(t)s + 1 + \rho_n(t)e^{-\psi_n(t)s}\right)\right]^{-1} \tag{3.16}$$

where M_{s0} and M_{p0} are constants. $\delta_n(t)$, $\rho_n(t)$, and $\psi_n(t)$ are variables control the instantaneous nonlinearities as proposed by Shera model [97, 98].

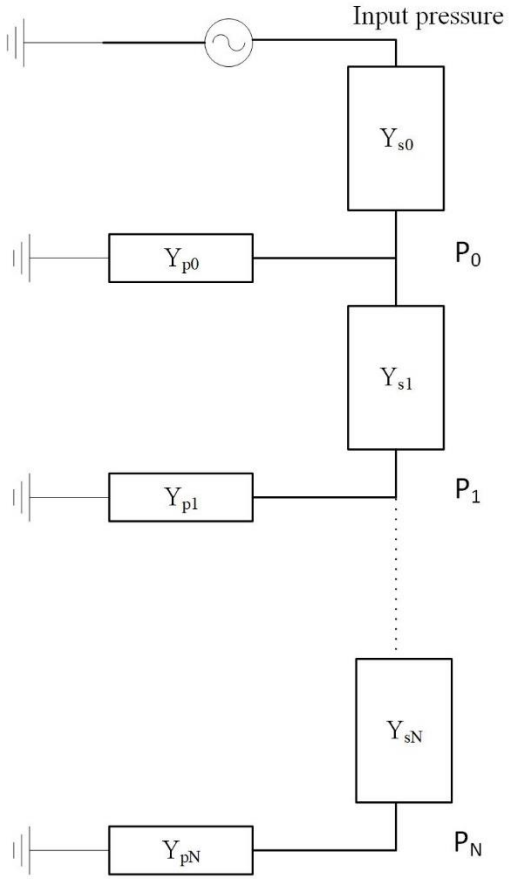

Figure 3.7. Schematic diagram of the electrical equivalent of the transmission line cochlear model [97].

3.4.7 Auditory-nerve (AN) fiber responses model (Zilany model)

Zilany and Bruce [99] introduced a computational auditory-periphery model to simulate the high spontaneous rate (HSR) auditory nerve fiber responses. As shown in Figure 3.8, the model includes two parallel filter paths (C1 and C2) which represent the active and passive modes of basilar membrane vibration, respectively. The output of the first filter (*i.e.,* C1) closely resembles the active mode of vibration of the basilar membrane. The second filter (*i.e.,* C2) has been used as a second mode of excitation to the inner hair cell (IHC) and this filter is critical for simulating the transition region effects at high levels. The feed-forward control path regulates the gain and bandwidth of the C1 filter to account for several level-dependent characteristics in the cochlea. The control path consists of: (1) a time-varying third-order Gammatone filer, (2) a nonlinear (Boltzmann) function followed by a third-order low-pass filter, and (3) a nonlinear function. The low-pass filter used to control the dynamic range and the time course of compression. The nonlinear function in the last stage is used to convert the output of the low-pass filter to a time-varying constant for the C1 filter [99, 100].

The idea of this model is to simulate the auditory nerve responses where the cochlea vibrations are passed to a low-pass filter (modeling the IHC), a time-varying three-store-diffusion model of the IHC-AN synapse, and the final stage is the spike generator. The parameters of this model were chosen to match the auditory-nerve fiber responses in cats [99, 101]. In this dissertation, the code for Zilany model (the humanized version) is used from the AMtoolbox [74]. Moreover, the code related to the basilar membrane stage of the humanized model was used in this dissertation because our focus is on the basilar membrane vibrations.

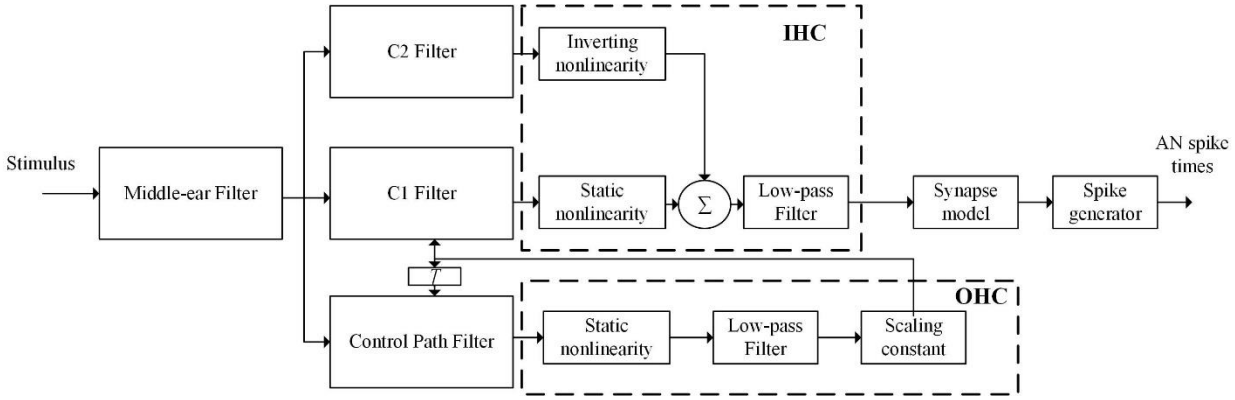

Figure 3.8. Schematic diagram of the Auditory-nerve (AN) fiber responses model [99].

For the implementation of the Zilany model, the outer ear is not included in original design because it's used to predict physiological data for acoustic stimulus that was delivered directly to the tympanic membrane in the middle ear via earbars. Outer ear transfer function is considered in this model to build a complete auditory system to evaluate the input acoustic signal from the free-field.

In Zilany's model, the middle ear filter is implemented by using digital filters. A second-order digital filter system is formed by cascading the following filters [99]

$$ME_1(\mathrm{Z}) = 0.0127\left(\frac{1.0000+1.0000Z^{-1}}{1.0000-0.9986Z^{-1}}\right) \quad (3.17)$$

$$ME_2(\mathrm{Z}) = \frac{1.0000-1.9998Z^{-1}+0.9998Z^{-2}}{1.0000-1.9777Z^{-1}+0.9781z^{-2}} \quad (3.18)$$

$$ME_3(\mathrm{Z}) = \frac{1.0000-1.9943Z^{-1}+0.9973Z^{-2}}{1.0000-1.9856Z^{-1}+0.9892z^{-2}} \quad (3.19)$$

As mentioned before, the C1 filter produces the tuning characteristics for the basilar membrane response. The C1 filter was designed with an asymmetrical orientation of the poles and zeros in the complex plane. It consists of two second-order poles (at the same position), one

first-order pole and a fifth-order zero on the real axis. The order of the C1 filter was chosen to be equal to 10 [99]. The order of the filter has a major impact on the sharpness of the tuning. If the order of the filter is too high, the filter remains sharply tuned even for high SPL stimulus [99, 102]. The configuration of the relative positions and the limits of the poles and zeros movement of the C1 filter can be expressed as below [99]

$$P_{01} = 1/\tau_{C1} = 0.7 \times (2\pi CF)/(2Q_{10}) \tag{3.20}$$

$$P_w = 1.01 \times 2\pi CF - 50 \tag{3.21}$$

$$P_b = 0.2343 \times 2\pi CF - 1104 \tag{3.22}$$

$$\log_{10}(P_a - 2000) = \log_{10}(CF) \times 0.9 + 0.55 \tag{3.23}$$

$$\log_{10}(Z_L - 500) = \log_{10}(CF) \times 0.7 + 1.6 \tag{3.24}$$

where P_{01} is the real part of the pole. τ_{C1} is the estimated time constant of the C1 filter. CF is the characteristic frequency in Hz. Q_{10} is a normalized measure of the filter sharpness. P_w is the imaginary part of the pole. P_b is the relative imaginary parts of the poles. P_a is the relative real parts of the poles. Z_L is the location of the zeros on the real axis. All zeros are placed at the same location in the complex plane for simplicity. The selection of the above functions was motivated by several physiological observations [99].

CHAPTER 4

COMPARISON OF NEW METRICS FOR ASSESSMENT OF RISKS OF OCCUPATIONAL NOISE

The conventional metrics for noise evaluation (*i.e.*, the equivalent sound pressure level, the A-weighting sound pressure level, and the C-weighting sound pressure level) cannot accurately assess the exposure risks to high-level complex noise, which commonly occurs in many industrial and military fields. Recently, two advanced models, an adaptive weighting (F-weighting sound pressure level) and a complex velocity level (CVL) auditory fatigue model, have been developed to evaluate the risks of occupational noise. In this chapter, five noise metrics, including equivalent SPL (L_{eq}), A-weighted SPL (L_{Aeq}), C-weighted SPL (L_{Ceq}), F-weighted sound pressure level (L_{Feq}), and CVL model based SPL (L_{CVL}) will be evaluated and compared using animal experimental data. The animal data includes 22 groups of chinchillas exposed to different types of noise (Gaussian and non-Gaussian). Linear regression analysis is applied to evaluate the correlations between the five noise metrics and the chinchillas' NIHL data. The results show that the F-weighting and the CVL model have high correlations with animal hearing loss data compared with the conventional noise metrics (*i.e.*, L_{eq}, L_{Aeq} and L_{Ceq}). These findings indicate that both developed models may provide accurate assessment of risks of high-level occupational noise in military and industrial applications. The results also suggest that the CVL model is more accurate than the F-weighting sound pressure level on assessment of occupational noise.

4.1 Introduction

Various international standards have been developed to estimate NIHL, for example, CHABA [103], NOISH98 [104], MIL STD-1472F [105]. These standards were designed based on either auditory weighting function (e.g., A-weighting) or based on waveform empirical strategies (e.g., peak pressure and pulse duration) [106, 107]. In current guidelines, the noise metrics are developed depending on the equal energy hypothesis (EEH), which states that NIHL mainly depends on the total acoustic energy of the exposure and it is independent on the temporal characteristics of that noise [36, 108].

The primary metric used to assess the exposure levels of the noise is the A-weighted equivalent sound pressure level, L_{Aeq}. However, previous studies on NIHL indicated that L_{Aeq} is applicable for continuous noise (*i.e.*, Gaussian noise) but not for impact, impulsive or complex noises [36, 40, 108-110]. A number of animal studies showed that complex noises can cause more hearing loss than continuous noise with the same energy level [20, 111-114]. Other studies also showed that the A-weighting filter is more appropriate to assess the low SPL, while the C-weighting filter is suitable for the high SPL [115]. In addition, some researchers claimed that the EEH based metrics cannot provide a physical insight about NIHL, because they do not reflect the physical properties of the ear [45].

To accurately evaluate high-level complex noise, new noise models have been developed for assessment of the NIHL, including an adaptive weighting filter (F-weighting) [41] and the complex velocity level (CVL) auditory fatigue model [43, 52]. In this chapter, the performance of the F-weighting metric and the CVL model will be further evaluated using experimental noise exposure data on chinchilla, and compared with the conventional noise metrics (*i.e.*, L_{eq}, L_{Aeq}, and L_{Ceq}.).

4.2 A-weighting and C-weighting

A-weighting is used to evaluate relatively quiet sounds and C-weighting is used for detection of the peak SPLs [41, 115]. Both A-weighting and C-weighting were developed to mimic the frequency responses of the human auditory system [116]. A-weighting was designed to be the best predictor for the ear's sensitivity to tones at low SPLs, while C-weighting was designed to follow the frequency sensitivity of the human ear at high SPLs. Therefore, the C-weighting function has a better estimation of the auditory system's response to high level sounds than the A-weighting (in terms of the magnitude perspective) [25].

A-weighting function, *AW(f)*, and C-weighting function, *CW(f)*, can be expressed by the following magnitude function [117]

$$AW(f) = K_A \frac{\left(\frac{f}{f_1}\right)^2}{1+\left(\frac{f}{f_1}\right)^2} \frac{\left(\frac{f}{f_2}\right)}{\sqrt{1+\left(\frac{f}{f_2}\right)^2}} \frac{\left(\frac{f}{f_3}\right)}{\sqrt{1+\left(\frac{f}{f_3}\right)^2}} \frac{1}{1+\left(\frac{f}{f_4}\right)^2} \tag{4.1}$$

$$CW(f) = K_C \frac{\left(\frac{f}{f_1}\right)^2}{1+\left(\frac{f}{f_1}\right)^2} \frac{1}{1+\left(\frac{f}{f_4}\right)^2} \tag{4.2}$$

where K_A, K_C, f_1, f_2, f_3, and f_4 are constants given by approximate values: K_A = 1.258905, K_C = 1.007152, f_1= 20.60 Hz, f_2= 107.7 Hz, f_3 = 737.9 Hz, f_4 = 12194 Hz. The A-weighting and C-weighting are defined to have a unity gain at 1 kHz.

The A-weighted filter shows reduction at low frequencies (less than 400 Hz), while the C-weighted filter is quite flat and has a very broad bandwidth [see Figure 3.2] [117]. Due to their abbreviated form, both A-weighted and C-weighted noise metrics have limitations on accurate assessment of a complex noise. Therefore, it is necessary and meaningful to develop

new noise metrics, which can be used for more accurate assessment of the auditory risk for high-level complex noise [118, 119].

4.3 Adaptive weighting (F-weighting)

Sun *et al.* [41] developed an adaptive weighting metric which is based on the idea of blending the two conventional weighting functions (*i.e.*, A-weighting and C-weighting). F-weighting can achieve a universal criterion for better evaluation of different types of complex noises. The F-weighting is defined below [41]

$$P_{feq}(t) = \alpha_{A,T}\left(AW(t) * P(t)\right) + \alpha_{C,T}\left(CW(t) * P(t)\right) \tag{4.3}$$

where $AW(t)$ and $CW(t)$ refer to A-weighed and C-weighted filters, respectively, '*' represents the convolution calculation. The parameters $\alpha_{A,T}$ and $\alpha_{C,T}$ are given by [41]

$$\alpha_{A,T} = \exp(\beta K_T O_T)\frac{1}{|ln(O_T)|+1} \tag{4.4}$$

$$\alpha_{C,T} = \exp(\beta K_T O_T)\frac{|ln(O_T)|}{|ln(O_T)|+1} \tag{4.5}$$

where K_T is the kurtosis and O_T is the oscillation coefficient. β is a positive constant used to let the amplification component ($exp(\beta K_T O_T)$) equal to one approximately in the case of the Gaussian noise.

The kurtosis can be defined as the standardized fourth population moment about the mean of the data [120]

$$K_T = \frac{E[(x-\mu)^4]}{(E[(x-\mu)^2])^2} = \frac{\mu_4}{\sigma^4} \tag{4.6}$$

where E represents the expectation operator, μ represents the mean of x, μ_4 represents the fourth moment about the mean, and σ represents the standard deviation. A large kurtosis value implies

more impulsive components in the noise [34, 35]. The kurtosis of the Gaussian noise is approximately equal to 3. The kurtosis statistic is used to measure the departure from normality (*i.e.*, deviation from the Gaussian) [121].

The other parameter, oscillation coefficient O_T, can be defined as [41]

$$O_T = \frac{\sum_{n=2}^{N-1} |(x_n - x_{n-1})(x_n - x_{n+1})|}{\sum_{n=2}^{N-1} x_n^2} \tag{4.7}$$

The oscillation coefficient is used to calculate the energy density distribution of the complex noise. O_T is relevant to the local transition level and the frequency of the noise signal. The product of the differential values in the O_T formula reflects the local transitions' strength of the noise signal. This parameter is derived from the concept of the Teager energy operator [122]. The oscillation coefficient has been commonly used to obtain the energy density distribution of a signal.

4.4 Auditory fatigue model

Sun *et al.* [51] developed an auditory fatigue model to predict gradually developing hearing loss. The fatigue model combines an auditory filter, which can obtain the velocities distributions on the Basilar Membrane (BM) in cochlea, and a fatigue theory which is based on the Miner rule to calculate hearing loss associated with BM velocity.

4.4.1 Outer ear and middle ear transfer function

The main function of the outer ear and the middle ear is to gather the sound energy into the inner ear. The primary path for conducting the sound from the environment to the cochlea is through the coupled motion of tympanic membrane (TM), ossicles, and stapes footplate. Figure 4.1 shows the transfer function for the outer ear and the middle ear of a chinchilla [51, 123, 124]. The transfer function of an outer ear has a higher gain in mid-range frequencies (1000 – 8000

Hz). The transfer function of a middle ear is characterized by stapes velocity transfer function (SVTF), which is defined as the ratio between the linear velocity of the stapes and the sound pressure near TM in the ear canal.

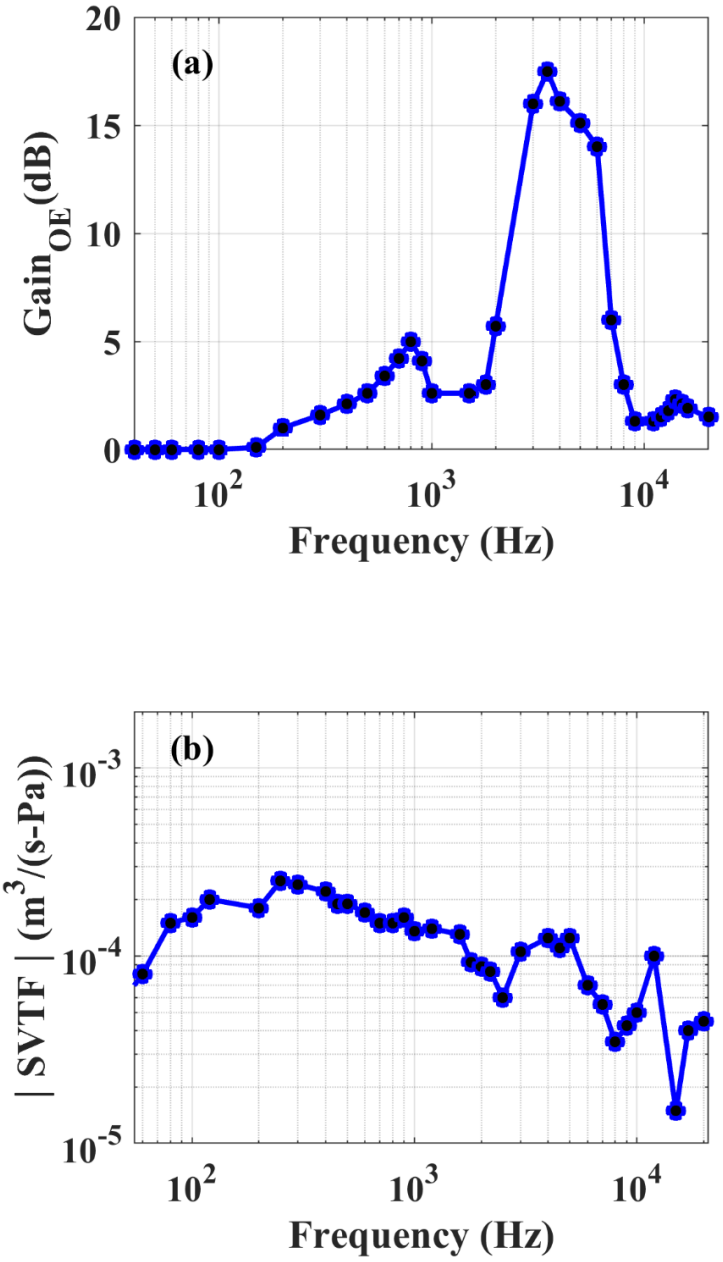

Figure 4.1. The transfer function of chinchilla (a) the outer ear [123], and (b) the middle ear [124].

4.4.2 Inner ear

The cochlea in an inner ear can be considered as a two-chambered, fluid-filled box with rigid side walls [42]. The motion of the stapes produces pressure within the cochlea vestibule. The stimulus sound can be transferred as vibrations on the BM [125]. The triple-path nonlinear (TRNL) filter [88] was applied to obtain the BM responses along the cochlea partitions. The detailed description of the TRNL filter is mentioned in section 3.4.4.2. Moreover, the model parameters of the TRNL filter are summarized in Table 4.1.

Table 4.1. TRNL filter parameters used to simulate the chinchilla inner ear [51, 55, 88].

	0.8 kHz	**5.5 kHz**	**7.25 kHz**	**9.75 kHz**	**10 kHz**	**12 kHz**	**14 kHz**
Linear							
GT cascade	5	5	5	5	5	5	5
LP cascade	7	7	7	7	7	7	7
CF_{lin}	750	5000	7400	9000	9000	11000	13000
BW_{lin}	450	3000	2500	3000	3500	5000	4000
LP_{lin}	750	6000	7400	9000	8800	12000	13500
Gain, g	500	190	3000	300	500	500	350
Nonlinear							
GT cascade	3	3	3	3	3	3	3
LP cascade	4	4	4	4	4	4	4
CF_{lin}	730	5850	7800	9800	10000	12000	15000
BW_{lin}	350	1800	2275	1650	1800	2000	3200
LP_{nl}	730	5850	7800	9800	10000	12000	15000
Gain, a	850	3000	15000	9000	15000	22500	3000
Gain, b	0.03	0.04	0.06	0.05	0.06	0.07	0.045
Exponent, c	0.25	0.25	0.25	0.25	0.25	0.25	0.25
Linear all-pass							
Gain, K	10	0.4	20	1	2	20	20

4.4.3 Complex velocity level (CVL) fatigue model

Sun *et al.* [51] proposed a complex velocity level (CVL) fatigue model based on the Miner's rule to calculate the noise induced cumulative hazard. The Miner's rule has been used to predict the materials' high-cycle fatigue life. The CVL model takes into account the amplitude transition and the mean value of the BM velocities that is correlated with hearing loss.

In real life, the occupational noise is considered a complex load. The BM velocities can be demonstrated as a complex distribution. The hearing loss $H_{i,CVL}$ of the complex input loads (*i.e.*, the velocities of BM) is the integration of different types of the inputs along the time axis and can be described as [52]

$$H_{i,CVL} = \sum_{j \subset k} N_j . |V_{amplitude}(i,j) . V_{mean}(i,j)| \tag{4.8}$$

where k is the load categories total number with jth velocity type. i is the ERB band. V is the BM velocities and N is the corresponding failure cycle.

The hearing loss based on the CVL model at the ERB band i can be obtained as [51]

$$L_{i,CVL} = 10 \log_{10} \frac{\sum {H^2}_{i,CVL}}{{H^2}_o} \tag{4.9}$$

where $L_{i,CVL}$ is the hearing loss metric log scale at the ith ERB.

4.5 Experimental data

Chinchilla noise exposure data is used to evaluate the performance of the five noise metrics in this chapter. The five metrics are: L_{eq}, L_{Aeq}, L_{Ceq}, F-weighted SPL (L_{Feq}), and the CVL model based SPL (L_{CVL}). The chinchilla noise exposure data provided by collaborators at the State University of New York at Plattsburgh contains 263 chinchillas divided into 22 groups [20, 34, 39], each of the 22 animal groups containing 9–16 chinchillas. Animals were exposed for

five successive days to a certain noise for 24 hours per day. The 22 noise samples include 3 Gaussian noises at (90, 95, and 100 dBA), and 19 complex noises (one sample at 95 dBA, two samples at 90 dBA, and 16 samples at 100 dBA). The hearing threshold level (HTL) was measured at 0.5, 1, 2, 4, 8, and 16 kHz for each animal from the auditory evoked potential (AEP) before the exposure, daily, and 30 days after noise exposure. Permanent threshold shift (PTS) is defined as the permanent hearing loss measured 30 days after the noise exposure, and temporary threshold shift (TTS) refers to temporary hearing loss measured immediately after the noise exposure. Both PTS and TTS at 0.5, 1, 2, 4, 8, and 16 kHz octave bands were calculated based on the AEP data. The noise data was digitally recorded for 5-min with a sampling frequency at 48 kHz. The noise data and the experimental protocols with detailed descriptions are available in several previous publications [20, 34, 39, 126]. Table 4.2 summarized the PTS and the TTS values of each animal group for each octave band at the center frequency 0.5, 1, 2, 4, 8, and 16 kHz.

To assess the hearing loss, the National Institute for Occupational Safety and Health (NIOSH) guidelines defines the unacceptable occupational hearing loss as having 25-dB or higher hearing threshold level (HTL) averaged at 1, 2, 3, and 4 kHz [104]. However, the PTS values of chinchillas were measured at 0.5, 1, 2, 4, 8, and 16 kHz (missing the 3 kHz band). So that, in this study the hearing threshold shift at 0.5, 1, 2, and 4 kHz will be used instead of 1, 2, 3, and 4 kHz as an approximation. The formula for the PTS_{5124} can be define as follows [40]

$$PTS_{5124} = (PTS_{0.5} + PTS_1 + PTS_2 + PTS_4)/4 \tag{4.10}$$

where $PTS_{0.5}$, PTS_1 , PTS_2, and PTS_4 are the PTS average measured at 0.5, 1, 2, and 4 kHz from chinchillas in each group. Moreover, the formula for the TTS_{5124} can be define as follows

$$TTS_{5124} = (TTS_{0.5} + TTS_1 + TTS_2 + TTS_4)/4 \tag{4.11}$$

where $TTS_{0.5}, TTS_1, TTS_2,$ and TTS_4 are the TTS average measured at 0.5, 1, 2, and 4 kHz from chinchillas in each group. Table 4.2 summarizes the PTS_{5142} and the TTS_{5124} values of each animal group.

Table 4.2. PTS and TTS values of chinchillas of each group measure at six octave bands with center frequency at 0.5,1, 2, 4, 8, and 16 kHz. PTS_{5124} is the average of the PTS measured at 0.5, 1, 2, and 4 kHz from chinchillas in each group. TTS_{5124} is the average of the TTS measured at 0.5, 1, 2, and 4 kHz from chinchillas in each group.

Animal group index	PTS(dB)						$PTS_{5124(dB)}$	TTS(dB)						$TTS_{5124(dB)}$
	0.5 kHz	1 kHz	2 kHz	4 kHz	8 kHz	16 kHz		0.5 kHz	1 kHz	2 kHz	4 kHz	8 kHz	16 kHz	
G-44	17.1	26.2	39.4	42.9	46.5	43.7	31.4	58.6	70.1	79.3	85.4	85.8	70.6	73.4
G-49	22.1	34.3	47.2	54.6	46.8	47.2	39.6	62.6	75.3	77.6	86.5	79.9	70.6	75.5
G-50	7.7	10.1	8.0	15.8	14.1	17.7	10.4	37.2	57.6	63.4	76.1	79.8	69.2	58.6
G-51	15.7	19.5	29.0	24.3	27.8	25.1	22.1	59.7	63.9	73.2	75.9	81.9	67.9	68.2
G-52	18.5	24.5	36.8	32.9	28.3	23.3	28.2	63.9	72.4	76.4	81.2	80.1	69.6	73.5
G-53	19.0	24.4	34.5	31.7	29.9	28.1	27.4	59.4	68.0	77.4	85.0	84.3	69.0	72.4
G-54	16.2	18.5	29.9	31.4	25.4	29.1	24.0	55.7	65.3	75.6	82.5	80.0	66.3	69.8
G-55	18.8	21.7	36.5	46.8	60.1	47.5	30.9	67.1	74.1	76.2	82.3	80.3	68.8	74.9
G-60	20.7	27.8	34.1	34.1	29.3	27.8	29.2	59.3	68.4	70.8	75.7	75.9	65.2	68.5
G-61	2.6	5.0	10.0	20.5	18.2	24.0	9.5	36.1	45.6	50.4	74.4	80.4	72.0	51.6
G-63	25.4	31.4	43.8	36.2	32.3	28.9	34.2	63.4	69.8	76.2	76.4	73.4	65.0	71.5
G-64	15.8	17.4	24.7	22.1	19.0	13.5	20.0	60.0	66.3	73.8	79.4	73.9	67.1	69.9
G-65	17.2	14.4	25.0	39.6	49.5	48.3	24.1	62.5	62.8	68.1	74.4	75.8	70.7	67.0
G-66	7.5	9.3	19.2	32.9	44.8	36.2	17.2	49.4	58.9	70.0	82.9	76.1	70.4	65.3
G-68	12.9	13.9	21.7	39.7	47.3	47.3	22.1	65.9	69.2	71.1	81.1	75.0	73.3	71.8
G-69	4.8	10.9	9.3	11.3	5.5	8.0	9.1	28.8	47.4	48.8	49.3	47.8	50.1	43.6
G-70	12.1	17.9	27.6	43.2	30.4	35.1	25.2	59.9	69.9	75.0	84.8	76.8	71.0	72.4
G-47	0.3	-0.3	3.3	1.9	7.5	6.7	1.3	22.4	34.3	41.6	60.9	68.7	60.7	39.8
G-48	3.0	6.8	9.4	5.4	11.2	10.8	6.2	26.9	35.9	37.6	41.5	58.0	63.9	35.5
G-56	2.9	1.7	4.5	8.9	14.7	8.9	4.5	29.5	30.5	29.2	39.3	52.0	50.9	32.1
G-57	6.8	5.8	6.7	16.7	23.3	18.9	9.0	35.5	41.4	52.1	66.4	71.8	66.0	48.8
G-58	7.8	8.8	18.9	17.5	15.0	17.9	13.2	44.5	50.3	59.1	62.1	62.1	63.6	54.0

4.6 Results and discussion

The linear regression analysis of the five noise metrics (*i.e.*, L_{eq}, L_{Aeq}, L_{Ceq}, L_{Feq}, and L_{CVL}), and the hearing loss indicators (*i.e.*, PTS and TTS) were conducted using all 22 groups of animal experimental data. The coefficient of determination (r^2) is used to evaluate the performance of each metric. The r^2 value indicates the correlation between the metrics and the hearing loss indicators. When the value of the r^2=1, it indicates a perfect correlation and when r^2=0 it means there is no correlation between noise metrics and hearing loss data. The purpose of the correlation analysis is to measure and to interpret the strength of the linear relationship between the two continuous variables [127]. In this study, it will be between the noise metric and the hearing loss indictor. The linear regression equation is expressed as

$$HLI = K_0 + K_1 L_m + \epsilon \tag{4.12}$$

where HLI is the hearing loss indictor represented by PTS or TTS. L_m refers to one of the noise metrics (*i.e.*, L_{eq}, L_{Aeq}, L_{Ceq}, L_{Feq}, or L_{CVL}). ϵ is the error to be minimized. k_0, and k_1 are constants determined by the best fitting regression line.

Table 4.3 summarizes the r^2 values between the hearing loss indicators (*i.e.*, PTS and TTS), and the five noise metrics (*i.e.*, L_{eq}, L_{Aeq}, L_{Ceq}, L_{Feq}, and L_{CVL}) at six octave bands centered at 0.5, 1, 2, 4, 8, and 16 kHz. The results show that L_{CVL} achieves the best correlation with the PTS at 0.5, 2, 4, 8, and 16 kHz. The L_{Aeq} has the best correlation with the PTS at 1 kHz. For the TTS, L_{CVL} has the best correlation at 0.5, 2, 8, and 16 kHz. L_{Aeq} has the best correlation with the TTS at 1 kHz. At 4 kHz, L_{eq}, L_{Aeq}, and L_{Ceq} achieve the best correlation with the TTS. Overall, the CVL model has a higher correlation with the hearing loss indicator compared to the other metrics. The higher correlation between the hearing loss and the CVL model indicates that it can be used to predict NIHL accurately.

Table 4.3. Comparison of the regression analysis results of the two hearing loss indicators (*i.e.*, PTS and TTS) and the five metrics (*i.e.*, L_{eq}, L_{Aeq}, L_{Ceq}, L_{Feq}, and L_{CVL}) at six octave bands centered at 0.5, 1, 2, 4, 8, and 16 kHz.

	r^2											
	PTS						***TTS***					
Metric	**0.5 kHz**	**1 kHz**	**2 kHz**	**4 kHz**	**8 kHz**	**16 kHz**	**0.5 kHz**	**1 kHz**	**2 kHz**	**4 kHz**	**8 kHz**	**16 kHz**
L_{eq}	0.13	0.59	0.21	0.65	0.30	0.13	0.33	0.67	0.37	**0.80**	0.51	0.53
L_{Aeq}	0.16	**0.61**	0.21	0.65	0.33	0.17	0.37	**0.69**	0.37	**0.80**	0.48	0.55
L_{Ceq}	0.13	0.59	0.21	0.65	0.33	0.17	0.33	0.67	0.37	**0.80**	0.48	0.55
L_{Feq}	0.20	0.58	0.24	0.62	0.33	0.18	0.44	0.66	0.41	0.72	0.47	0.53
L_{CVL}	**0.24**	0.40	**0.62**	**0.70**	**0.52**	**0.54**	**0.56**	0.64	**0.75**	0.77	**0.60**	**0.56**

Furthermore, Figure 4.2 shows the linear fitting lines between the five metrics (*i.e.*, L_{eq}, L_{Aeq}, L_{Ceq}, L_{Feq}, and L_{CVL}) and the hearing loss indicators (*i.e.*, PTS and TTS) at 0.5, 1, 2, 4, 8, and 16 kHz octave bands. The lines in the figure represent the fitting results of the distributions of the symbols. All the five metrics are positive proportional to the PTS and TTS. It indicates that all the metrics can be used to effectively evaluate hearing loss. In addition, the slopes of these fitting lines are close, which means that the new metrics (*i.e.*, L_{Feq}, and L_{CVL}) are comparable to the other three conventional metrics (*i.e.*, L_{eq}, L_{Aeq}, and L_{Ceq}) on the evaluation of hearing loss.

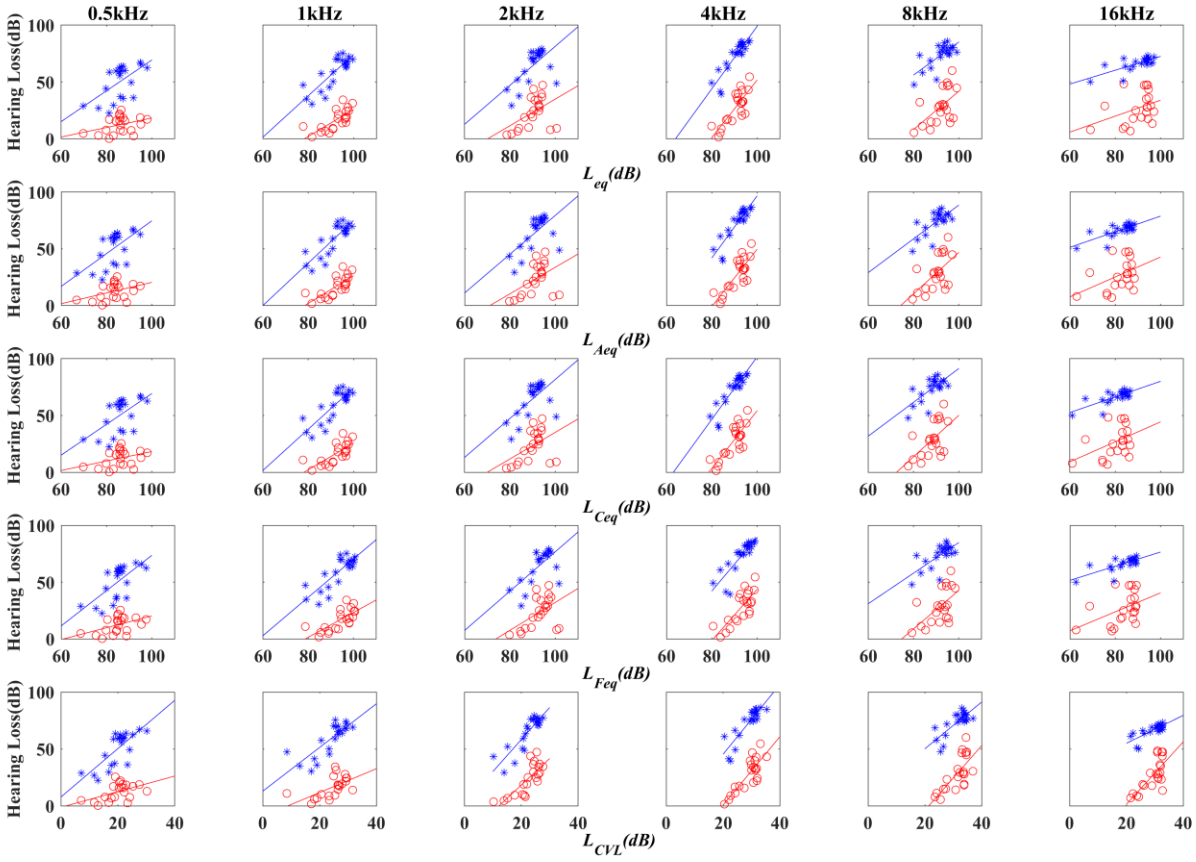

Figure 4.2. Scatting plots and fitting lines between the five noise metrics (*i.e.*, L_{eq}, L_{Aeq}, L_{Ceq}, L_{Feq}, and L_{CVL}) and the hearing loss indicators (*i.e.*, PTS and TTS) at six octave bands with center frequency at 0.5, 1, 2, 4, 8, and 16 kHz. The red color represents the PTS and the blue color represents the TTS.

Moreover, the linear regression analysis of five noise metrics (*i.e.*, L_{eq}, L_{Aeq}, L_{Ceq}, L_{Feq}, and L_{CVL}) and NIHL indicators (*i.e.*, TTS_{5124} and PTS_{5124}) are conducted. The correlations between the five noise metrics and the NIHL indicators are summarized in Table 4.4. The results show that the CVL fatigue model achieves the highest r^2 values for both PTS_{5124} (r^2=0.61) and TTS_{5124} (r^2=0.84) among all of the five noise metrics. It indicates that the CVL model is more accurate than the other four metrics for the assessment of NIHL. Furthermore, L_{Feq} also has higher correlations with PTS_{5124} than the other three conventional noise metrics (*i.e.*, L_{eq}, L_{Aeq}, and L_{Ceq}). For TTS_{5124}, L_{Feq} achieves same r^2 as L_{Ceq}, and both are higher than L_{eq} and L_{Aeq}.

Therefore, the F-weighting metric can be more accurate for assessment of NIHL compared with the L_{eq}, L_{Aeq}, and L_{Ceq}.

Table 4.4. Regression analysis results of the five noise metrics (*i.e.*, L_{eq}, L_{Aeq}, L_{Ceq}, L_{Feq}, and L_{CVL}) and the NIHL indicators (*i.e.*, PTS_{5124} and TTS_{5124}).

	r^2	
Metric	PTS_{5124}	TTS_{5124}
L_{eq}	0.44	0.69
L_{Aeq}	0.50	0.68
L_{Ceq}	0.50	0.71
L_{Feq}	0.55	0.71
L_{CVL}	**0.61**	**0.84**

Additionally, Figure 4.3 shows scatting plots and fitting lines of the linear regression analysis between the five noise metrics and the NIHL indicators. The fitting lines show a positive proportion between the five noise metrics and NIHL indictors (PTS_{5124} and TTS_{5124}). The positive relationship indicates that these metrics can be used to evaluate hearing loss effectively. The results are consistent with Table 4.4.

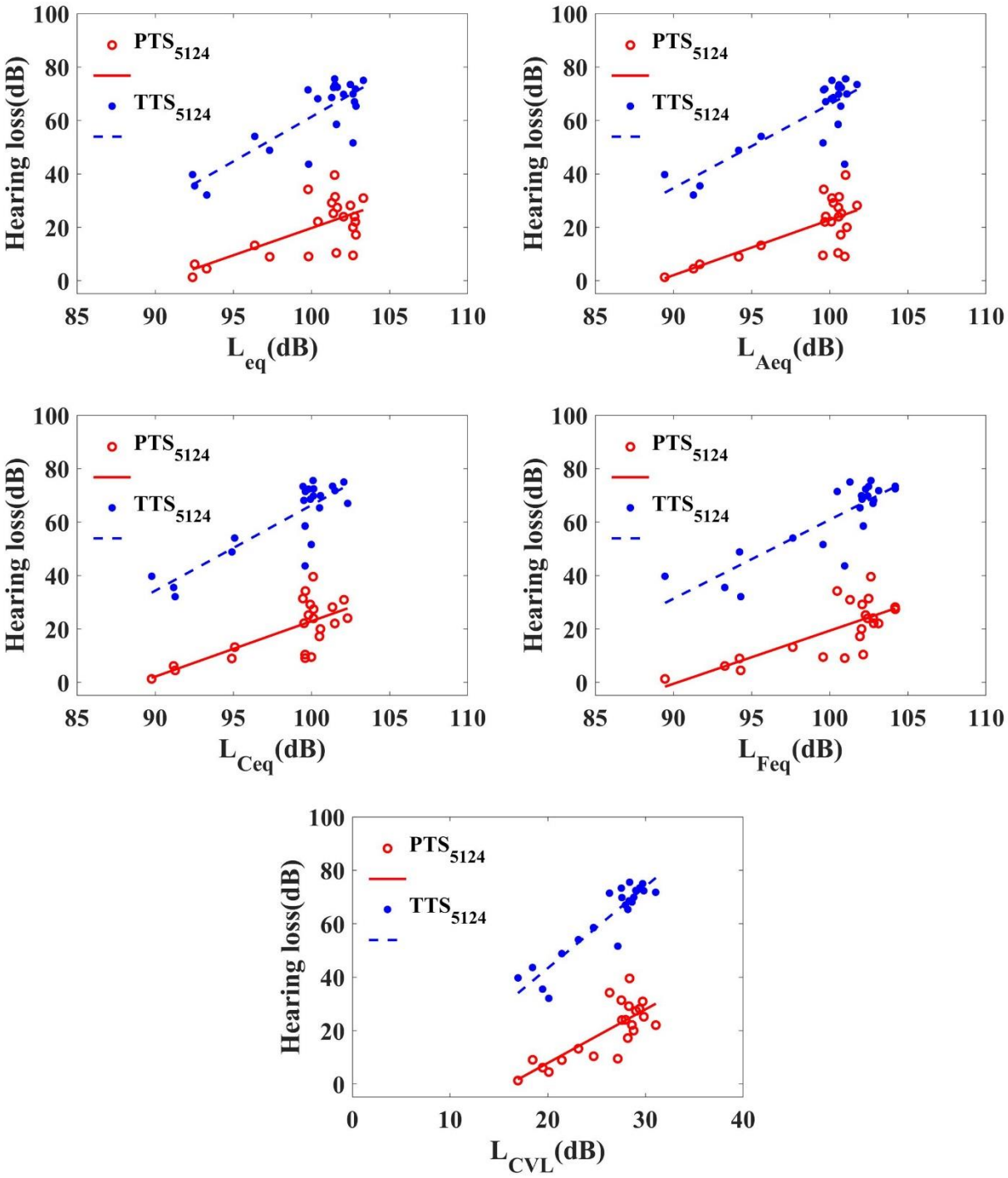

Figure 4.3. Scatting plots and fitting lines of the five noise metrics (*i.e.*, L_{eq}, L_{Aeq}, L_{Ceq}, L_{Feq}, and L_{CVL}) and the NIHL indicators (PTS_{5124} and TTS_{5124}). The red color represents PTS_{5124} and the blue color represents TTS_{5124}.

4.7 Conclusion

In this chapter, the performances of two newly developed noise models (*i.e.*, F-weighting and CVL fatigue model) were compared with conventional noise metrics (*i.e.*, L_{eq}, L_{Aeq}, and L_{Ceq}) using animal noise exposure data. Linear regression analysis was used to evaluate the correlations between the five noise metrics (L_{eq}, L_{Aeq}, L_{Ceq}, L_{Feq}, and L_{CVL}) and hearing loss indicators (PTS and TTS centered at 0.5, 1, 2, 4, 8, and 16 kHz octave bands). Moreover, to evaluate effective hearing loss, the linear regression analysis was conducted between five noise metrics and the NIHL indictors (PTS_{5124} and TTS_{5124}). The results show that the CVL fatigue model demonstrates the highest correlations with the hearing loss indicators and NIHL indictors among five noise metrics. The F-weighting also achieves higher correlations with hearing loss data compared with the three conventional noise metrics (*i.e.*, L_{eq}, L_{Aeq}, and L_{Ceq}). It indicates that both developed metrics (*i.e.*, CVL model and F-weighting) can predict the NIHL better than the conventional EEH-based noise metrics in the current noise measurement standard. The F-weighting and CVL fatigue model can be applied to assess occupational noise-induced hearing loss in various industrial and military applications.

CHAPTER 5

INVESTIGATIONS OF AUDITORY FILTERS BASED EXCITATION PATTERNS FOR ASSESSMENT OF NOISE-INDUCED HEARING LOSS

The excitation pattern (EP) has been considered as one of the techniques to estimate the movements of the basilar membrane in the cochlea. In this chapter, two auditory filters (dual resonance nonlinear filter and rounded-exponential filter) are applied to create two EPs which are the velocity EP and the loudness EP. Two noise hazard metrics are used to evaluate hazardous levels caused by different types of signals. Gaussian noise and a tone are simulated to evaluate performances of the proposed EPs and the noise metrics. The results show that both EPs can demonstrate the response of the BM to the Gaussian noise and the tone. For the Gaussian noise, there is a frequency shift between the velocity EP and the loudness EP. For the tone case, both EPs can demonstrate the frequency of the input signal. The results suggest that both EPs can be potentially used for NIHL assessment.

5.1 Introduction

Intrinsically, NIHL can be partially explained as an auditory fatigue phenomenon, in which the motions of stretching and squeezing of the basilar membrane could damage the hearing cells (*i.e.*, outer and inner hair cells) in the cochlea [43, 51, 52, 90]. The mechanical motions of the BM can be considered as one of the major factors that cause NIHL in the cochlea [128, 129]. The motions of the BM in response to the noise stimulus is a function of frequency which can be defined as an excitation pattern (EP). Therefore, investigating the EP is very useful for the NIHL research [44].

An EP represents the distribution of movements along the BM caused by a sound [54, 130]. In psychoacoustic, the EP is defined as the output of each auditory filter plotted as a

function of the filter's center frequency [84]. The EPs are normally calculated and plotted as the gain of each auditory filter equal to 0 dB at its center frequency. For example, a tone with a 60 dB sound pressure level and at 1 kHz center frequency will cause an excitation level equal to 60 dB and at 1 kHz [54, 75, 131].

The human auditory models (AMs) are the fastest way to estimate the EPs over the BM partitions in the cochlea [87]. Several AMs have been developed based on observations of input-output behavior of the human auditory system with reference to psychological or physiological responses [51]. Such AMs include Gammatone filters, dual-resonance nonlinear (DRNL) filters, rounded-exponential (ROEX) filters, dynamic-compressive gammachirp filters, etc. Hohmann [72] developed a 4^{th}-order linear Gammatone filter based AM for speech processing in hearing aids. This linear model can reconstruct acoustical signals in an auditory system, but it does not include nonlinear features [72]. Lopez-Poveda and Meddis [55, 87] proposed a nonlinear DRNL filter, which successfully simulates the two-tone suppression and the phase responses in the BM. Irino and Patterson [132] developed a gammachirp filterbank with nonlinear and compressive features. The developed gammachirp filter has a group of linear passive gammachirp filters. It can also be used for the applications on speech enhancement, speech coding, and hearing aids [132].

Moreover, the AMs can be categorized as mechanical or perceptual [73]. The mechanical AMs are designed to estimate mechanical vibrations on BM in the cochlea [87]; while the perceptual AMs are developed to mimic the psychoacoustic data [132]. In this chapter, a mechanical AM (*i.e.*, DRNL filter) and a perceptual AM (*i.e.*, ROEX) are used to investigate EPs on the human BM. As a cascade filter model, the DRNL filter was developed to simulate the nonlinear mechanical response of the BM in reaction to stapes motion [55]. The output of DRNL

filters is the velocity of the BM, which can be described as a velocity EP of the BM in the cochlea. Such velocity EP intuitively can be used to assess the auditory fatigue based NIHL [51].

On the other hand, the ROEX filter as a perceptual model can be used to demonstrate loudness in the cochlea. Loudness is one of the most important parameters for evaluation of the acoustical quality in various applications, from hearing aid optimizing to automatic music mixing systems [76]. The loudness estimations directly reflect the characteristics of the human auditory system, such as masking adaption, integration along a perceptual frequency axis, and integration and compression along time axis. In previous studies, loudness contours based models have been developed for evaluations of the annoyance of environment noise, including community noise, industrial noise, and transportation noise [22, 30, 41].

The DRNL filter and the ROEX filter were used to create two EPs, the velocity EP and the loudness EP, respectively. To evaluate the performance of the proposed EPs, Gaussian noise and tone signals with various parameters (e.g., amplitude and frequency) are simulated. In addition, two noise metrics are used based on two proposed EPs to estimate the hazardous levels caused by different types of signals.

5.2 Transfer functions of external ear and middle ear

The DRNL filter and the ROEX filter have the same transfer function of the external ear in this chapter. As shown in Figure 5.1, the transfer function of the external ear is the same as it was described in Moore's work [76] and ANSI-S3-2007 [86]. For the middle ear transfer function, the stapes velocity transfer function (SVTF) which converts the acoustical pressure to stapes velocity is used for the DRNL filter as shown in Figure 5.2a [55]. On the other hand, the transfer function that is used in the procedure of loudness computation of Moore's work [76] is used for the ROEX filter. Figure 5.2b shows the transfer function used for the ROEX filter.

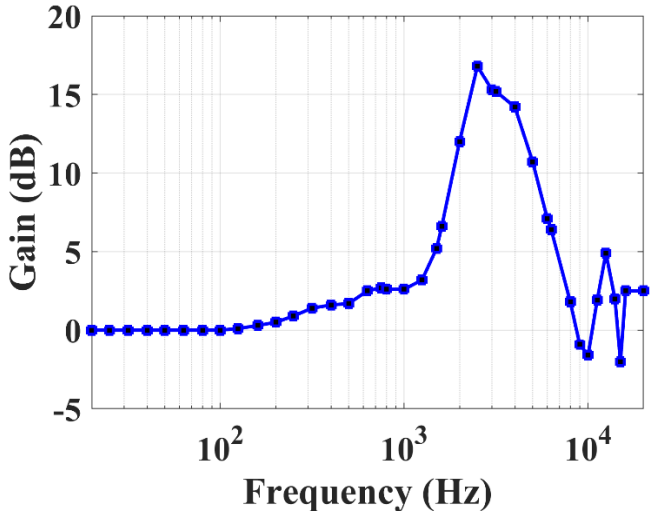

Figure 5.1. The transfer function of an external human ear [76].

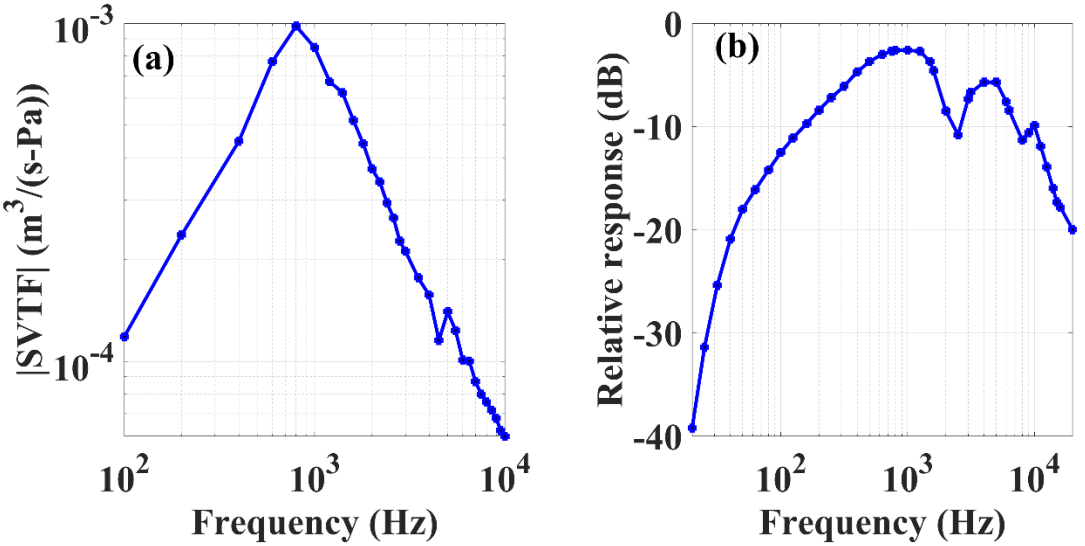

Figure 5.2. The transfer functions of the middle ear of the human, which are applied to (a) the DRNL filter [52], and (b) the ROEX filter [76].

5.3 Dual resonance nonlinear (DRNL) filter

In this chapter, a DRNL filter is utilized to obtain the BM movements in the human cochlea [55]. The detailed descriptions of the DRNL filter is mentioned in section 3.4.4.1 in this dissertation. Moreover, the model parameters of the DRNL filter are summarized in Table 5.1.

Table 5.1. DRNL filter parameters used to simulate the human inner ear [87].

	0.25kHz	0.5kHz	1kHz	2kHz	4kHz	8kHz
Linear						
GT cascade	2	2	2	2	2	2
LP cascade	4	4	4	4	4	4
CF_{lin}	235	460	945	1895	3900	7450
BW_{lin}	115	150	240	390	620	1550
LP_{lin}	235	460	945	1895	3900	7450
Gain, g	1400	800	520	400	270	250
Nonlinear						
GT cascade	3	3	3	3	3	3
LP cascade	3	3	3	3	3	3
CF_{lin}	250	500	1000	2000	4000	8000
BW_{lin}	84	103	175	300	560	1100
LP_{nl}	250	500	1000	2000	4000	8000
Gain, a	2124	4609	4598	9244	30274	76354
Gain, b	0.45	0.28	0.13	0.078	0.06	0.035
Exponent, c	0.25	0.25	0.25	0.25	0.25	0.25

5.4 Rounded-exponential (ROEX) filter

The detailed descriptions of the ROEX filter is mentioned in section 3.4.3 in this dissertation.

5.5 Excitation pattern based noise metrics

Previous studies have demonstrated that the EPs of the BM are highly correlated with the NIHL in the human cochlea [44, 51, 133]. To investigate hearing loss, two EPs based-metrics are proposed to assess the potential hazardous levels (HLs) caused by different types of signals. Since the EP represents the temporal responses of the organ of Corti in the cochlea, one can integrate the local responses and obtain the cumulative HLs. Therefore, two proposed noise metrics, ${HL_i}^D$ and ${HL_i}^R$, can be defined as [44]

$$ {HL_i}^D = 10\log_{10}\sum_{t=1}^{t=n} V(i,t)^2/{V_o}^2 \tag{5.1} $$

$$ {HL_i}^R = 10\log_{10}\sum_{t=1}^{t=n} N(i,t)^2/{N_o}^2 \tag{5.2} $$

where ${HL_i}^D$ represents the hazard level based on the velocity EP, and $V(i,t)$ refers to the BM velocity at the ith frequency of BM at a time t. V_0 represents the BM velocity located at the center frequency equal to 1 kHz. ${HL_i}^R$ represents the hazard level based on the loudness EP, and $N(i,t)$ refers to the loudness level at the ith frequency of BM at a time t. N_0 is the loudness level at center frequency equal to 1 kHz. By Equation (5.1) and Equation (5.2), the developed EPs have been successfully translated to the amount of HLs, which can be potentially used for the assessment of NIHL.

Moreover, total hazard level (THL) can be defined as summation of HLs as shown below

$$ {THL}^D = \sum_i {HL_i}^D \tag{5.3} $$

$$ {THL}^R = \sum_i {HL_i}^R \tag{5.4} $$

where THL^{D} and THL^{R} represent THLs based on the velocity EP and the loudness EP, respectively.

5.6 Simulation of signals

In this chapter, two different types of signals (*i.e.*, Gaussian noise and a tone) have been simulated to evaluate the performance of the two proposed EPs. The Gaussian noise signals are simulated using the "randn" function in MATLAB, in which the probability distribution function of the Gaussian noise is given by [134]

$$P(t) = \frac{1}{\sigma\sqrt{2\pi}} \exp^{-\frac{(t-\mu)^2}{2\sigma^2}} \tag{5.5}$$

where μ is the mean, and σ is the standard deviation. μ is equal to zero in this chapter.

The tone signal in this chapter is given by

$$y(t) = A\cos 2\pi f t \tag{5.6}$$

where A is the amplitude of the signal, and f is the frequency.

5.7 Results and discussion

5.7.1 Time-Frequency (T-F) representations of the two EPs

In this section, the simulated Gaussian noise and a tone are fed into the DRNL filter and the ROEX filter to obtain the proposed velocity EP and loudness EP. Both EPs can be represented in the joint time and frequency (T-F) domain. Figure 5.3a and 5.3b show the T-F representations of the velocity EP and the loudness EP responding to a simulated Gaussian noise at 100 dB SPL. Figure 5.3c and 5.3d show the T-F representations of the velocity EP and the loudness EP responding to a tone with 100 dB SPL and 1 kHz frequency. The results show that both EPs can reflect the amplitudes and transitions of the Gaussian noise and the tone. The velocity EP as a mechanical model can illustrate both positive and negative vibrations of the BM

in the cochlea. The velocity EP reflects more realistic representations of the stretching and squeezing of the hair cells in the cochlea. On the other hand, the loudness EP as a perceptual model can only represent the positive amount of loudness as a response to input stimulus. The loudness EP doesn't directly reflect the BM vibrations in the cochlea.

Moreover, along the time axis, the velocity EP presents a higher temporal resolution than the loudness EP for the Gaussian noise. It indicates that the temporal resolution of the DRNL filter is better than the ROEX filter. Along the frequency axis, for the Gaussian noise, the peak frequency of the velocity EP is around 2 kHz and is lower than the corresponding value of the loudness EP which is around 4 kHz. For a tone, both EPs present the peak frequencies at 1 kHz, which reflects the frequency of the input tone signal. However, the velocity EP shows vibrations around 1 kHz since it reflects the BM motion while the loudness EP shows only one peak since it is a perceptual model that reflects the amount of psychoacoustic data.

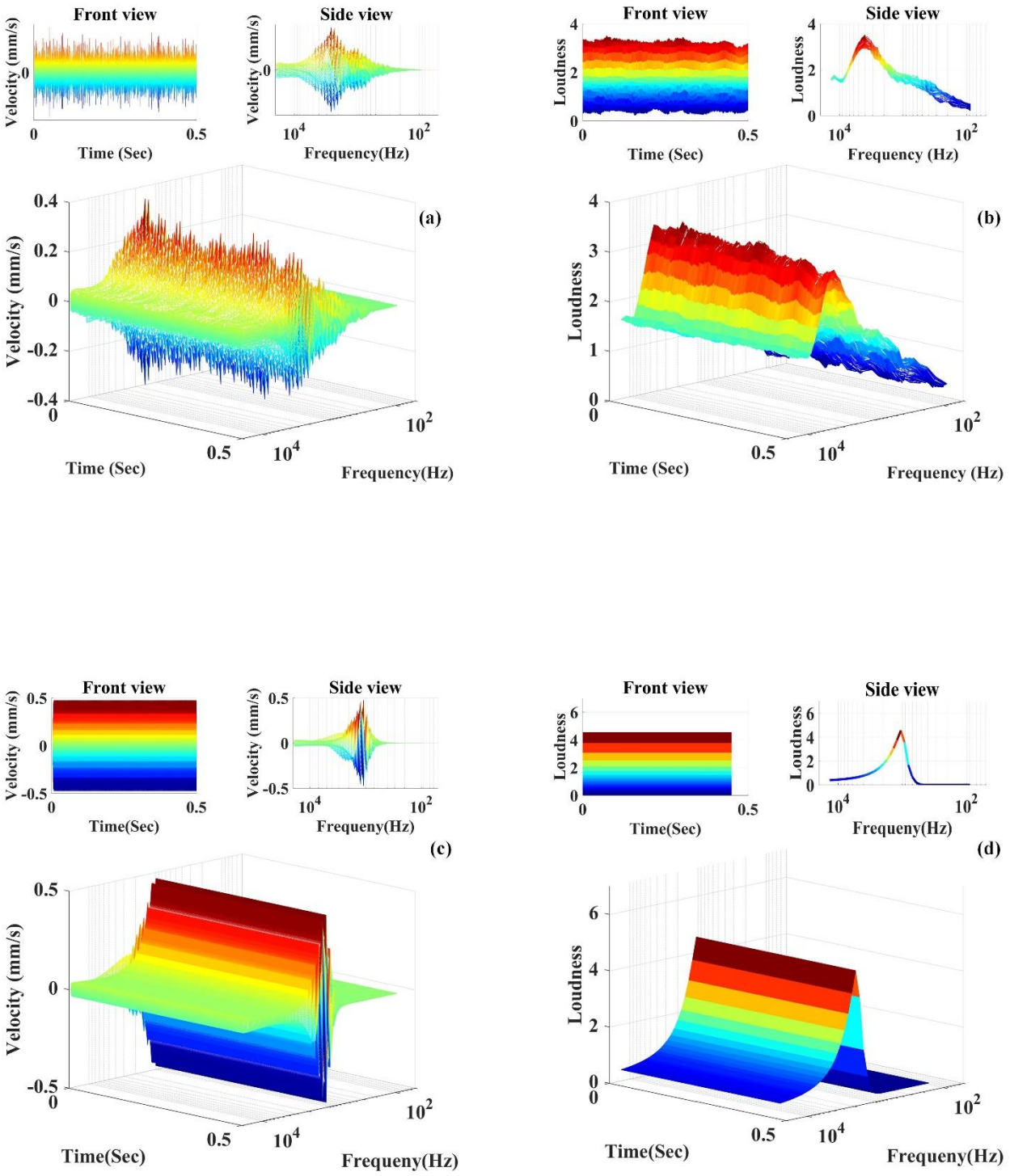

Figure 5.3. The T-F representations of (a) the velocity EP, (b) the loudness EP responding to a Gaussian noise at 100 dB SPL, (c) the velocity EP, and (d) the loudness EP with respect to a tone at 100 dB SPL and 1 kHz.

5.7.2 Time-Frequency (T-F) representations of the two EPs for a tone signal at different frequencies

Figure 5.4 shows the T-F representations of the velocity EP and the loudness EP produced by tone signals with 100 dB SPL at various frequencies equal to 0.5, 1, 2, 4, and 6 kHz. For the velocity EP (as shown in the left side of Figure 5.4), the amplitudes have both positive and negative values which reflects the BM vibrations. Moreover, all the velocity EPs peak at a similar center frequency to the frequency of the input tones. It also can be observed that the peaks of the velocity EPs are decreasing when the frequency is higher than 2 kHz because of the bandpass filtering effects in the middle ear. Furthermore, the loudness EP (as shown in the right side of Figure 5.4) presents only positive amplitudes, and the peaks match the frequencies of the stimulated tones. The peak of the loudness EP increases first and then decreases when the frequency increases, and the maximum peak amplitude appears at 4 kHz.

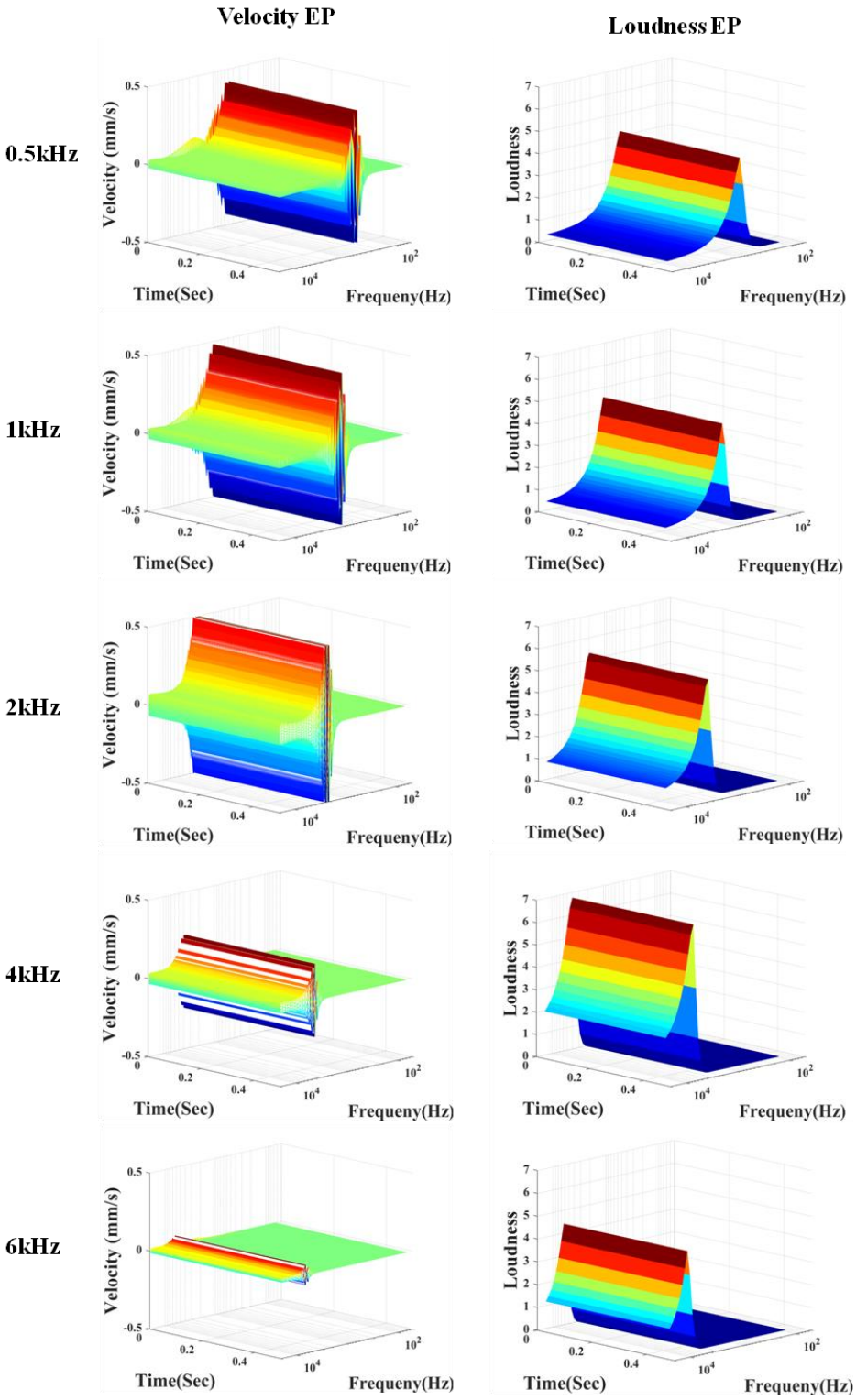

Figure 5.4. The T-F distributions of the two proposed EPs obtained by simulated tone signals at 100 dB SPL with frequencies at 0.5, 1, 2, 4, and 6 kHz, respectively.

5.7.3 Hazardous level evaluation

5.7.3.1 Frequency distributions of the hazardous levels for the Gaussian noise

The performances of the two EPs are evaluated using the two proposed metrics (*i.e.*, $HL_i{}^D$ and $HL_i{}^R$) which are used to depict the hazardous level **(**HL) at the frequency locations on the BM. Figure 5.5 shows the frequency distributions of the normalized HLs generated by the simulated Gaussian noise signals at SPL ranges from 70 to 120 dB with a 10 dB increase. For both velocity EP and loudness EP, the HLs rise when the SPL increases. Overall, the loudness EP shows a broader frequency response compared with the velocity EP. The results also show that there is a frequency shift between the two EPs. The peak HLs of the velocity EP are around 2 kHz while the peak HLs of the loudness EP are around 4 kHz. Since the BM motions are associated with hearing loss in the cochlea, the peak frequency shift between the two EPs indicates that the maximum hearing loss predicted by these two EPs may occur at different partitions of BM.

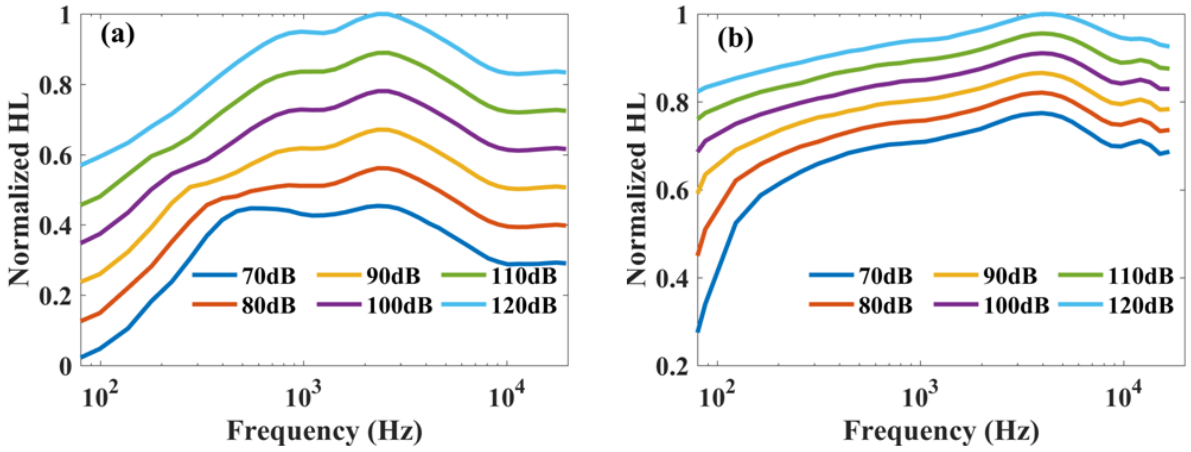

Figure 5.5. The frequency distributions of the normalized HLs based on (a) the velocity EP and (b) the loudness EP generated by simulated Gaussian noise signals at SPL = 70 to 120 dB with 10 dB interval.

5.7.3.2 Frequency distributions of the hazardous levels for the tone signal

Figure 5.6 shows the normalized HLs generated by simulated tones at 1 kHz and SPL ranges from 70 to 120 dB with a 10 dB increase. Both the velocity EP and the loudness EP show the peak frequency at 1 kHz, which is the same as the frequency of the input tone. It can be found that the HLs are rising when SPLs are increasing in both EPs. As shown in Figure 5.6a, the HLs of the velocity EP gradually increase when the frequency is smaller than 1 kHz and then gradually decrease after the frequency is greater than 1 kHz. Comparatively, as shown in Figure 5.6b, the HLs of the loudness EP show a different frequency behavior than the velocity EP. The HLs of the loudness EP almost equal to zero when the frequency is smaller than 500 Hz and then rapidly increase to peak at 1 kHz. Finally, the HLs of the loudness EP start gradually decreasing after 1 kHz. This is because the loudness EP is based on the ROEX filter, which is derived from psychophysical data. Therefore, the loudness EP may not reflect the real motion of the BM in the cochlea.

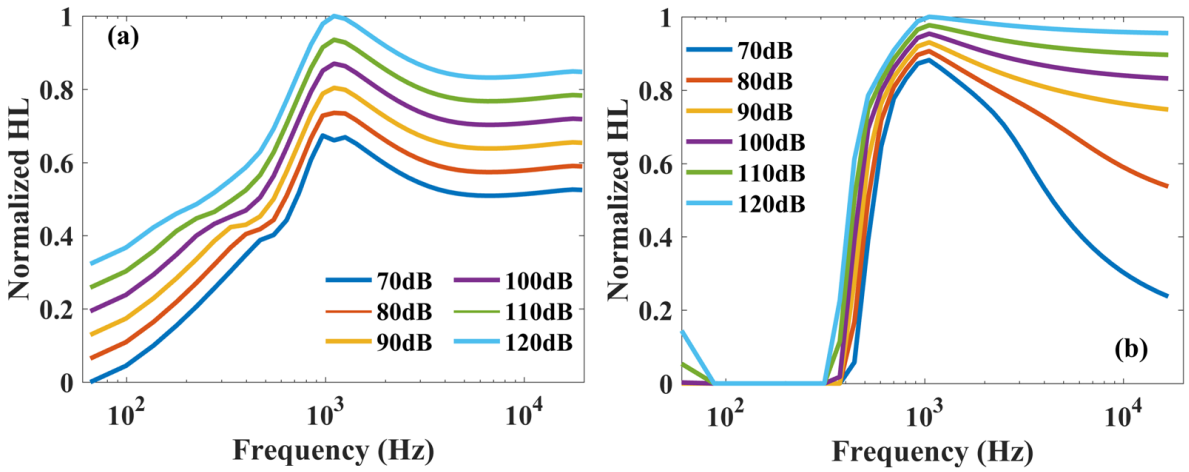

Figure 5.6. The frequency distributions of the normalized hazardous levels based on (a) the velocity EP and (b) the loudness EP, obtained at 1 kHz tone and SPL = 70 to 120 dB with 10 dB interval.

Figure 5.7 shows the normalized HLs generated by the simulated tones at different frequencies (0.5, 1, 2, 4, and 6 kHz) with SPL equal to 100 dB. Both velocity EP and loudness EP can reflect the corresponding frequencies of the input tone signals. The peak of the HL for the velocity EP (as shown in Figure 5.7a) starts decreasing when the frequency gets greater than 2 kHz, while the peak of the HL for the loudness EP slightly decreases when the frequency is higher than 4 kHz (as shown in Figure 5.7b). In the velocity EP, the highest peak occurs around 2 kHz, while in the loudness EP the highest peak appears around 4 kHz.

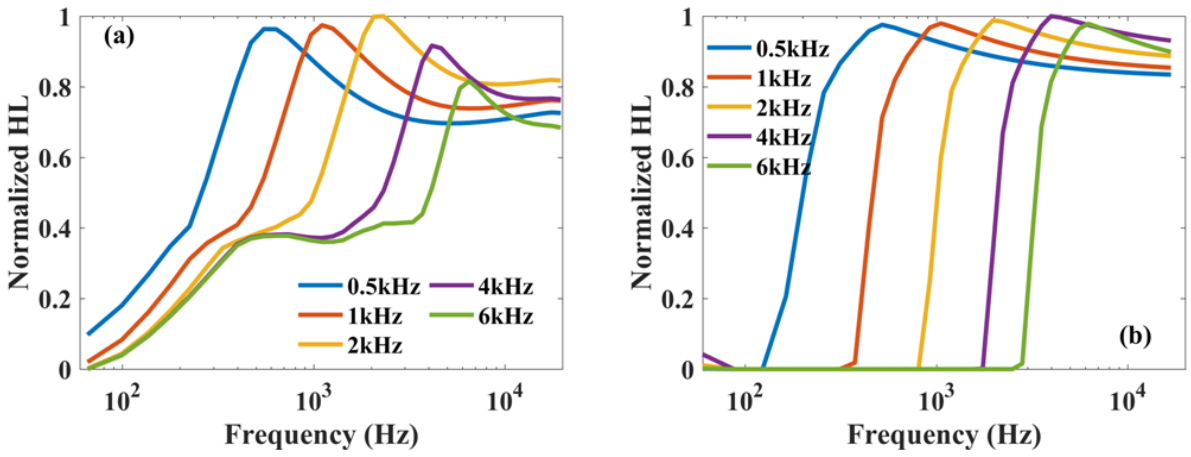

Figure 5.7. The frequency distributions of the normalized hazardous levels based on (a) the velocity EP and (b) the loudness EP, obtained at various frequencies (0.5, 1, 2, 4, and 6 kHz) with fixed SPL = 100 dB.

5.7.4 Total hazardous levels evaluation

The total hazardous levels (*i.e.*, THL^{D} and THL^{R}) can be calculated based on the velocity EP and the loudness EP. THLs can be used to assess the hazard level of high noise exposure and potentially can be used to investigate NIHL.

5.7.4.1 Total hazardous levels for the Gaussian noise

Figure 5.8 shows the normalized THLs for the Gaussian noise at SPLs from 70 to 120 dB. The result shows that THLs of both EPs are increasing when SPL increases. The velocity EP surges higher than the loudness EP. Also, under 100 dB SPL the loudness EP is higher than the velocity EP. However, above 100 dB SPL the velocity EP surpasses the loudness EP.

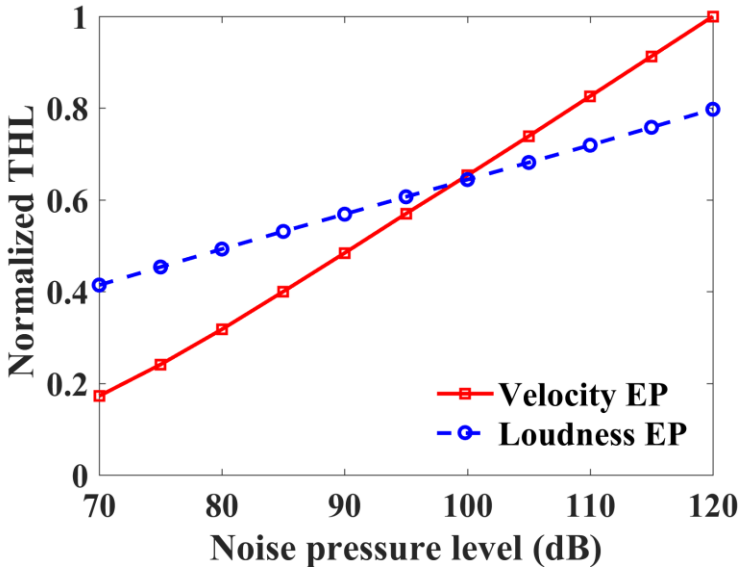

Figure 5.8. The normalized THLs for the Gaussian noise at SPL from 70 to 120 dB for the velocity EP and the loudness EP.

5.7.4.2 Total hazardous levels for the tone signal

Figure 5.9a shows the normalized THLs of both EPs produced by the simulated tones when increasing SPL from 70 to 120 dB with a fixed frequency at 1 kHz. The THLs of both EPs are rising when SPL is increasing. Specifically, the velocity EP increases faster than the loudness EP. The result indicates that the velocity EP is more sensitive to SPL increases than the loudness EP. It also can be found that the THLs of the velocity EP are constantly higher than the corresponding values of the loudness EP.

Figure 5.9b shows the normalized THLs of both EPs generated by the simulated tones where SPL is equal to 100 dB with varying frequencies from 0.5 kHz to 8 kHz. For both EPs, the THLs first increase and then decrease when the frequency starts increasing. The peak THL of the velocity EP is at 2 kHz, while the THL of the loudness EP peaks at 4 kHz. In addition, the velocity EP shows a fast degradation of the THL when the frequency increase mores than 2 kHz.

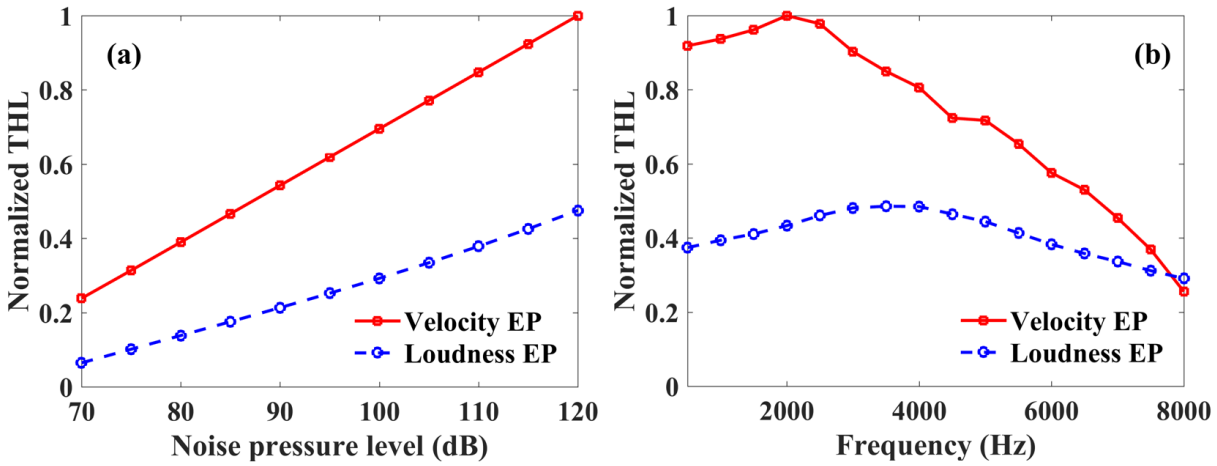

Figure 5.9. The normalized THLs for the tone (a) at 1 kHz and SPL from 70 to 120 dB and (b) at fixed SPL = 100 dB and frequencies from 0.5 to 8 kHz for the velocity EP and the loudness EP.

5.8 Conclusion

In this chapter, two auditory filters (*i.e.*, the DRNL filter and the ROEX filter) have been applied to develop the velocity EP and the loudness EP. Two different types of stimulus (*i.e.*, Gaussian noise and a tone) have been simulated to evaluate the two proposed EPs. For Gaussian noise, the results show that the maximum velocity obtained by the DRNL filter occurs around 2 kHz, while the peak loudness obtained by the ROEX filter is about 4 kHz. For a tone, both velocity EP and loudness EP can reflect the corresponding frequencies of the input tone signals. To evaluate the effectiveness of the two EPs for the prediction of NIHL, we proposed two noise

metrics, HL^D and HL^R, based on the velocity EP and the loudness EP. The results show that both EPs can potentially be used as noise hazardous level indexes for assessment of NIHL. The velocity EP based metric demonstrates a higher sensitivity than the loudness EP based metric.

CHAPTER 6

METRICS FOR NOISE-INDUCED HEARING LOSS ASSESSMENT BASED ON THE EXCITATION PATTERNS OF THE AUDITORY MODELS

It has been widely considered that the current noise metrics (like L_{eq}, and L_{Aeq}) underestimate the risk of the complex noises because they are based on the EEH. In addition, these metrics cannot provide a physical insight into the processes of the hearing damage inside the cochlea. In contrast, the mammalian auditory model can be utilized to develop more advanced metric for the assessment and the prediction of the NIHL. In this study, six noise metrics ($L_{Gammatone,}$ $L_{Loudness}$, L_{DRNL}, L_{CARFAC}, $L_{Verhulst}$, and L_{Zilany}) derived from six different auditory models (Gammatone, loudness, DRNL, CARFAC, Verhulst, and Zilany, respectively) were developed to assess the hearing loss caused by different types of noise based on the excitation pattern. The vibration of the basilar membrane caused by a noise stimulus as a function of the frequency of the stimulus can be referred as an excitation pattern. So that, the excitation pattern can be used to build an advance noise metric for more accurate evaluation of the hearing loss. The proposed noise metrics can be used for more accurate assessment of risks of complex noises because they are based on the EP of the auditory models. Furthermore, an existing chinchilla noise exposure data are used to validate the effectiveness of the proposed metrics. The results of the regression analysis demonstrate that the proposed noise metrics can accurately assess the hearing loss measured in chinchillas. Moreover, the overall results of the proposed noise metrics show better correlation with the permanent hearing loss compared with the conventional metrics.

6.1 Introduction

The current noise guidelines were developed based on the EEH [86]. The EEH states that the NIHL depends on the total acoustic energy of exposure to the noise and its independent to the temporal characteristics of the noise [135]. A-weighted equivalent sound pressure level, L_{Aeq}, has been considered as the main metric to assess levels of the noise exposure. However, a number of studies showed that L_{Aeq} is appropriate for continuous noise (Gaussian noise for example) but not for impulsive or non-Gaussian noises [90, 108, 109].The noise environments in many workplaces are often non-Gaussian and contain high-level noise bursts [20]. Noise levels in these environments may change from relatively slowly levels, as in warehouses, to high level bursts of noise, as in the work environments of firefighters. A number of animal exposure studies showed that the interaction effect between the impulse and continuous noise may actually exacerbate the NIHL [111, 112, 136].

However, the results from most of the researchers showed that hearing damage was larger than would have been predicted by the equivalent energy. Several factors can partake in the hearing system damage, such as: peak SPL, pulse repetition rate, duration, absence or presence of the background noise, and the frequency component of the background noise [137]. Therefore, lately, controversy has arisen over the need for an advance method for better assessment of the NIHL. Recently, several auditory filter based models have been developed for better assessment of the NIHL [42-44]. Such auditory filter based models can reflect the fundamental physical properties of the ear [45]. This may lead to a better understanding of the NIHL based on the characteristics of the conductive path of the ear [43, 46].

The auditory models play a major role as powerful analytical tools to understand the auditory processing. The auditory models have been utilized as realistic sound processors for

many hearing applications. The overarching goal of this chapter is to use different types of the existing auditory models to design new noise metrics based on EP. The proposed metrics will be utilized for better evaluation of the NIHL. The performance of the proposed metrics will be assessed using chinchilla noise exposure data. Six auditory models (Gammatone, loudness, DRNL, CARFAC, Verhulst, and Zilany) will be used to develop six noise metrics ($L_{Gammatone,}$ $L_{Loudness}$, L_{DRNL}, L_{CARFAC}, $L_{Verhulst}$, and L_{Zilany}, respectively). Although the auditory models have different approaches (*i.e.*, mechanical or perceptual), the EP will be used to in this chapter to develop the new noise metrics. The EP method can be estimated from the mechanical or the perceptual model.

6.2 Chinchilla outer ear and middle ear transfer function

The transfer function of the outer ear for chinchilla in this chapter will be the same one that is used in chapter four of this dissertation which is shown in Figure 4.1(a). In this chapter, the outer ear transfer function will be added because some of the auditory models do not contain the outer ear in their original implementation which are Gammatone, DRNL, CARFAC, Verhulst, and Zilany. For the case of the loudness model, the original outer ear transfer function will be replaced by the one for the chinchilla. The idea of adding the transfer function of the outer ear and the middle ear is to build a complete auditory system (*i.e.*, outer, middle, and inner ear) that can evaluate the noise signal from the free field to the inner ear. This will help to give more realistic assessment for the NIHL. Moreover, the reason behind choosing the chinchilla outer ear transfer function is because later the chinchilla hearing loss data will be used to evaluate each auditory model for hearing loss assessment.

The transfer function of the middle ear for chinchilla is shown in Figure 6.1 [124]. In this chapter, the middle ear transfer function will be used for Gammatone, and CARFAC because

these models do not contain the middle ear transfer function in their original implementation. The reason behind choosing this transfer function is because it can be applied for the Gammatone model and the CARFAC model. For the other models (*i.e.*, DRNL, loudness, Verhulst, and Zilany), the original implementation of the middle ear transfer function will be used.

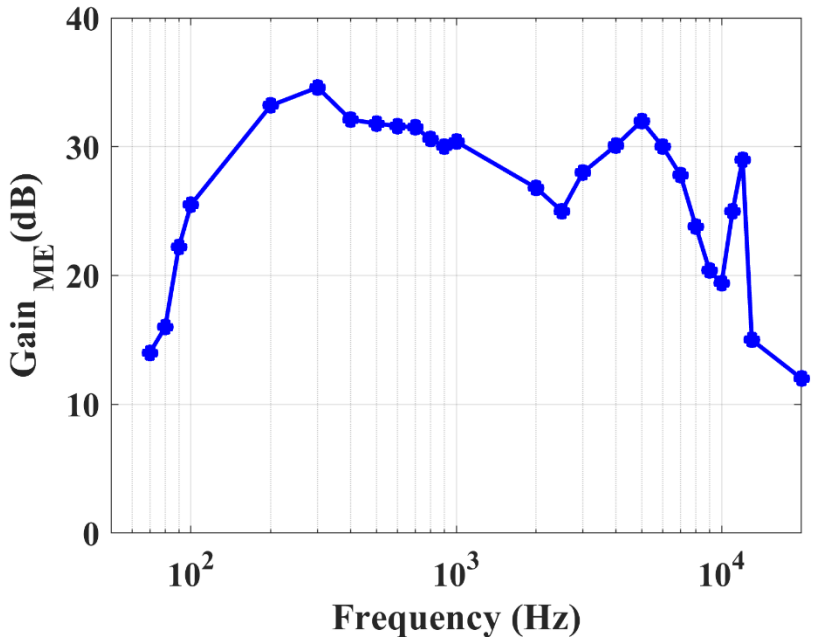

Figure 6.1. Chinchilla middle ear transfer function [124].

6.3 Auditory models

The detailed descriptions of the six auditory models used in this chapter (*i.e.*, Gammatone, Loudness, DRNL, CARFAC, Verhulst, and Zilany) are mentioned in sections 3.4.1, 3.4.2, 3.4.4, 3.4.5, 3.4.6, and 3.4.7, respectively.

6.4 Excitation patterns

The mechanical movement of the BM can be considered as an essential feature that causes hearing loss in the case of the high sound pressure level [49]. In the mammalian cochlea, the vibrations of the BM caused by an input of an acoustic signal as a function of the stimulus frequency can be defined as the excitation pattern (EP) [44, 73, 91]. for the case of a mechanical model (*i.e.*, a model can predict the mechanical vibrations of the BM), the EP can be assessed by calculating the root-mean-square (RMS) energy value of the mechanical vibration at each cochlear location [73, 138]. In the perceptual model case (*i.e.*, a model can reproduce psychoacoustic data only without making explicit predictions of the cochlea mechanics), the EP can be assessed at the output of each perceptual filter in response to the input stimulus [73, 139].

In this chapter, excitation patterns of six auditory models were constructed by calculating the RMS energy at the output of the channels for each model. The input SPL of the stimuli were chosen from 70dB SPL to 120dB SPL with 10dB SPL step. The reason behind selecting this range is that the exposure level above 85 dB is considered to be hazardous for workers according to WHO [1]. Moreover, the EP calculations of the auditory models in this range will help to give a clear idea about the performance of each model with high SPL. Also, the stimuli have 100-ms long tones with center frequencies at 0.5, 1, 2, 4, 8, 16 kHz. The tones also contained a squared-cosine rise of 10ms decay time to minimize the influence of the spectral splatter [73]. The reason behind choosing these six center frequencies is because the chinchilla exposure data measured at these bands and later will be used for the hearing loss evaluation based on EP.

6.5 Design of noise metric based excitation patterns for hearing loss evaluation

A number of studies have demonstrated that EPs are highly associated with hearing loss [44, 133]. The EP method generates an assessment for the magnitude of the BM motion along the cochlear duct which can be used to estimate the hazard level in the case of high SPL. The six auditory filters in this chapter have different approaches (*i.e.,* mechanical or perceptual), and they are not expected to yield the same results. The EP output of each auditory filter will be divided by the EP of a 10dB SPL Gaussian noise signal of the same auditory model. This should result in a unit-less value of each auditory filter for the comparison purposes. The length of the generated Gaussian noise signal has the same length of the chinchilla exposure data. For the case of NIHL assessment, EP of each auditory model will be used to design a noise metric to evaluate the hazard level by measuring the output energy. The form below represents the proposed metric equation

$$L_{AM,CH} = 10\log_{10}(EP_{AM,CH}^2/EP_{AM0}^2) \tag{6.1}$$

where $L_{AM,CH}$ represents the output level in dB based on EP calculation of the given auditory model (*AM*) at each channel (*CH*). $EP_{AM,CH}$ represents the EP output of the given auditory model (*AM*) at each channel (*CH*), and EP_{AM_0} represents the EP of the 10dB Gaussian noise signal for the given auditory model.

The reason behind adding the denominator (*i.e.,*EP_{AM_0}) is to make the final result (*i.e.,*$L_{AM,CH}$) unit-less to compare the result of each auditory model with the other models using linear regression analysis. Moreover, for further evaluation of NIHL, the below form will be used

$$L_{AM,5124} = (L_{AM,0.5} + L_{AM,1} + L_{AM,2} + L_{AM,4})/4 \quad (6.2)$$

where $L_{AM,0.5}$, $L_{AM,1}$, $L_{AM,2}$, and $L_{AM,4}$ are the equivalent output levels of the given auditory model (*AM*) at 0.5, 1, 2, 4 kHz full-octave components, respectively. The form of the $L_{AM,5124}$ equation is chosen to match the form of the NIHL defined in Equation (4.10). By Equation (6.1) and Equation (6.2), the EP has been successfully translated to measure the hazard level. Therefore, the proposed equations can be used for the NIHL assessment.

6.6 Experimental data

In this chapter, the derived metrics will be evaluated using existing animal data that was obtained by exposing 23 groups of chinchillas to different types of noise [20, 34, 39]. The same chinchilla noise exposure data used in chapter four will be utilized here again. The details about this data is mentioned in section 4.5.

6.7 Results and discussion

6.7.1 Excitation patterns

The simulated excitation patterns of the six auditory models are demonstrated in Figure 6.2 and Figure 6.3. EPs were assessed by calculating the RMS energy at the output of the channels for each auditory model. Figure 6.2 illustrates the EP simulation of the six auditory models in this chapter in response to 70 dB to 120 dB SPL tones at 1 kHz center frequency. All of the figures are normalized by their peaks. The results show that all the auditory models were able to capture the center frequency of the input stimulus (*i.e.*, 1 kHz). Even though all of the auditory models' excitation patterns peak at 1 kHz, the sharpness and the tail slopes of the curves are different. Moreover, Figure 6.3 shows the EP simulation in response to 100 dB SPL tone with six different center frequencies at 0.5, 1, 2, 4, 8, and 16 kHz, respectively. The results show

that each EP of the auditory models peak at a common location which is similar to the frequency of the input stimulus. This is indicating that all the auditory models were able to capture the correct center frequency.

Although several modifications were made for the auditory models here by adding and/or modifying the outer ear and the middle ear by using the one for chinchilla; the excitation patterns peak of all the auditory models were able to predict the correct center frequency. From the frequency selectivity point of view, in comparison with other models, the Gammatone model shows a sharp curve around the peak. The Gammatone filters are linear and unable to simulate the nonlinear features of the cochlea, so that the shape of the output will be symmetric. Moreover, the rest of the auditory models have different sharpness, tail slope, and area under the curve because they have different cochlear processing features (such as nonlinearity, compression, number of channels, etc.) in the original implementation.

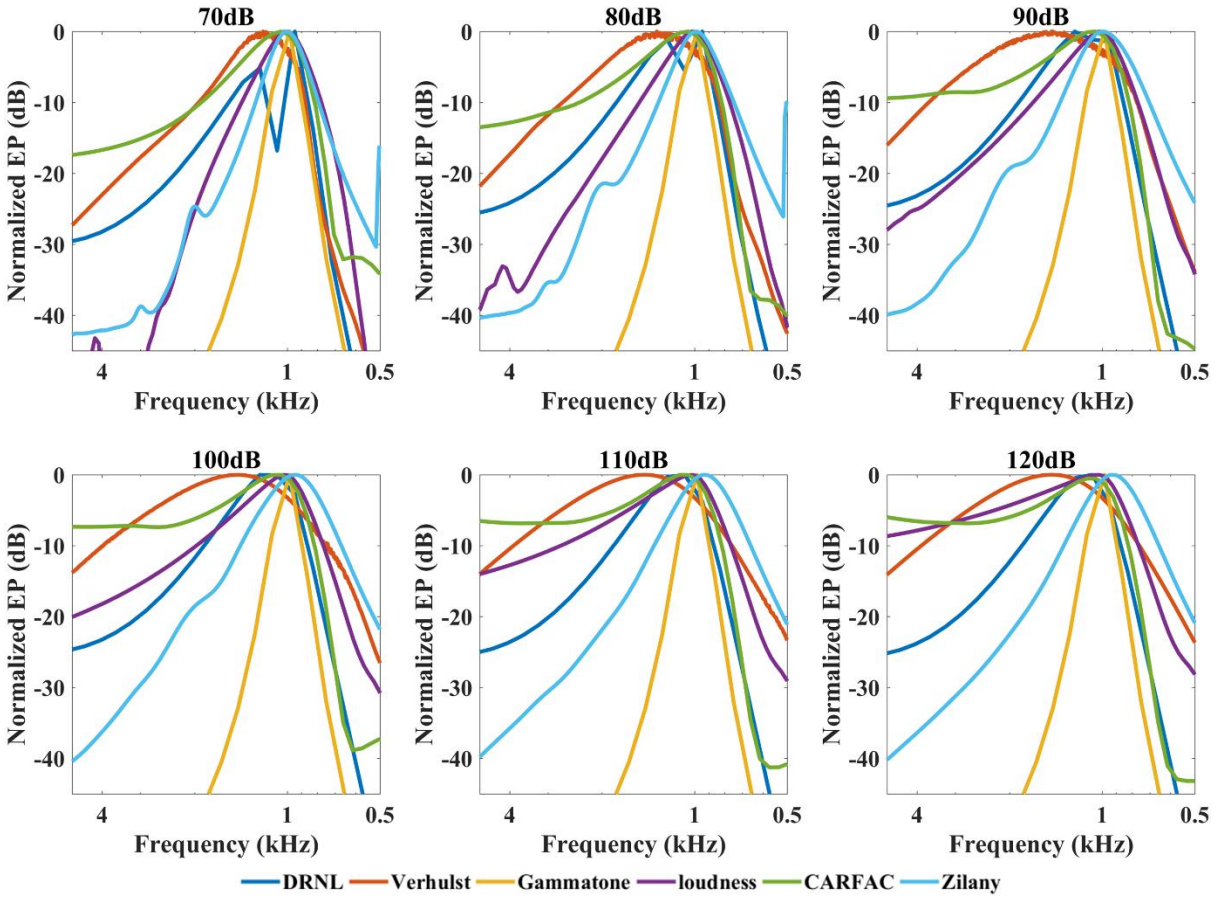

Figure 6.2. EP for each auditory model calculated with response to tones at 70 dB to120 dB SPL with 10 dB step and center frequency at 1 kHz. The excitation patterns were normalized by their maxima for each auditory model implementation.

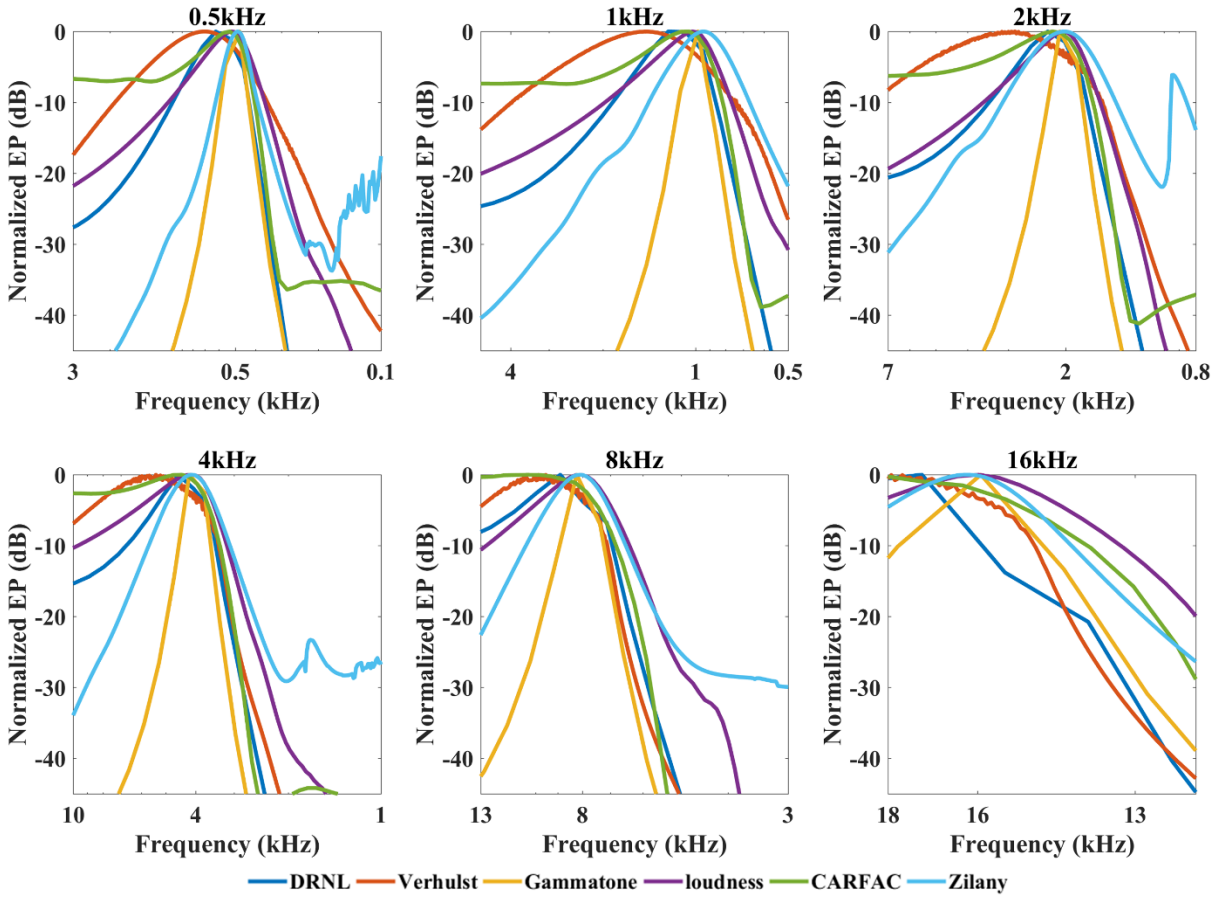

Figure 6.3. EP for each auditory model calculated with response to tones at 100 dB SPL with six center frequency at 0.5, 1, 2, 4, 8, and 16 kHz, respectively. The excitation patterns were normalized by their maxima for each auditory model implementation.

6.7.2 Analysis of hearing loss with the proposed noise metrics based excitation patterns at six full-octave bands

The EP method will be used to generate a noise metric for each auditory model. The performance of the proposed noise metric based EP is evaluated by its correlation with the NIHL. The purpose of the correlation analysis is to measure and to interpret the strength of the linear relationship between the two continuous variables [127] (in this chapter, it will be between

the proposed metric and the hearing loss index represented by the PTS). The linear regression equation is expressed as

$$PTS = K_0 + K_1 L_{AM,CH} + \epsilon \quad (6.3)$$

where $L_{AM,CH}$ refers to the proposed noise metric, and ϵ is the error to be minimized. k_0, and k_1 are constants determine by the best fitting regression line.

The correlation analysis of the noise metric and hearing loss (represented by PTS) is conducted by applying the linear regression analysis to 22 pairs of the proposed noise metric and the PTS data at 0.5, 1, 2, 4, 8, and 16 kHz full-octave frequency components. Both of the conventional metrics (*i.e.*, L_{eq}, and L_{Aeq}) and the proposed noise metrics (*i.e.*, $L_{Gammatone,}$ $L_{Loudness}$, L_{DRNL}, L_{CARFAC}, $L_{Verhulst}$, and L_{Zilany}) are calculated using 10 second window of the digitally recorded noise time history. The sampling frequency of the 22 noises were recorded at 48 kHz. Figure 6.4 shows the fitting lines and the scattering plots of the hearing loss against the proposed metrics with the regressed line. The hearing loss was measured at 0.5, 1, 2, 4, 8, and 16 kHz. The six full-octave bands will cover the frequency range of the BM along the cochlear duct. The proposed noise metrics are calculated at 0.5, 1, 2, 4, 8, and 16 kHz, respectively. Each point represents the hearing loss-proposed metric pair of the 22 animal groups, and the lines indicate the fitting results of the symbols distribution. It can be found in Figure 6.4 that all the proposed metrics can accurately predict the noise induced hearing loss in chinchilla, but with different correlation. The results indicate that the proposed noise metrics based EP can be used as a noise guideline to assess NIHL.

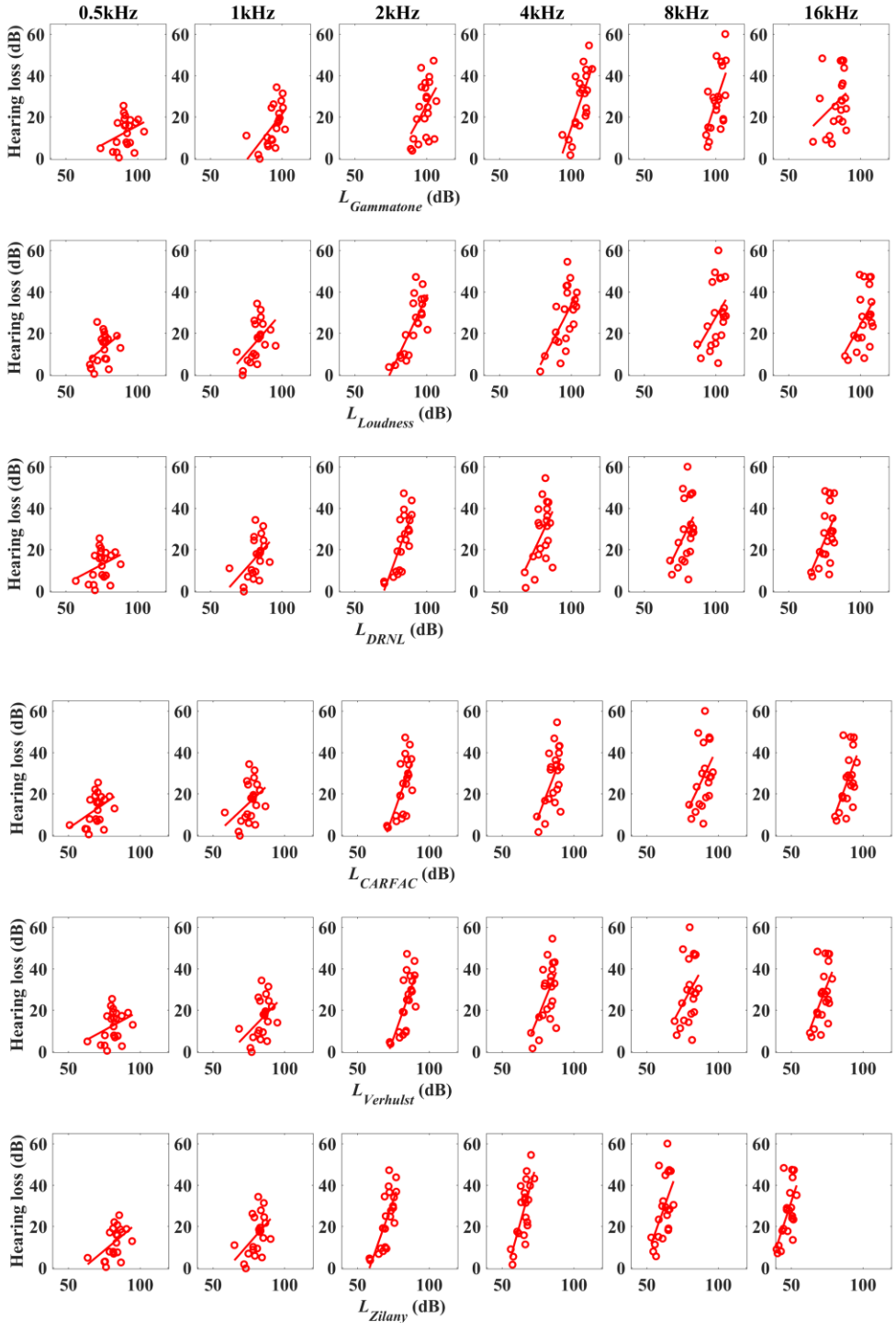

Figure 6.4. Scattering plots and fitting lines of the hearing loss vs. the proposed metric for the 22 animal groups at six full-octave frequency bands. The hearing loss is represented by the PTS (red color) measured at 0.5, 1, 2, 4, 8, and 16 kHz. The proposed noise metrics are represented by $L_{Gammatone}$, $L_{Loudness}$, L_{DRNL}, L_{CARFAC}, $L_{Verhulst}$, and L_{Zilany}, respectively. The (r^2) values have been summarized in Table 6.1.

Moreover, the coefficient of determination (r^2) value is used to show the linear correlation between the metric and the hearing loss. The r^2 measure (with a range of 0-1) is the fraction of the variability between the hearing loss and the metric through their linear relationship, or vice versa. When $r^2 = 1$ it indicates a perfect correlation between the metric and the hearing loss. If $r^2 = 0$ it indicates no correlation between the metric and the hearing loss. Table 6.1 summarizes the results of r^2 values of the conventional metrics (*i.e.*, L_{eq}, and L_{Aeq}) and the proposed noise metrics (*i.e.*, $L_{Gammatone,}$ $L_{Loudness}$, L_{DRNL}, L_{CARFAC}, $L_{Verhulst}$, and L_{Zilany}) of this study. The hearing loss is indicated by the PTS values measured at 0.5, 1, 2, 4, 8, and 16 kHz. The PTS indicates the permanent hearing loss that happens after certain recovery time [140]. L_{Zilany} metric shows the highest correlation with the PTS (r^2=0.25) at 0.5 kHz and (r^2=0.41) at 16 kHz. The L_{Aeq} metric shows the highest correlation with the PTS (r^2=0.63) at 1 kHz. The $L_{Loudness}$ metric shows the highest correlation with the PTS (r^2=0.61) at 2 kHz. At 4 kHz, L_{eq} shows the highest correlation with the PTS (r^2=0.60). $L_{Gammatone}$ shows the highest correlation with the PTS (r^2=0.37) at 8 kHz. The results are consistent with Figure 6.5.

Furthermore, the r^2 results for the proposed noise metrics (*i.e.*, $L_{Gammatone,}$ $L_{Loudness}$, L_{DRNL}, L_{CARFAC}, $L_{Verhulst}$, and L_{Zilany}) show that all these metrics can successfully predict hearing loss. Also, the proposed metrics have overall better correlation with the PTS at 0.5, 2, 8, and 16 kHz compared with the conventional metrics. These results indicate that the proposed noise metrics have better assessment of the complex noise than the conventional metrics.

Table 6.1. Results of the regression analysis of the metrics. The (r^2) values represent the linear correlation between the proposed metric and the hearing loss (represented by PTS) at six full-octave bands centered at 0.5, 1, 2, 4, 8, and 16 kHz.

Metric	r^2					
	0.5 kHz	**1 kHz**	**2 kHz**	**4 kHz**	**8 kHz**	**16 kHz**
L_{eq}	0.12	0.61	0.18	**0.60**	0.26	0.10
L_{Aeq}	0.16	**0.63**	0.18	0.59	0.28	0.14
$L_{Gammatone}$	0.11	0.36	0.21	0.53	**0.37**	0.11
$L_{Loudness}$	0.19	0.26	**0.61**	0.41	0.18	0.25
L_{DRNL}	0.11	0.24	0.56	0.29	0.19	0.29
L_{CARFAC}	0.18	0.16	0.47	0.36	0.19	0.33
$L_{Verhulst}$	0.12	0.18	0.50	0.34	0.15	0.31
L_{Zilany}	**0.25**	0.22	0.56	0.55	0.31	**0.41**

6.7.3 Analysis of the hearing loss indicator (PTS_{5124}) with the proposed noise metrics based excitation patterns

Most standards use A-weighted sound level (L_{Aeq}) as the basis for assessing the potential of a noise to produce NIHL from long-term exposures to noise [25, 36, 41]. The use of A-weighting metric reflects the fact that humans hear best in their mid-frequency range of audibility [25]. In this chapter, the hearing loss indicator which is based on the mid- range frequency will be used to assess the performance of the developed metrics. The indicator is the PTS_{5124} which is the permanent threshold shift measured at 0.5, 1, 2, and 4 kHz.

For further evaluation of the proposed noise metrics on the NIHL prediction, PTS_{5124} will be used with the regression analysis. Figure 6.5 shows the scattering plots and the fitting lines of the pairs of all metrics in this study (*i.e.*, the conventional metrics and the proposed metrics) and the hearing loss indicator (PTS_{5124}). Each point in the figure characterizes the pair of the average hearing loss (*i.e.*, PTS_{5124}) of the chinchilla groups exposed to specific noise type and the metric

calculated for that noise. It can be found that all of the proposed metrics can successfully predict the hearing loss in chinchillas, but with different correlation.

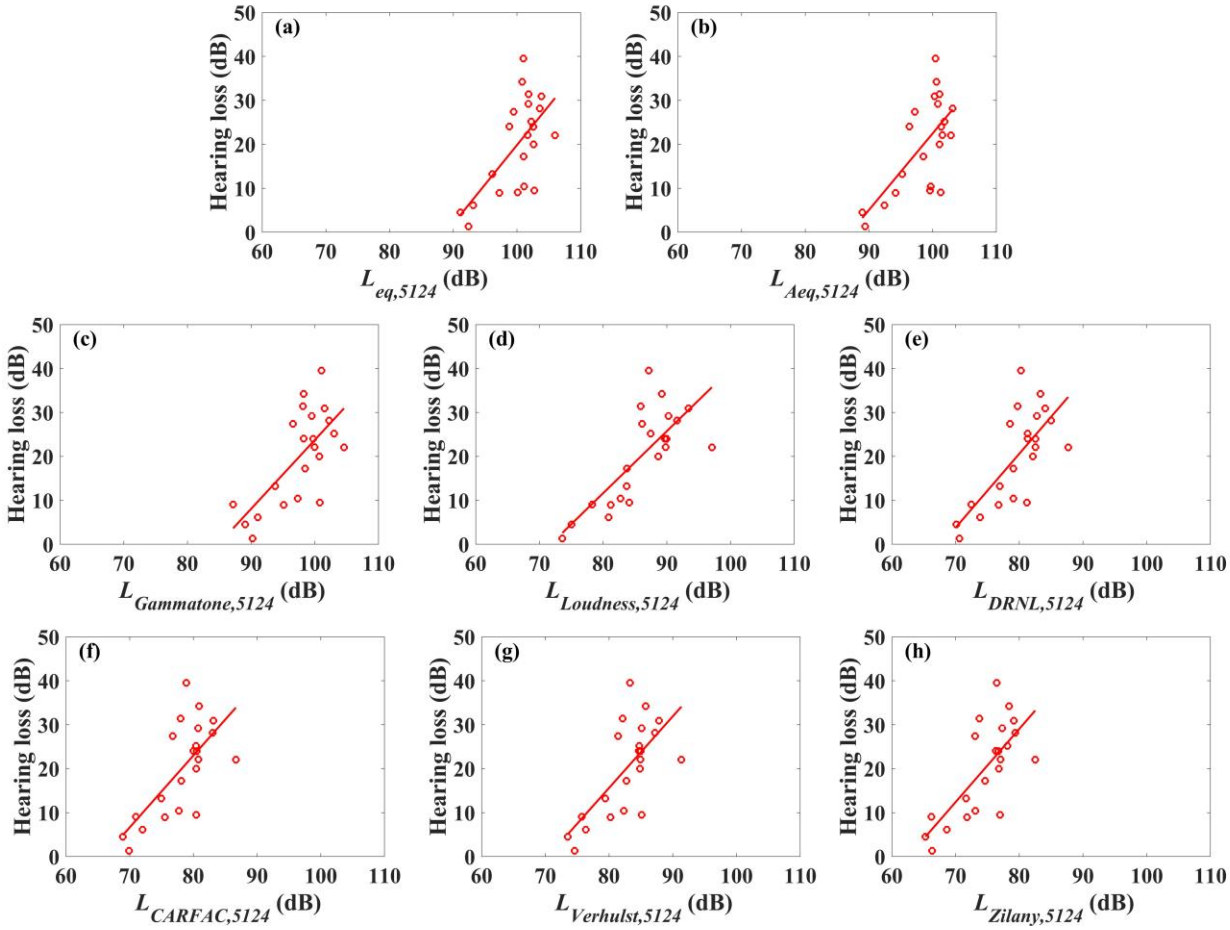

Figure 6.5. Scattering plots and fitting lines of the hearing loss against the metric values with the regressed lines. Each point characterizes the pair of the average hearing loss (*i.e.*, PTS_{5124}) of the chinchilla groups exposed to specific noise and the metric calculated for that noise. The hearing loss represented by the PTS_{5124} (red color). The metrics represented by the current noise metrics (*i.e.*, $L_{eq,5124}$, and $L_{Aeq,5124}$) and the proposed noise metrics ($L_{Gammatone,5124}$, $L_{Loudness,5124}$, $L_{DRNL,5124}$, $L_{CARFAC,5124}$, $L_{Verhulst,5124}$, and $L_{Zilany,5124}$) from (a) to (h) respectively. The (r^2) values have been summarized in Table 6.2.

Moreover, Table 6.2 shows the results of r^2 values for the conventional metrics and the proposed metrics with respect to the PTS_{5124}. The results show that the $L_{Loudness,5124}$ metric has the highest correlation ($r^2 = 0.58$) with the permanent hearing loss indicator (PTS_{5124}). Furthermore, as mentioned before, L_{Aeq} is the primary metric to evaluate the noise exposure levels. In this

chapter, all of the proposed metrics show stronger correlation with the hearing loss indicator (PTS_{5124}) than the conventional metrics. The r^2 values of the proposed metrics ($L_{Gammatone,5124}$, $L_{Loudness,5124}$, $L_{DRNL,5124}$, $L_{CARFAC,5124}$, $L_{Verhulst,5124}$, and $L_{Zilany,5124}$) are 0.48, 0.58, 0.52, 0.48, 0.47, and 0.53, respectively. The r^2 values of the conventional metrics ($L_{eq,5124}$, and $L_{Aeq,5124}$) are 0.42, and 0.45, respectively. These results indicate that the proposed metrics are more accurate on the assessment of the auditory risk exposure to hazardous occupational noise than the current noise guidelines. This finding will give the advantage to use the proposed metrics over the conventional guidelines because the proposed metrics are based on the auditory models. The models of the auditory system will provide more physiological insight about the ear than the weighted metrics (like L_{eq} and L_{Aeq}), especially for high level of exposure [42].

Furthermore, in this study, 19 complex noise samples combining different forms of impulse noise with a continuous Gaussian noise were used [20, 21, 33, 39]. Each of the complex noise sample has several pulses with a peak level over 120 dB. The loss at these high noise levels is more like a sprain, and it grows as a linear function of the number of the pulses [45, 141]. Such high levels are identified to damage the active mechanism of the BM [12]. The active mechanism depends on the operation of the outer hair cells (OHCs), and it functions in a nonlinear way. The passive mechanism depends on the mechanical properties of the BM and the surrounding structures. The passive mechanism of the BM operates in a roughly linear way [12]. The auditory models can successfully simulate the active mechanism and the passive mechanism while the conventional metrics cannot provide such details. This explains why the auditory filters in this chapter have higher correlation with the hearing loss compared with the conventional metrics.

Table 6.2. Results of the regression analysis of the metrics. The (r^2) values represent the linear correlation between the metric and the average hearing loss represented by PTS_{5124}. PTS_{5124} is defined as the NIHL indicator as shown in Equation (4.10).

Metric	r^2
$L_{eq,5124}$	0.42
$L_{Aeq,5124}$	0.45
$L_{Gammatone,5124}$	0.48
$L_{Loudness,5124}$	**0.58**
$L_{DRNL,5124}$	0.52
$L_{CARFAC,5124}$	0.48
$L_{Verhulst,5124}$	0.47
$L_{Zilany,5124}$	0.53

6.8 Conclusion

It has been widely considered that the current noise metrics (like L_{eq}, and L_{Aeq}) underestimate the risk of the complex noises because they are based on the EEH. The current noise metrics cannot provide physiological understanding of the auditory system because they are based on the overall SPL and the exposure time only. To address this problem, six noise metrics ($L_{Gammatone,}$ $L_{Loudness}$, L_{DRNL}, L_{CARFAC}, $L_{Verhulst}$, and L_{Zilany}) derived from six different auditory models (Gammatone, loudness, DRNL, CARFAC, Verhulst, and Zilany, respectively) were developed to assess the hearing loss caused by different types of noise based on the excitation pattern. The proposed noise metrics can be used for more accurate assessment of risks of complex noises because they are based on the EP of the auditory models. The six noise metrics were assessed by their correlations with animal noise exposure data obtained by exposing 22 groups of chinchillas to different types of noise. The correlation analysis was conducted by comparing the metric values calculated from the noise and the PTS values measured in chinchillas exposed to the noise. For the full-octave bands correlation study, the

results show that the proposed metrics have better correlation with the PTS at 0.5, 2, 8, and 16 kHz compared with the conventional metrics.

Moreover, for the NIHL correlation analysis, the loudness metric ($L_{Loudness,5124}$) shows the highest correlation with the hearing loss indicator (PTS_{5124}). NIHL indicator (*i.e.*, PTS_{5124}) was defined in this study as the average of the PTS at 0.5, 1, 2, and 4 kHz. The r^2 value (the coefficient of determination) of the correlation of the best metric (*i.e.*, $L_{Loudness,5124}$) was 0.58 compared to 0.45 of the current noise metric (*i.e.*, $L_{Aeq,5124}$). Moreover, all of the proposed metrics show a stronger correlation with the hearing loss indicator (PTS_{5124}) than the conventional metrics. The r^2 values of the correlation of the proposed metrics ($L_{Gammatone,5124}$, $L_{Loudness,5124}$, $L_{DRNL,5124}$, $L_{CARFAC,5124}$, $L_{Verhulst,5124}$, and $L_{Zilany,5124}$) are 0.48, 0.58, 0.52, 048, 0.47, and 0.53, respectively. This indicates that the proposed metrics would be more accurate on the assessment of the auditory risk of exposure to hazardous military and industrial noise.

Practically, the approach in this chapter maybe questioned in relation to developing noise metrics. The proposed metrics require additional processing like the digital recording of the noise and the computer analysis for that noise. However, this problem should be a minor issue considering that the modern computers have very powerful and very fast implementation.

Moreover, the use of chinchilla exposure data in this study should not cause a major difference from humans, because both chinchillas and humans have very similar audiometric characteristics [36, 40]. Bohne and Harding [142] found that the chinchilla is an excellent model for studying the effects of noise on humans. The audibility curve of the chinchilla is similar to that of humans, and the patterns and progression of noise-induced damage look to be very similar to humans [137, 142].

CHAPTER 7

CONCLUSION AND FUTURE WORK

In this final chapter, the main findings and the contributions of this dissertation are summarized. Several research directions for future work are outlined as well.

7.1 Conclusion

This dissertation as a whole has focused on comparing the existing noise metrics and on the designing of new noise metrics for better assessment of the NIHL. The key point for the designed metrics is to develop an advance method for more accurate evaluation of the complex noises. Moreover, the proposed metrics are developed to reflect response characteristics of the ear in their design. This approach will offer better assessment for the hearing loss than the conventional metrics. In the following, the main objectives accomplished in each chapter of this dissertation are briefly reviewed:

- In chapter four, the performances of the F-weighting and the CVL fatigue model were compared with the conventional noise metrics (*i.e.*, L_{eq}, L_{Aeq}, and L_{Ceq}) using animal noise exposure data. Linear regression analysis was used to evaluate the correlations between the five noise metrics (L_{eq}, L_{Aeq}, L_{Ceq}, L_{Feq}, and L_{CVL}) and the hearing loss indicators (PTS and TTS). The results show that the F-weighting and the CVL fatigue model demonstrates better correlations with the hearing loss indicators among the five noise metrics. It indicates that both developed metrics can predict the NIHL better than the conventional EEH based noise metrics.
- In chapter five, The DRNL auditory filter and the ROEX auditory filter were applied to develop the velocity EP and the loudness EP, respectively. Two types of stimulus (Gaussian noise and a tone) were used to evaluate the two proposed EPs. The results of

the Gaussian noise stimulus showed different response for the characteristic frequency along the cochlea. The maximum velocity obtained by the velocity EP model occurs around 2 kHz, while the peak loudness obtained by the loudness EP model is about 4 kHz. For a tone stimulus, both velocity EP and loudness EP can reflect the corresponding frequencies of the input tone signals. Two noise metrics used to evaluate the effectiveness of the two EPs for the NIHL prediction. The results show that both EPs can potentially be used as noise hazardous level indexes for assessment of NIHL. The velocity EP based metric demonstrates higher sensitivity than the loudness EP based metric.

- In chapter six, six noise metrics ($L_{Gammatone,}$ $L_{Loudness}$, L_{DRNL}, L_{CARFAC}, $L_{Verhulst}$, and L_{Zilany}) derived from six different auditory models (Gammatone, loudness, DRNL, CARFAC, Verhulst, and Zilany, respectively) were developed to assess the NIHL based on the excitation pattern. The proposed noise metrics were assessed by their correlations with chinchilla noise exposure data. The correlation analysis was conducted by comparing the metric values and the PTS values measured in chinchillas exposed to the noise. For the full-octave bands analysis, the results show that the proposed metrics have better correlation with the PTS at 0.5, 2, 8, and 16 kHz compared with the conventional metrics. For the NIHL correlation analysis, the loudness metric ($L_{Loudness,5124}$) shows the highest correlation with the hearing loss indicator (PTS_{5124}).

7.2 Future research directions

Several potential directions based on the results in this dissertation can be further extended as future work are highlighted below:

- Consolidate the findings in this dissertation using human hearing loss data to evaluate the designed metrics instead of the chinchilla data. The human hearing loss data can be used for more validation for the proposed metrics with the NIHL.
- Apply fatigue theory instead of the excitation pattern in the assessment of the hearing loss. The basilar membrane can be considered as a material that is subjected to cyclic loading. The fatigue theory can elucidate the process of the hearing loss happens due to the motions of stretching and squeezing of the basilar membrane.
- Using advance kurtosis statistics for better assessment of the spikes distribution in the complex noise. This will result in a better assessment of the temporal domain of the noise signal which cannot be obtain from the conventional metrics like the A-weighting sound pressure level.
- Design a model using an Artificial Neural Network (ANN) that can assess the NIHL. The ANN consists of artificial neurons as processing units that can be trained to perform complex calculations. Through this advance method other several factors which can affect the hearing loss will be included such as: age, gender, genetics, nonuse of hearing protection, smoking, etc. The ANN can be trained using the previous factors and the excitation pattern method used in this dissertation for better assessment of the hearing loss. Moreover, the ANN can be used as a predictor for the NIHL as well.

REFERENCES

1. World Health Organization. *Deafness and hearing loss*. 2018 [cited 2018 15 Oct]; Available from: http://www.who.int/mediacentre/factsheets/fs300/en/.
2. Agrawal, Y., E.A. Platz, and J.K. Niparko, *Prevalence of hearing loss and differences by demographic characteristics among US adults: data from the National Health and Nutrition Examination Survey, 1999-2004.* Archives of internal medicine, 2008. **168**(14): p. 1522-1530.
3. Sahota, R.S., *Noise-induced Hearing Loss: treatment and prevention*. 2017, Department of Medical and Social Care Education.
4. Le, T.N., L.V. Straatman, J. Lea, and B. Westerberg, *Current insights in noise-induced hearing loss: a literature review of the underlying mechanism, pathophysiology, asymmetry, and management options.* Journal of Otolaryngology-Head & Neck Surgery, 2017. **46**(1): p. 41.
5. Ramazzini, B., *De morbis artificum diatriba [diseases of workers]*. American journal of public health, 2001. **91**(9): p. 1380-1382.
6. Tak, S., R.R. Davis, and G.M. Calvert, *Exposure to hazardous workplace noise and use of hearing protection devices among US workers—NHANES, 1999–2004.* American journal of industrial medicine, 2009. **52**(5): p. 358-371.
7. Masterson, E.A., *Hearing impairment among noise-exposed workers—United States, 2003–2012.* MMWR. Morbidity and mortality weekly report, 2016. **65**.
8. Alamgir, H., D.L. Tucker, S.-Y. Kim, J.A. Betancourt, C.A. Turner, N.S. Gorrell, N.J. Wong, H.K. Sagiraju, S.P. Cooper, and D.I. Douphrate, *Economic burden of hearing loss*

for the US military: a proposed framework for estimation. Military medicine, 2016. **181**(4): p. 301-306.

9. Kirchner, D.B., E. Evenson, R.A. Dobie, P. Rabinowitz, J. Crawford, R. Kopke, and T.W. Hudson, *Occupational noise-induced hearing loss: ACOEM Task Force on occupational hearing loss.* Journal of Occupational and Environmental Medicine, 2012. **54**(1): p. 106-108.
10. Hétu, R., L. Getty, and H.T. Quoc, *Impact of occupational hearing loss on the lives of workers.* Occupational medicine (Philadelphia, Pa.), 1995. **10**(3): p. 495.
11. Zwerling, C., P.S. Whitten, C.S. Davis, and N.L. Sprince, *Occupational injuries among older workers with visual, auditory, and other impairments: a validation study.* Journal of occupational and environmental medicine, 1998. **40**(8): p. 720-723.
12. Moore, B.C., *Cochlear hearing loss: physiological, psychological and technical issues*. 2007: John Wiley & Sons.
13. Hussain, M.S.M., *Conductive Hearing Loss*. 2008, Nottingham.
14. Hong, O., M.J. Kerr, G.L. Poling, and S. Dhar, *Understanding and preventing noise-induced hearing loss.* Dis Mon, 2013. **59**(4): p. 110-8.
15. Kuhn, M., S.E. Heman-Ackah, J.A. Shaikh, and P.C. Roehm, *Sudden sensorineural hearing loss: a review of diagnosis, treatment, and prognosis.* Trends in amplification, 2011. **15**(3): p. 91-105.
16. Tate, M., *Principles of hearing aid audiology*. 2013: Springer.
17. Plomp, R., *The intelligent ear: On the nature of sound perception*. 2001: Psychology Press.
18. Martin, F.N. and J.G. Clark, *Introduction to audiology*. 1997: Allyn and Bacon Boston.

19. Singal, S., *Noise pollution and control strategy*. 2005: Alpha Science Int'l Ltd.

20. Hamernik, R.P., W. Qiu, and B. Davis, *The effects of the amplitude distribution of equal energy exposures on noise-induced hearing loss: The kurtosis metric.* The Journal of the Acoustical Society of America, 2003. **114**(1): p. 386-395.

21. Hamernik, R.P., W. Qiu, and B. Davis, *Hearing loss from interrupted, intermittent, and time varying non-Gaussian noise exposure: The applicability of the equal energy hypothesis.* The Journal of the Acoustical Society of America, 2007. **122**(4): p. 2245-2254.

22. Qin, J., P. Sun, and J. Walker. *Measurement of field complex noise using a novel acoustic detection system*. in *AUTOTESTCON, 2014 IEEE*. 2014. IEEE.

23. Smalt, C.J., J. Lacirignola, S.K. Davis, P.T. Calamia, and P.P. Collins, *Noise dosimetry for tactical environments.* Hearing research, 2017. **349**: p. 42-54.

24. Kinsler, L.E., A.R. Frey, A.B. Coppens, and J.V. Sanders, *Fundamentals of acoustics.* Fundamentals of Acoustics, 4th Edition, by Lawrence E. Kinsler, Austin R. Frey, Alan B. Coppens, James V. Sanders, pp. 560. ISBN 0-471-84789-5. Wiley-VCH, December 1999., 1999: p. 560.

25. Houser, D.S., W. Yost, R. Burkard, J.J. Finneran, C. Reichmuth, and J. Mulsow, *A review of the history, development and application of auditory weighting functions in humans and marine mammals.* The Journal of the Acoustical Society of America, 2017. **141**(3): p. 1371-1413.

26. Acoustical Society of America, *Z 243-1936: American Tentative Standard for Sound Level Meter for Measurement of Noise and other Sound.* J. Acoust. Soc. Am_, 1936. **8**: p. 147-152.

27. Dobie, R.A. and S. Van Hemel, *Hearing loss: Determining eligibility for social security benefits.* Basics of Sound, the Ear, and Hearing, 2004.

28. Alves-Pereira, M., J.J. de Melo, J. Motylewski, E. Kotlicka, and N.A.C. Branco, *Legislation Hinders Research into Low Frequency Noise.* Proc SSGRR 2003w, 2003.

29. Pierre Jr, R.L.S., D.J. Maguire, and C.S. Automotive. *The impact of A-weighting sound pressure level measurements during the evaluation of noise exposure*. in *Conference NOISE-CON*. 2004.

30. Schomer, P.D., Y. Suzuki, and F. Saito, *Evaluation of loudness-level weightings for assessing the annoyance of environmental noise.* The Journal of the Acoustical Society of America, 2001. **110**(5): p. 2390-2397.

31. Cohen, A., J.R. Anticaglia, and P.L. Carpenter, *Temporary Threshold Shift in Hearing from Exposure to Different Noise Spectra at Equal dB A Level.* The Journal of the Acoustical Society of America, 1972. **51**(2B): p. 503-507.

32. Lei, S.F., W.A. Ahroon, and R.P. Hamernik, *The application of frequency and time domain kurtosis to the assessment of hazardous noise exposures.* The Journal of the Acoustical Society of America, 1994. **96**(3): p. 1435-1444.

33. Hamernik, R.P. and W. Qiu, *Energy-independent factors influencing noise-induced hearing loss in the chinchilla model.* The Journal of the Acoustical Society of America, 2001. **110**(6): p. 3163-3168.

34. Qiu, W., R.P. Hamernik, and B. Davis, *The kurtosis metric as an adjunct to energy in the prediction of trauma from continuous, nonGaussian noise exposures.* The Journal of the Acoustical Society of America, 2006. **120**(6): p. 3901-3906.

35. Qiu, W., R.P. Hamernik, and R.I. Davis, *The value of a kurtosis metric in estimating the hazard to hearing of complex industrial noise exposures.* The Journal of the Acoustical Society of America, 2013. **133**(5): p. 2856-2866.

36. Zhu, X., J.H. Kim, W.J. Song, W.J. Murphy, and S. Song, *Development of a noise metric for assessment of exposure risk to complex noises.* The Journal of the Acoustical Society of America, 2009. **126**(2): p. 703-712.

37. Zhu, X. and J. Kim, *Application of the analytic wavelet transform for time-frequency analysis of impulsive sound signals*. 2005, SAE Technical Paper.

38. Zhu, X. and J. Kim, *Application of analytic wavelet transform to analysis of highly impulsive noises.* Journal of sound and vibration, 2006. **294**(4-5): p. 841-855.

39. Hamernik, R.P., W. Qiu, and B. Davis, *Cochlear toughening, protection, and potentiation of noise-induced trauma by non-Gaussian noise.* The Journal of the Acoustical Society of America, 2003. **113**(2): p. 969-976.

40. Goley, G.S., W.J. Song, and J.H. Kim, *Kurtosis corrected sound pressure level as a noise metric for risk assessment of occupational noises.* The Journal of the Acoustical Society of America, 2011. **129**(3): p. 1475-1481.

41. Sun, P., J. Qin, and W. Qiu, *Development and validation of a new adaptive weighting for auditory risk assessment of complex noise.* Applied Acoustics, 2016. **103**: p. 30-36.

42. Price, G.R. and J.T. Kalb, *Insights into hazard from intense impulses from a mathematical model of the ear*. The Journal of the Acoustical Society of America, 1991. **90**(1): p. 219-227.

43. Sun, P. and J. Qin. *Auditory fatigue models for prediction of gradually developed noise induced hearing loss*. in *2016 IEEE-EMBS International Conference on Biomedical and Health Informatics (BHI)*. 2016.

44. Sun, P. and J. Qin. *Excitation patterns of two auditory models applied for noise induced hearing loss assessment*. in *Biomedical and Health Informatics (BHI), 2016 IEEE-EMBS International Conference on*. 2016. IEEE.

45. Price, G.R., *Impulse noise hazard: From theoretical understanding to engineering solutions.* Noise Control Engineering Journal, 2012. **60**(3): p. 301-312.

46. Price, G.R., *Predicting mechanical damage to the organ of Corti.* Hearing research, 2007. **226**(1): p. 5-13.

47. Price, G.R. *Auditory hazard units an index of risk from intense sounds*. in *National Institute for Occupational Safety and Health Best Practices Workshop: Impulsive Noise, Cincinnati, OH*. 2003.

48. Price, G.R., *Weapon noise exposure of the human ear analyzed with the AHAAH model.* now a paper in this series, 2003.

49. Price, G.R., *Validation of the auditory hazard assessment algorithm for the human with impulse noise data.* The Journal of the Acoustical Society of America, 2007. **122**(5): p. 2786-2802.

50. Price, G.R., *Impulse noise and the cat cochlea*. 2003, Army Research Lab.

51. Sun, P., J. Qin, and K. Campbell, *Fatigue Modeling via Mammalian Auditory System for Prediction of Noise Induced Hearing Loss.* Computational and mathematical methods in medicine, 2015. **2015**.

52. Sun, D. Fox, K. Campbell, and J. Qin, *Auditory fatigue model applications to predict noise induced hearing loss in human and chinchilla.* Applied Acoustics, 2017. **119**: p. 57-65.

53. Unoki, M., T. Irino, B. Glasberg, B.C. Moore, and R.D. Patterson, *Comparison of the roex and gammachirp filters as representations of the auditory filter.* The Journal of the Acoustical Society of America, 2006. **120**(3): p. 1474-1492.

54. Chen, Z., G. Hu, B.R. Glasberg, and B.C. Moore, *A new method of calculating auditory excitation patterns and loudness for steady sounds.* Hearing research, 2011. **282**(1): p. 204-215.

55. Meddis, R., L.P. O'Mard, and E.A. Lopez-Poveda, *A computational algorithm for computing nonlinear auditory frequency selectivity.* The Journal of the Acoustical Society of America, 2001. **109**(6): p. 2852-2861.

56. Rosowski, J.J., *Outer and middle ears*, in *Comparative Hearing: Mammals*. 1994, Springer. p. 172-247.

57. Song, W.J., *Study on human auditory system models and risk assessment of noise induced hearing loss*. 2010, University of Cincinnati.

58. Oghalai, J.S., *The cochlear amplifier: augmentation of the traveling wave within the inner ear.* Current opinion in otolaryngology & head and neck surgery, 2004. **12**(5): p. 431.

59. Ashmore, J., *Cochlear outer hair cell motility.* Physiological reviews, 2008. **88**(1): p. 173-210.

60. Pulkki, V. and M. Karjalainen, *Communication acoustics: an introduction to speech, audio and psychoacoustics*. 2015: John Wiley & Sons.

61. Fletcher, H. and W.A. Munson, *Loudness, its definition, measurement and calculation.* Bell Labs Technical Journal, 1933. **12**(4): p. 377-430.

62. Churcher, B. and A. King, *The performance of noise meters in terms of the primary standard.* Journal of the institution of Electrical Engineers, 1937. **81**(487): p. 57-81.

63. Robinson, D.W. and R.S. Dadson, *A re-determination of the equal-loudness relations for pure tones.* British Journal of Applied Physics, 1956. **7**(5): p. 166.

64. ISO, B., *226: 2003: Acoustics–Normal equal-loudness-level contours.* International Organization for Standardization, 2003. **63**.

65. Rimell, A.N., N.J. Mansfield, and G.S. Paddan, *Design of digital filters for frequency weightings (A and C) required for risk assessments of workers exposed to noise.* Industrial health, 2014: p. 2013-0003.

66. International Electrotechnical Commission, *Electroacoustics: sound level meters-Part 1: Specifications (IEC 61672-1)*. 2002: Geneva, Switzerland.

67. ANSI S1.42-2001, *American National Standard Design Response of Weighting Networks for Acoustical Measurements*. 2001, Acoustical Society of America New York.

68. Zweig, G., R. Lipes, and J. Pierce, *The cochlear compromise.* The Journal of the Acoustical Society of America, 1976. **59**(4): p. 975-982.

69. Lyon, R.F., A.G. Katsiamis, and E.M. Drakakis. *History and future of auditory filter models*. in *Circuits and Systems (ISCAS), Proceedings of 2010 IEEE International Symposium on*. 2010. IEEE.

70. Patterson, R., I. Nimmo-Smith, J. Holdsworth, and P. Rice. *An efficient auditory filterbank based on the gammatone function*. in *a meeting of the IOC Speech Group on Auditory Modelling at RSRE*. 1987.

71. Patterson, R.D., K. Robinson, J. Holdsworth, D. McKeown, C. Zhang, and M. Allerhand, *Complex sounds and auditory images.* Auditory physiology and perception, 1992. **83**: p. 429-446.

72. Hohmann, V., *Frequency analysis and synthesis using a Gammatone filterbank.* Acta Acustica united with Acustica, 2002. **88**(3): p. 433-442.

73. Saremi, A., R. Beutelmann, M. Dietz, G. Ashida, J. Kretzberg, and S. Verhulst, *A comparative study of seven human cochlear filter models.* The Journal of the Acoustical Society of America, 2016. **140**(3): p. 1618-1634.

74. Søndergaard, P. and P. Majdak, *The auditory modeling toolbox*, in *The technology of binaural listening*. 2013, Springer. p. 33-56.

75. Glasberg, B.R. and B.C. Moore, *Derivation of auditory filter shapes from notched-noise data.* Hearing research, 1990. **47**(1-2): p. 103-138.

76. Moore, B.C., B.R. Glasberg, and T. Baer, *A model for the prediction of thresholds, loudness, and partial loudness.* Journal of the Audio Engineering Society, 1997. **45**(4): p. 224-240.

77. Zwicker, E. and B. Scharf, *A model of loudness summation.* Psychological review, 1965. **72**(1): p. 3.

78. Zwicker, E., *BASIC-Program for calculating the loudness of sounds from their 1/3-oct band spectra according to ISO 532 B.* Acustica, 1984. **55**: p. 63-67.

79. Zwicker, E. and H. Fastl, *Psychoacoustics: Facts and models*. Vol. 22. 2013: Springer Science & Business Media.

80. ANSI, *ANSI S3. 4-2007. Procedure for the computation of loudness of steady sounds*. 2007, American National Standards Institute New York.

81. ISO532-2, *Acoustics–Methods for Calculating Loudness–Part 2: Moore–Glasberg Method*. 2016, International Organization for Standardization Geneva, Switzerland.

82. Glasberg, B.R. and B.C. Moore, *A model of loudness applicable to time-varying sounds.* Journal of the Audio Engineering Society, 2002. **50**(5): p. 331-342.

83. Patterson, R.D., *Auditory filter shapes derived with noise stimuli.* The Journal of the Acoustical Society of America, 1976. **59**(3): p. 640-654.

84. Moore, B.C. and B.R. Glasberg, *Suggested formulae for calculating auditory-filter bandwidths and excitation patterns.* The Journal of the Acoustical Society of America, 1983. **74**(3): p. 750-753.

85. Acoustical Society of, A., A. Acoustical Society of, S. Standards, I. American National Standards, and B. Accredited Standards Committee S, *American National Standard : procedure for the computation of loudness of steady sounds*. 2005, Melville, N.Y.: Standards Secretariat, Acoustical Society of America.

86. ANSI, S., *4: Procedure for the computation of loudness of steady sounds.* ANSI S3, 2007: p. 4-2007.

87. Lopez-Poveda, E.A. and R. Meddis, *A human nonlinear cochlear filterbank.* The Journal of the Acoustical Society of America, 2001. **110**(6): p. 3107-3118.

88. Lopez-Najera, A., R. Meddis, and E.A. Lopez-Poveda, *A computational algorithm for computing cochlear frequency selectivity: Further studies*, in *Auditory Signal Processing*. 2005, Springer. p. 14-20.

89. Robles, L. and M.A. Ruggero, *Mechanics of the mammalian cochlea.* Physiological reviews, 2001. **81**(3): p. 1305-1352.

90. Al-Dayyeni, W. and J. Qin, *Comparison of New Metrics for Assessment of Risks of Occupational Noise.* Journal of Applied Sciences and Arts, 2017. **1**(3): p. 4.

91. Al-Dayyeni, W.S., P. Sun, and J. Qin, *Investigations of Auditory Filters Based Excitation Patterns for Assessment of Noise Induced Hearing Loss.* Archives of Acoustics, 2018. **43**(3): p. 477–486.

92. Hartmann, W.M., *Signals, sound, and sensation*. 1997: Springer Science & Business Media.

93. Lyon, R.F., *Cascades of two-pole–two-zero asymmetric resonators are good models of peripheral auditory function.* The Journal of the Acoustical Society of America, 2011. **130**(6): p. 3893-3904.

94. Lyon, R.F., *Filter cascades as analogs of the cochlea*, in *Neuromorphic systems engineering*. 1998, Springer. p. 3-18.

95. Brandmeyer, A., R. Lyon, and R. Weiss. *Cascade of asymmetric resonators with fast-acting compression cochlear model*. 2015; Available from: https://github.com/google/carfac.

96. Verhulst, S., T. Dau, and C.A. Shera, *Nonlinear time-domain cochlear model for transient stimulation and human otoacoustic emission.* The Journal of the Acoustical Society of America, 2012. **132**(6): p. 3842-3848.

97. Altoè, A., V. Pulkki, and S. Verhulst, *Transmission line cochlear models: Improved accuracy and efficiency.* The Journal of the Acoustical Society of America, 2014. **136**(4): p. EL302-EL308.

98. Shera, C.A., *Intensity-invariance of fine time structure in basilar-membrane click responses: Implications for cochlear mechanics.* The Journal of the Acoustical Society of America, 2001. **110**(1): p. 332-348.

99. Zilany, M.S. and I.C. Bruce, *Modeling auditory-nerve responses for high sound pressure levels in the normal and impaired auditory periphery.* The Journal of the Acoustical Society of America, 2006. **120**(3): p. 1446-1466.

100. Bruce, I.C., M.B. Sachs, and E.D. Young, *An auditory-periphery model of the effects of acoustic trauma on auditory nerve responses.* The Journal of the Acoustical Society of America, 2003. **113**(1): p. 369-388.

101. Zilany, M.S. and I.C. Bruce, *Representation of the vowel/ɛ/in normal and impaired auditory nerve fibers: model predictions of responses in cats.* The Journal of the Acoustical Society of America, 2007. **122**(1): p. 402-417.

102. Tan, Q. and L.H. Carney, *A phenomenological model for the responses of auditory-nerve fibers. II. Nonlinear tuning with a frequency glide.* The Journal of the Acoustical Society of America, 2003. **114**(4): p. 2007-2020.

103. Smoorenburg, G.F., *Damage Risk Criteria for Impulse Noise [microvorm]*. 1980: Institute for Perception, TNO.

104. Health, U.D.o. and H. Services, *Criteria for a Recommended Standard: Occupational Noise Exposure Revised Criteria.* Cincinnati, OH, 1998: p. 1-122.

105. AMSC, N. and A.A. HFAC, *DEPARTMENT OF DEFENSE DESIGN CRITERIA STANDARD.* Signal. **44**(5.3): p. 4.

106. Azizi, M.H., *Occupational noise-induced hearing loss.* The international journal of occupational and environmental medicine, 2010. **1**(3 July).

107. Murphy, W.J. and C.A. Kardous, *A case for using a-weighted equivalent energy as a damage risk criterion.* National Institute for Occupational Safety and Health, EPHB Report No, 2012.

108. Hamernik, R.P., W.A. Ahroon, R.I. Davis, and S.F. Lei, *Hearing threshold shifts from repeated 6-h daily exposure to impact noise.* The Journal of the Acoustical Society of America, 1994. **95**(1): p. 444-453.

109. Henderson, D. and R. Hamernik, *Impulse noise: critical review.* The Journal of the Acoustical Society of America, 1986. **80**(2): p. 569-584.

110. Starck, J. and J. Pekkarinen, *Industrial impulse noise: crest factor as an additional parameter in exposure measurements.* Applied Acoustics, 1987. **20**(4): p. 263-274.

111. Hamernik, R.P., D. Henderson, J.J. Crossley, and R.J. Salvi, *Interaction of continuous and impulse noise: audiometric and histological effects.* The Journal of the Acoustical Society of America, 1974. **55**(1): p. 117-121.

112. Blakeslee, E., K. Hynson, R. Hamernik, and D. Henderson, *Interaction of spectrally-mismatched continuous and impulse-noise exposures in the chinchilla.* The Journal of the Acoustical Society of America, 1977. **61**(S1): p. S59-S59.

113. Hamernik, R.P. and W. Qiu, *Correlations among evoked potential thresholds, distortion product otoacoustic emissions and hair cell loss following various noise exposures in the chinchilla.* Hearing research, 2000. **150**(1): p. 245-257.

114. Qin, J. and P. Sun, *Applications and comparison of continuous wavelet transforms on analysis of a-wave impulse noise.* Archives of Acoustics, 2015. **40**(4): p. 503-512.

115. Parmanen, J., *A-weighted sound pressure level as a loudness/annoyance indicator for environmental sounds–Could it be improved?* Applied Acoustics, 2007. **68**(1): p. 58-70.

116. Walworth, H.T., *Guidelines for Noise Exposure Control: Intersociety Committee Report.* Journal of Occupational and Environmental Medicine, 1967. **9**(11): p. 571-575.

117. Havelock, D., S. Kuwano, and M. Vorländer, *Handbook of signal processing in acoustics*. 2008: Springer Science & Business Media.

118. Dunn, D.E., R.R. Davis, C.J. Merry, and J.R. Franks, *Hearing loss in the chinchilla from impact and continuous noise exposure.* The Journal of the Acoustical Society of America, 1991. **90**(4): p. 1979-1985.

119. Steele, C., *A critical review of some traffic noise prediction models.* Applied acoustics, 2001. **62**(3): p. 271-287.

120. DeCarlo, L.T., *On the meaning and use of kurtosis.* Psychological methods, 1997. **2**(3): p. 292.

121. Pearson, K., *" Das Fehlergesetz und Seine Verallgemeinerungen Durch Fechner und Pearson." A Rejoinder.* Biometrika, 1905. **4**(1/2): p. 169-212.

122. Hamila, R., J. Astola, F.A. Cheikh, M. Gabbouj, and M. Renfors, *Teager energy and the ambiguity function.* IEEE Transactions on Signal Processing, 1999. **47**(1): p. 260-262.

123. Rosowski, J.J., *The effects of external-and middle-ear filtering on auditory threshold and noise-induced hearing loss.* The Journal of the Acoustical Society of America, 1991. **90**(1): p. 124-135.

124. Slama, M.C., M.E. Ravicz, and J.J. Rosowski, *Middle ear function and cochlear input impedance in chinchilla.* The Journal of the Acoustical Society of America, 2010. **127**(3): p. 1397-1410.

125. Rhode, W.S. and N.P. Cooper, *Nonlinear mechanics in the apical turn of the chinchilla cochlea in vivo.* Aud. Neurosci, 1996. **3**(101): p. U121.

126. Hamernik, R.P., J.H. Patterson, G.A. Turrentine, and W.A. Ahroon, *The quantitative relation between sensory cell loss and hearing thresholds.* Hearing research, 1989. **38**(3): p. 199-211.

127. Zou, K.H., K. Tuncali, and S.G. Silverman, *Correlation and simple linear regression.* Radiology, 2003. **227**(3): p. 617-628.

128. Calford, M., R. Rajan, and D. Irvine, *Rapid changes in the frequency tuning of neurons in cat auditory cortex resulting from pure-tone-induced temporary threshold shift.* Neuroscience, 1993. **55**(4): p. 953-964.

129. Ohlemiller, K.K., *Contributions of mouse models to understanding of age-and noise-related hearing loss.* Brain research, 2006. **1091**(1): p. 89-102.

130. Fletcher, H., *Auditory patterns.* Reviews of modern physics, 1940. **12**(1): p. 47.

131. Zwicker, E., *Masking and psychological excitation as consequences of the ear's frequency analysis.* Frequency analysis and periodicity detection in hearing, 1970: p. 376-394.

132. Irino, T. and R.D. Patterson, *A dynamic compressive gammachirp auditory filterbank.* Audio, Speech, and Language Processing, IEEE Transactions on, 2006. **14**(6): p. 2222-2232.

133. Crane, H., *Mechanical impact: a model for auditory excitation and fatigue.* The Journal of the Acoustical Society of America, 1966. **40**(5): p. 1147-1159.

134. Hussain, Z.M., A.Z. Sadik, and P. O'Shea, *Digital signal processing: an introduction with MATLAB and applications*. 2011: Springer Science & Business Media.

135. Ahroon, W.A., R.P. Hamernik, and R.I. Davis, *Complex noise exposures: An energy analysis.* The Journal of the Acoustical Society of America, 1993. **93**(2): p. 997-1006.

136. Hamernik, R., W. Ahroon, D. Henderson, and R. Salvi. *The interaction between continuous and impulse noise: Frequency effects*. in *The 2 Nd International Conference on the Combined Effects of Environmental Factors*. 1987.

137. Suter, A.H. *Occupational Hearing Loss from Non-Gaussian Noise*. in *Seminars in Hearing*. 2017. Thieme Medical Publishers.

138. Ren, T., *Longitudinal pattern of basilar membrane vibration in the sensitive cochlea.* Proceedings of the National Academy of Sciences, 2002. **99**(26): p. 17101-17106.

139. Patterson, R.D., *Auditory filters and excitation patterns as representations of frequency resolution.* Frequency selectivity in hearing, 1986.

140. Moore, B.C., *An introduction to the psychology of hearing*. 2012: Brill.

141. Ward, W.D., *Effect of temporal spacing on temporary threshold shift from impulses.* The Journal of the Acoustical Society of America, 1962. **34**(9A): p. 1230-1232.

142. Bohne, B.A. and G.W. Harding, *Degeneration in the cochlea after noise damage: primary versus secondary events.* Otology & Neurotology, 2000. **21**(4): p. 505-509.

APPENDIX-A

PERMISSION FOR THE REUSE FROM THE COPYRIGHT OWNER

A.1: Permission for the reuse of Figure 3.1 on page 18

JOHN WILEY AND SONS LICENSE TERMS AND CONDITIONS

Mar 06, 2019

This Agreement between Southern Illinois University -- Wisam Al-Dayyeni ("You") and John Wiley and Sons ("John Wiley and Sons") consists of your license details and the terms and conditions provided by John Wiley and Sons and Copyright Clearance Center.

License Number	4543150204283
License date	Mar 06, 2019
Licensed Content Publisher	John Wiley and Sons
Licensed Content Publication	Wiley Books
Licensed Content Title	Communication Acoustics: An Introduction to Speech, Audio and Psychoacoustics
Licensed Content Author	Matti Karjalainen Ville Pulkki
Licensed Content Date	Jan 1, 2015
Licensed Content Pages	1
Type of use	Dissertation/Thesis
Requestor type	University/Academic
Format	Print and electronic
Portion	Figure/table
Number of figures/tables	1
Original Wiley figure/table number(s)	Figure 7.1
Will you be translating?	No
Title of your thesis / dissertation	DEVELOPMENT AND VALIDATION OF NEW MODELS AND METRICS FOR THE ASSESSMENTS OF NOISE-INDUCED HEARING LOSS
Expected completion date	May 2019
Expected size (number of pages)	140
Requestor Location	Southern Illinois University 1230 Lincoln Drive MC 6603 CARBONDALE, IL 62901 United States Attn: Southern Illinois University
Publisher Tax ID	EU826007151
Total	0.00 USD

VITA

Graduate School
Southern Illinois University

Wisam Subhi Talib Al-Dayyeni

wisam.subhi@gmail.com

Al-Nahrain University at Baghdad, Iraq
Bachelor of Science, Electronics and Communications Engineering, May 2005

Al-Nahrain University at Baghdad, Iraq
Master of Science, Modern Communications Engineering, February 2009

Dissertation Paper Title:

DEVELOPMENT AND VALIDATION OF NEW MODELS AND METRICS FOR THE ASSESSMENTS OF NOISE-INDUCED HEARING LOSS

Major Professor: Dr. Jun Qin

Publications:

1. **Al-Dayyeni, W.S.**, P. Sun, and J. Qin, *Investigations of Auditory Filters Based Excitation Patterns for Assessment of Noise Induced Hearing Loss.* Archives of Acoustics, 2018. 43(3): p. 477–486.

2. **Al-Dayyeni, W.S.**, and J. Qin, *Comparison of New Metrics for Assessment of Risks of Occupational Noise.* Journal of Applied Sciences and Arts, 2017. 1(3): p. 4.